UNIVERSITY OF CALIFORNIA, MERCED

# Enhancing Device-Level Models for Ignition and Sheath Characteristics of Field Emission Assisted Microdischarges

A dissertation submitted in partial satisfaction of the
requirements for the degree
Doctor of Philosophy

in

Physics

by

Jiba Nath Dahal

Committee in charge:

Jay sharping, Chair
Venkattraman Ayyaswamy, Graduate Advisor
Roland Winston, Committee Member

2018

The dissertation of Jiba Nath Dahal is approved, and it is acceptable in quality and form for publication on microfilm and electronically:

---

(Venkattraman Ayyaswamy, Graduate Advisor)

---

(Roland Winston, Committee Member)

---

(Jay sharping, Chair)

University of California, Merced

2018

DEDICATION

To my parents

Father: Tikaram Dahal

Mother: Yakumaya Dahal

# EPIGRAPH

*Imagination is more*
*important than knowledge.*
—Albert Einstein

TABLE OF CONTENTS

LIST OF FIGURES

ACKNOWLEDGEMENTS

I would like to express the deepest gratitude to my adviser Professor Venkattraman Ayyaswamy for his guidance and continual support in the planning and development of my research. I cannot imagine where am I without his guidance. I got the complete freedom while working on this academic project. Without him, this work will never be in this form. I am always in debt for his time , support, and the way of his guiding. Each of the members of my Dissertation Committee has provided me extensive personal and professional guidance and taught me a great deal about both scientific research and life in general. So, I would like to express my appreciation to my committee members, Professor Roland Winston and Professor Jay Sharping for their constant support and encouragement since qualifying exam to final dissertation defense. My sincere gratefulness goes to the Department of Physics for providing me an opportunity to pursue doctorate degree with full financial support.

I personally thankful to Dean of graduate division and Professor Marjorie Zatz and Vice Chancellor for Student Affairs Dr. Charles Nies for their continuous support in my leadership career while being executive member of graduate students association (GSA) as well as being as a graduate student. I would like to thank all faculties of the School of natural science and Department of Physics at University of California, Merced for being extremely helpful.

Staffs from the School of Natural Science are always in my memory for their support and assistance during my time at UC Merced. I express my appreciation to my friends especially to Gowa Lama, Dr. Lokendra Poudel, Dr Rudra Gyawali, Dr. Kamal Raj Dhakal and all the supportive ones who directly or indirectly helped me to make my thesis successful.

Last but not least I am grateful to my family whose love and support made me successful to accomplish whatever I have so far. I want to remember my late grandpa and grandma who always encouraged me to be successful person since my childhood. This journey is possible only because of my father Tikaram Dahal and Mother Yakumaya Dahal and I want to thank god for giving me such a wonderful parents. Words can not express how grateful I am for all of the sacrifices that you

have made on my behalf. Your prayer for me was what sustained me thus far. I especially want to thank to my brother Purna Prasad Dahal who always brings me smile even if I am in pain. My deep love to my wife Gita Adhikari Dahal who always makes me ready to struggle for our better future and my sons Sujit Dahal and Suyog Dahal for your jokes, laugh and happiness.

**$11^{th}$ August 2018 Saturday**

## VITA

| | |
|---|---|
| 2000-2004 | B.S. in Physics ,Tribhuvan University, Kirtipur, Nepal |
| 2004-2007 | M. Sc.in Physics, Tribhuvan University, Kirtipur, Nepal |
| 2011-2013 | M. S. in Physics and Material Science, The University of Memphis, Tennessee. |
| 2013-2018 | Ph. D. in Physics, University of California, Merced |

## PUBLICATIONS

**J.N.Dahal** and A. Venkattraman," Influence of applied voltage on electron energy distribution function and ioiation coefficient in microdischarge" (Submitted 2018)

**J.N. Dahal** and A. Venkattraman, Enhancing the predictive capability of modified Paschen curve models for direct current field emission assisted (FEA) microdischarges *Physics of Plasma* (Submitted 2018)

**J.N. Dahal** , K. S. Syed Ali, and J. Alam, S. R. Mishra Structural, Magnetic, and Mossbauer Spectral Study of $Gd_2Fe_{16}Ga_{0.5}TM_{0.5}$ (TM = Cr, Mn, Co,Ni, Cu, Zn) Compounds, *Journal of Alloy and Compounds* , 2018

**J.N. Dahal**, S.R. Mishra Synthesis and Magnetic Properties of exchange-coupled $SrFe_{12}O_{19}$ - x Wt.% - $La_{0.7}Sr_{0.3}MnO_3$ nanocomposites via autocombusiton method, *Journal of Alloys and Compounds*, 2018.

**J.N.Dahal**, L. Wang, S.R. Mishra, V.V. Nguyen, J.P. Liu "Synthesis and magnetic properties of $SrFe_{12-x-y}Al_xCo_yO_{19}$ nanocomposites prepared via autocombustion technique", *Journal of Alloy and Compounds*, 595, 2014.

ABSTRACT OF THE DISSERTATION

**Enhancing Device-Level Models for Ignition and Sheath Characteristics of Field Emission Assisted Microdischarges**

by

Jiba Nath Dahal
Doctor of Philosophy in Physics
University of California Merced, 2018
Jay sharping, Chair

Traditional plasma systems typically operate at low pressures and centimeter scale reactors. However, during the last decade or so, there is an active interest in the downscaling of devices and plasmas are no exception. Because of the popular *pd* (pressure times gap size) scaling, such plasmas have to operate at or near atmospheric pressure and are referred to as microplasmas or microdischarges. While downscaling the plasma device, field emission of electrons and their interaction with micro discharge due to high electric fields has shown to affect both pre-and post breakdown operation of these discharge. In this context, we present computational data for the ionization coefficient ($\alpha$) at high electric fields. A zero-dimensional Monte Carlo code is used to determine the variation of $\alpha$ as a function of electric field for various gases to use in device-level models. Results are also presented for the dependence of $\alpha$ in a spatially varying electric field. While $\alpha$ represents the volume process in a discharge, the most important surface process in microdischarge is field emission which is characterized by the field enhancement factor $\beta$. Comparison of experimental data with theoretical data for argon , hydrogen, carbon dioxide and dry air are presented to predict a inverse dependence of $\beta_{eff}$ on electric field.

Finally, device-level models are also formulated for the post-breakdown operation of field emission assisted microdischarges as motivated by novel cathodes with

excellent field emission properties. In this context we present a non-linear sheath model for direct current field emitted assisted microdischarges. The main focus of this work is to develop a self consistent sheath model that includes the effects of field induced electron emission without assuming a linear electric field. The results obtained from the non-linear sheath model for various parameters including current-voltage characteristics, and current density profiles of ion/electro are validated with PIC/MCC simulation of an argon microdicharge.

# Chapter 1

# Introduction

## 1.1 Plasma in General

When solid, liquid or gas are heated with sufficient temperature, they will change in the form of ionized particles which is called plasma. So, in general, plasma is a collection of randomly moving free charged particles. Plasma is called as fourth state of matter and it is believed that about 99 percent of the universe is made up plasma. Unlike the other state, plasma is not found freely on the earth at normal condition. Lightning and polar light are the example of naturally occurring plasma. Plasma can be produced by heating at sufficiently high temperature or apply high electric field so that the the electrons are completely free which makes plasma a good conductor of electricity. Plasmas resulting from ionization of neutral gases generally contain equal numbers of positive and negative charge carriers. In this situation, the opposite charges coupled together and neutralize electrically. Such plasmas are termed as quasi-neutral plasma [2]. Strongly non-neutral plasmas, which may even contain charges of only one sign, occur primarily in laboratory experiments. Their equilibrium depends on the existence of intense magnetic field, about which the charged fluid rotates.

The study of plasma started in early seventeenth century when natural plasmas like lighting and polar lights were observed by peoples at that time. During the nineteenth century, significant progress was made with regard to electric energy

and vacuum system[3]. The contribution due to Faraday and Sir William Crookes is remarkable during this time as they developed the direct current glow discharge and vacuum plasma. In 1920s, Langmuir named as *plasma* to describe the region containing balanced charges of ions and electrons in the ionized gas that contains ions and electrons in about equal numbers. This makes the the resultant space charge very small. He also invented Langmuir probe to determine the electron temperature, electron density and electric potential of plasma [7, 8].

In recent decades rapid progress in the development, diagnostics and applications of plasma is done. High temperature plasma used in Fusion started in 1960s [9]. As significant improvement were achieved in 1970s and 1980s and used *Tokamak* which produces about 500MW fusion output power for the first time [10]. Since 1990 the application of atmospheric pressure plasma eliminated the need of expensive vacuum chamber and pumping systems such as atmospheric pressure plasma which is widely used for environmental applications, surface modification of materials, biomedical applications and so on. The study of aurora and ionosphere has been done in late nineteenth century which helps to design and study of space craft. Effect of solar wind and Earth magnetic field is also done while studying about the space plasma.

## 1.2 Categories of Plasma

Plasmas can be categories on the basis of plasma densities as well as the relative temperatures between electrons, ions and neutrals. On the basis of plasma densities, plasma are divided in to two categories.

1. **High-Density Plasma** : High density plasma sometime refers as high pressure plasma. The number density N $> 10^{15-18} cm^{-3}$. The excitation or ionization collision in these type of plasma are generally high and therefore the ion bombardment rate is usually high. These type of plasma usually used for etching in microelectronics, decontaminating plasma and producing nanomaterials.

2. **Low-Density Plasma**: Low density plasma are also called low pressure plasma where the number density N$< 10^{12-14} cm^{-3}$. The collision rate in these type of plasma are very low or almost negligible. These type of plasma usually used in laser wakefield accelerator [11] where plasma density should be very low to have the propagation of lasers of optical or infrared frequency.

On the bases of temperature, plasma is mostly divided into two categories as thermal plasma and non-thermal plasma.

1. **Non Thermal Plasma**: Non thermal plasma are also called as low temperature plasmas where $T_e << T_{gas}$. Low temperature plasmas have been widely used for surface treatment of solid materials. All the plasmas used in the microelectronics industry are cold plasmas. In most low-pressure plasmas, the pressure is lower than 1 mTorr - 1 Torr. Correspondingly, the electron density $n_e$ is of the order of $10^8 - 10^{13} cm^{-3}$ and electron temperature Te= 1-10 eV. An ion remain at room temperature of $T_i$=300K and $T_i \ll T_e$ . For cold plasma discharge, the chemical bonds of the molecular gas can mostly be formed at 1-10 eV. This discharge produces electrons and destroys chemical bonds thus generating a variety of free radicals and positive ions in order to remove part of the materials or form a surface film. Direct current(DC), radio-frequency (RF) or microwave sources can all be used to generated low temperature plasma. Because the coupling efficiency of electromagnetic energy into the plasma is low, high frequency (HF) is not suitable for low-pressure plasmas. It can be obtained by low pressure discharges or in short pulse discharges as Dielectric Barrier Discharges. Arc plasma at normal pressure, low-pressure gas discharge etc. are also the example of non thermal plasma.

2. **Thermal Plasma**: Thermal plasma are generally called as high temperature plasma where $T_e \sim T_{gas}$. The time of the discharge must be quite long, in order to have equilibration between the electron gas and heavy particles. It is produced in plasma torches or in high pressure discharges. Fusion plasma is the example of this type of plasma. In most of the stars the thermonuclear fusion reaction occurs as particles are in plasma state are subjected to very high temperature.

## 1.3 Applications of Plasma

Plasma lamps are the common use of plasma in our daily life. We are getting light and heat from the sun which is formed by the fusion of plasma in the interior of sun. As mentioned earlier, 99% of the universe is covered by plasma, so plasma is everywhere. Researchers can understand the complex behavior of confined plasmas by formulating the simple fundamental equations of plasma physics. This foundational work and understanding of plasmas has led to important advances in fields as diverse as computers, lighting, waste handling, space physics, switches and relays and lasers. Plasma is also applicable for an effective, cheap and environmentally friendly process for the disinfection and degradation of organic pollutants in water. The ozonation process has stronger oxidation efficiency compare to traditional chlorination process. Corona discharge has been successfully used for ozone synthesis in many industrial fields for more than 150 years without any major modification [12, 13, 14]. Plasma light sources are also useful for the energy saving alternatives [15] in homes by using high intensity arc lamp which produces light by means of an electric arc between tungsten electrodes inside the transparent quartz tube. Corona discharge, glow discharge, arc discharge, capacitively coupled discharge,neon light, solar wind are also the other application of plasmas. Plasma are also widely used in aerospace engineering, biomedicine, textile technology, analytical chemistry, plasma spraying and physical vapor deposition and many more.

Two parameters n and $kT_e$ are the key parameters used to characterized plasmas where k is the Boltzmann constant and $T_e$ is the electron temperature. Many applications of plasmas cover wide range of n and $kT_e$. The following Figure 1.1 explains more details about the application of plasma over the wide range of plasma parameter. In case of gas Discharge it needs $kT_e \approx 2\text{eV}$ and $10^{14} < n < 10^{18} m^{-3}$. The meaning of one electron volt (eV) is the energy needed to move an electron ($e = 1.6 \times 10^{-19} C$) against the potential difference of 1V and the temperature corresponding to the thermal energy of 1eV is 11600K.

Gas discharges are used in mercury rectifiers, ignitions, spark gaps, welding arcs, neon, fluorescent light, lightning discharges etc. Plasma lamps are the common

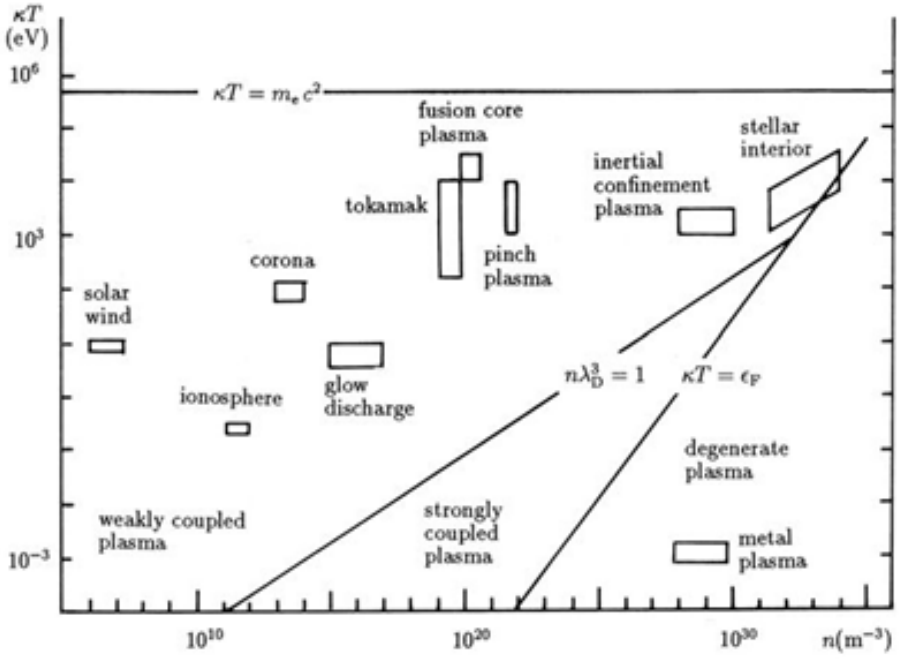


Figure 1.1: Various plasma domains in the $n - KT_e$ diagram. [1]

use of plasma in our daily life. Controlled thermonuclear fusion is another use of plasma where electrons are changed in the form of plasma in which thermal energies are in the range of 10 keV. Tokamack, pinch plasma *etc.* need more than 1000 eV of thermal energy to form the plasma. Many stellar interiors and atmosphere are hot enough to be in the plasma state where there is thermonuclear fusion reaction occurs. The plasma kinetic theory has been used to predict the development of galaxies. The radiation emitted by those stars and galaxies are received by the telescope to study about the surface temperature and many more.

The foundational work and understanding of plasmas has led to important advances in fields as diverse as computers, lighting, waste handling, space physics, switches and relays and lasers. Free electrons and holes in the semiconductor behaves as a plasma as they are exhibiting the some sort of oscillations and instabilities as a gaseous plasma. Quantum mechanical effects of those semiconductor can also be studied using plasma source. Gas lasers are also common use of plasma

nowadays.

## 1.4 Plasma parameter

There are three fundamental parameters that characterize a plasma: (a) the particle density n, (b) the temperature T of each species and (c) the steady-state magnetic field B.

For plasma to exist, ionization is necessary. As we know that when solid is heated to high temperature, it turns into liquid and when it is further heated it turns into gas and when the gas is sufficiently heated with high temperature, the molecule of the gas decomposes to form a gas of atoms that move freely in random direction as shown in the Figure 1.2. If the temperature is further increased, then the atoms decompose into freely moving charged particles (electron and ions) and the substance enters into the plasma state. This state is characterized by charged particle density ie charge density of electron( ne) = charge density of ion (ni) and are in equilibrium temperature as electron temperature ($T_e$) = ion temperature ($T_i$). The degree of ionization of a plasma is the proportion of atoms that have lost or gained electrons and is controlled mostly by temperature. The fractional ionization of plasmas is

$$x_{iz} = \frac{n_i}{n_g + n_i} \tag{1.1}$$

where $n_i$ is called ion number density and $n_g$ is called neutral gas density. For the fully ionized plasma, $n_g$ is almost zero and thus $x_{iz}$ will be approximately one but for weakly ionized plasma there are more $n_g$ and thus $x_{iz}$ is less than one .

The plasma properties will vary with the range of plasma scaling. Traditional plasma systems (relevant to, for example, materials processing technology) [16] typically operate at low pressures and centimeter scale reactors. However, during the last decade or so, there is active interest in the downscaling of devices and plasmas are no exception [17, 18, 19]. Because of the popular *pd* (pressure times

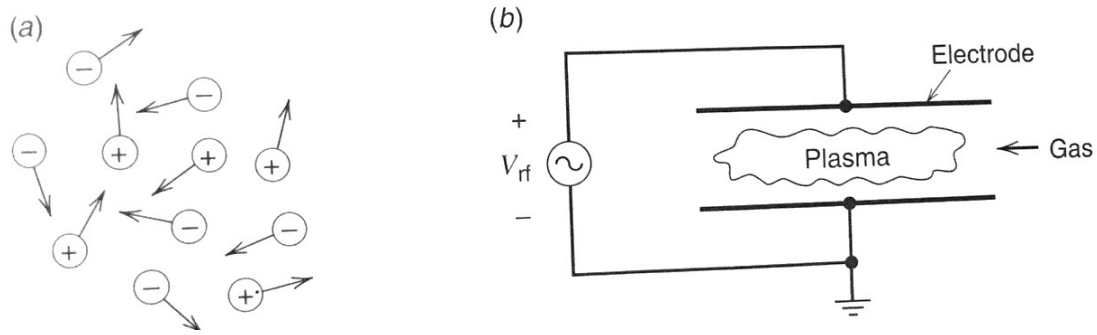


Figure 1.2: Schematic view of (a) a plasma and (b) a discharge. [2]

gap size) scaling, such plasmas need to be operated at or near atmospheric pressure and are referred to as microplasmas or microdischarges. While microplasmas were originally defined as electrical discharges/plasmas operating in gap sizes less than a millimeter, current thrust is on plasmas operating in micron-scale gaps with a constant push towards the $1\mu m$ limit [20]. Such devices are subjected to extremely high electric fields as a result of their small physical dimensions. If electric filed reaches $10^7$-$10^8$ V/m, field emission from the cathode into the gas take place. This type of technology is highly used in low gas pressure technology such as in vacuum technology [21],electron microscope [22] and vacuum electronics. One of the example of devices that is operating with small gap size are microelectromechanical systems (MEMS) where electrical breakdown must be avoided for the proper function of the devices. MEMS are considering as promising technology for the development of low-cost and low-power switches, actuators ad sensors. These devices are based on the field emission of electrons from the cathodes. In these devices, the mean free path of electron is much smaller than in vacuum technologies, and field-emitted electrons interact significantly with background gas atom and molecules via inelastic collisions, generating ions as well as other excited states. The continued interest in MEMS takes them to the rapid developments in MEMS fabrications in last few years though there are lots of challenges in dealing with the physics of these microscale systems. For the better designs, a complete understanding of the various physical process along with different strategies of the microscale gas break-

down need to be taken care of. Last two decades, many researchers are ruining to explore the role of field emission in microscale breakdown with the different tools such as computational, theoretical and experimental technique. Those research have shown that the field emission can produce comparatively less currents even below the breakdown threshold [23, 24, 25, 26]. The following sections provide the theoretical background of field emission driven microscale gas breakdown with the motivation for the work performed in this dissertation by pointing out how it extends previous relevant work.

## 1.5 Structure of plasma

Plasma is the state of matter where an ionized gaseous substance becomes highly conductive and affected by electric and magnetic filed. Plasma is electrically neutral at the steady state as number of electron and proton are equal so overall charge of the plasma is roughly zero. As electric field is applied across the electrode the electrons begins to flow from cathode to anode and if the electric field is sufficient the stream of electrons begin to occur which is called as electric discharge in general.

Plasma can be discharge using both direct current (DC) as well as alternating current (AC) also called as radio frequency (RF) discharge. In DC discharge there is a fixed cathode and a fixed anode where the electrons acquired energy to accelerate from cathode to anode and electrons undergoes many collisions along the way once applied the voltage across the electrode. If the voltage is too low, free electrons won't have enough energy to ionize the neutrals. If the voltage is too high, electrons will move too fast to avoid any collisions with neutrals. The optimum voltage range is a function of gas species and pressure. Unlike DC discharge there is no fixed cathode and anode when the plasma is treating using RF discharge. Both cathode and anode rely on the applied electric field. An alternating high voltage is applied on both electrodes. Majority of the free-moving electrons will be oscillating back and forth. Compared with DC discharge, they will have less chance of absorption by electrodes and higher chance of ionizing neutral particles.

Mostly are RF discharge are used if the layer to be treated is a semiconductor or an insulator. In this dissertation dc mode is taken care of in details while talking about the microplasma.

Electron Energy Distribution Function (EEDF) plays very important role in plasma modeling. It is needed to compute reaction rates for electron collision reactions. Because electron transport properties can also be derived from the EEDF, the choice of the EEDF we use influences the results of the plasma model. If the plasma is in thermodynamic equilibrium, the EEDF has a Maxwellian shape. In most plasmas, for technical purposes, deviations from the Maxwellian form occur.

EEDF can be computed by solving the Boltzmann equation. The Boltzmann equation describes the evolution of the distribution function in a six-dimensional phase space as,

$$\frac{\delta f}{\delta t} + v.\nabla f - \frac{e}{m}(E.\nabla_v f) = C[f] \tag{1.2}$$

## 1.6 Microdischarge

Many advantages of high temperature and low temperature plasma are already discussed in the earlier sections. Compare to high temperature plasma, Low temperature plasma is useful everywhere as it doesn't need high temperature. Since low temperature plasma also work for normal atmospheric pressure, they are useful on many electronics devices. The size of the electronic devices are also going down and nowadays most of them are working on microscale. Breakdown voltage plays an important role for the plasma discharge. Higher voltage can easily breakdown the devices where as small voltage cannot produce ionization. Study of breakdown voltage and current voltage characteristics need to be known before we use them for experimental purpose. Theoretical model will help to predict those parameter. Many studies have been done already but the data are not simplified so simple device model are necessary. Thus, present work focus on the microscale plasma at low temperature by formulating predictive model in order to address these issues.

Microplasmas, defined as plasmas where at least one dimension is in the millimeter rang. Microplasmas can be produced by applying voltage to electrodes or by focusing high power laser radiation into the discharge medium. Traditional plasma systems (relevant to, for example, materials processing) [16] technology typically operate at low pressures and centimeter scale reactors. However, during the last decade or so, downscaling of plasmas devices has focused many researcher [17, 20, 27].The attraction is based on As we are downscaling our electrical devices everyday, microcplasma is particularly important as it include high plasma number densities (more reactive) and requires low energy to make the discharge because the electric field is applied within the microscale gap size. For example, if 1V is applied for 1 mm gap size, the electric field across the electrode is $10^4$ V/m. This shows that even though we apply very small voltage across these micro-electrode, the electric field becomes very high. Thus, we are dealing with very high electric field while working on microplasma.

The first reviews in the field of microplasma was published in 2005 and 2006 [18, 17] and provided summaries of research into the basic properties of microplasma and results from some of the applications of microplasmas. Later till 2016 there are lots of topical reviews about the microplasmas and their applications are being published that include UV light sources [28], microdischarge based sensors [29], photonics devices [30], guided ionization waves in plasma jets [31, 32] etc. Many modeling and simulations helped to gain more sight into the physics of non-thermal microdischarges. The current thrust of understanding microplasmas will increase scientific knowledge to the development of new plasma technologies.

Due to the popular *pd* (pressure times gap size) scaling, such plasmas have to operate at or near atmospheric pressure and are referred to as microplasmas or microdischarges. While microplasmas were originally defined as electrical discharges/plasmas operating in gap sizes less than a millimeter, current thrust is on plasmas operating in micron-scale gaps with a constant push towards the $1\mu m$ limit. Such devices are subjected to extremely high electric fields as a result of their small physical dimensions. Therefore, physical mechanisms that were previously considered to be unimportant are rapidly gaining significance. For example, the in-

tense electric fields encountered by micron-scale devices triggers electron emission from metal electrodes thereby modifying the operating principles and creating new regimes of operation. This electric field-induced electron emission is referred to as field emission and is the primary focus of this dissertation. The gas breakdown in microgaps has been widely used for various applications. Traditionally, the breakdown of gases by production of charge particles in microscale gaps is described by the Paschen curve which explain the relation between breakdown voltage as a function of pressure and gap sizes between the anode and cathode popularly known as *pd*. The breakdown voltage expression using the Paschen theory is given as,

$$V_b = \frac{Bpd}{ln(Apd) - ln\left(ln\left(1 + 1/\gamma_{se}\right)\right)} \tag{1.3}$$

Where A and B are constants, $p$ is pressure, $d$ is gap sizes and $\gamma_{se}$ is coefficient of secondary electron emission at the cathode. The secondary electron are electrons emitted from the cathode when an ion strikes the cathode and $\gamma_{se}$ represents the probability of an electron being emitted when an ion strikes the cathode. It should be noted that the Paschen law predicts the breakdown voltage to depend on the product of pressure and gap size ($pd$) as opposed to pressure and gap size independently. Also, secondary electron emission coefficient is the only boundary phenomenon that determines the breakdown voltage. The gas-phase phenomena are contained in the gas-specific constants A and B with their values describing the ionization coefficient and its dependence on pressure and electric field for the gas under consideration. The understanding of ionization coefficient ($\alpha$) and its dependence on field emission is also the part of this dissertation which is explained in details in the following section.

## 1.7 Ionization Coefficient

Every elements are composed of electrons. There are various process to make electrons free from the elements. Thermionic emission, photoelectric effect etc are few examples. In plasma there are free electrons and ions where electron are colliding with near by molecules and creating additional electrons. Also, freely moving ions collides the cathode and knock out the electron. The electrons thus

produced are called secondary electrons and the probability of secondary electron emission when an incident ion strikes the cathode is measured by coefficient of secondary electron emission ($\gamma_{se}$). Some of those electrons also knock the cathode and creating extra electrons. All these electrons during the process of ionization are accelerated by electric field. If there are sufficient electrons and electric field the avalanche of electrons occurs which is called as plasma discharge. This way of creating electrons is called field emission where application of electric field changes the shape of the potential barrier. Larger the electric field the steeper the slope of the decreasing potential barrier. The electric field and the mean free path of the electron must allow free electrons to acquire an energy level that can cause impact ionization. If the electric field is too small, then the electrons do not acquire enough energy. If the mean free path is too short, the electron gives up its acquired energy in a series of non-ionizing collisions. If the mean free path is too long, then the electron reaches the anode before colliding with another molecule. Thus,an ionization coefficient is defined as the number of ions generated per electron per unit length of the cathode. If $dn$ number of ions pairs produced by $n$ electrons moving randomly and drifting $dx$ in the direction of uniform electric field $E$ than,

$$dn = n\alpha dx \tag{1.4}$$

where $\alpha$ is called the ionization coefficient.

If $n_o$ electrons cross the plane, x=0 and due to multiplication in the gas, $n$ electrons cross a plane at x=d (ie plane electrode separation),

integration gives,

$$\frac{n}{n_o} = \left(\frac{i}{i_o}\right) = e^{\alpha d} \tag{1.5}$$

Thus, if parallel plates are placed at x=0 and x=d, $i_o$ represents the electron current due to the steady emission of $n_o$ electrons per second and $i$ the total current flowing between the plates when uniform field $E$ is applied. It is found experimentally that the current $i_o$ is released from the cathode plate and the current $i$ that vary with distance as explained by equation (1.5). Thus with provided value of secondary effects at the cathode, $\alpha$ can be derived. Thus, micro scale breakdown voltage based on the Paschen theory as described in equation (1.3), the ionization coefficient $\alpha$

| Gas | $A$ | $B$ | $E/p$ | $C$ | $D$ | $E/p$ |
|---|---|---|---|---|---|---|
| | $cm^{-1}Torr^{-1}$ | $V/(cm \cdot Torr)$ | $V/(cm \cdot Torr)$ | $cm^{-1}Torr^{-1}$ | $V/(cm \cdot Torr)^{1/2}$ | $V/(cm \cdot Torr)$ |
| He | 3 | 34 | 20–150 | 4.4 | 14 | 100 |
| Ne | 4 | 100 | 100–400 | 8.2 | 17 | 250 |
| Ar | 12 | 180 | 100–600 | 29.2 | 26.6 | 700 |
| Kr | 17 | 240 | 100–1000 | 35.7 | 28.2 | 900 |
| Xe | 26 | 350 | 200–800 | 65.3 | 36.1 | 1200 |
| Hg | 20 | 370 | 150-600 | | | |
| $H_2$ | 5 | 130 | 150-600 | | | |
| $N_2$ | 12 | 342 | 100–600 | | | |
| $N_2$ | 8.8 | 275 | 27–200 | | | |
| Air | 15 | 365 | 100–800 | | | |
| $CO_2$ | 20 | 466 | 500–1000 | | | |
| $H_2O$ | 13 | 290 | 150–1000 | | | |

Figure 1.3: Values of constants A and B in equation (1.5) and C and D in equation (1.8) for different gas explained in ionization coefficient and regions of applicability. [3]

is explained by using the Townsend avalanche criterion as,

$$\gamma_{se}(e^{\alpha d} - 1) = 1 \tag{1.6}$$

where $\gamma_{se}$ is the secondary electron emission coefficient which is define as the probability of producing an electron when an ion strike the cathode and $d$ is the gap size.

Electrons generated at cathode due to field emission or other emission mechanisms ionize the gas in the gap producing ions that move towards the cathode. When these ion strike the cathode, it can lead to the production of additional electrons due to secondary electron emission which can then ionize the gas causing further and rapidly increase the number of electrons and ions. At the breakdown, the number of electron and ions increase rapidly and the gas in the gap becomes conducting. Apart from the secondary emission, the ions which are striking the cathode can also cause erosion of the surface and may modify the field enhancement factor as a function of time which is not directly included in the PIC/MCC simulations. Once the breakdown occur due by Townsend avalanche criterion ions

produced by the primary electron and reaching out to the cathode should produce one secondary electron which can then take the role of a primary electron and sustain the process. Traditionally, $\alpha$ is described by the semi-empirical formula. [33]

$$\alpha = A_p p exp\left(-\frac{B_p p}{E}\right) \tag{1.7}$$

where $p$ is the pressure, $E$ is the electric field, $A_p$ and $B_p$ are the Paschen curve parameters defined by Raizer [3]. Usually, for $\alpha$ calculation, parameters $A_p$ and $B_p$ are calculated using experimental data for the macroscale gaps around 1mm but are not relevant for microscale gap sizes like MEMS devices.

This expression for $\alpha$ doesn't include the semi-empirical correction proposed by Venkattraman et.al. [34] using the simulation of dark discharges in opposition of linearly varying electric field. For inert gas, better fit to experimental data for ionization coefficient ($\alpha$) can be obtained by using the another relation as,

$$\alpha = Cpexp\left(-D\sqrt{\frac{p}{E}}\right) \tag{1.8}$$

where $C$ and $D$ are constants with units on $cm^{-1}Torr^{-1}$ and these constants are different for different gases as in Figure 1.3

Many experiments has been done in order to find the ionization coefficient of different gases. Many different gases are studied and the data published previously provides only for small electric field. In this context, this dissertation presents the careful study of experimental data for ten different gases and purpose the new computational model for higher electric field and compare both data in order to validate the model. The experimental The broad range of ionization coefficient for different gases are presented. In order to perform the experiment, the researcher can use the data from the model in order to operate at higher electric field. This dissertation also presents the ionization coefficient ($\alpha$) for non-uniform electric field and the results are also presented for the dependence of $\alpha$ in a spatially varying electric field.

## 1.8 Field Emission and Modified Paschen's Law

Many research on micro discharge on plasma are done and topical reviews are published in many journal as discussed in section 1.5. Many computational and experimental work explains much more about the micro discharge in micrometer scale. For over a century, gas breakdown has been described and predicted by Paschen Law [35] which relates the breakdown voltage ($V_b$) to the parameter pressure (p) multiplied by the distance (d), usually called as *pd*. This relationship between ($V_b$) and *pd* produces the Paschen's curve is in the solid line in the Figure 1.4 in the left. The major consequences of Paschens law is its prediction of breakdown as a function of gap size. Specifically, the right branch shifts up as $\gamma_{se}$ decreases and left branch shifts up as  decreases. It is seen from the Paschens curve that the voltage reaches a minimum value as gap size decreases but when the gap size decreases from 5-10 $\mu m$ than the breakdown voltage begins to increase as the gap size continues to decrease. It is possible because in the smaller gap distance, electron can reach from cathode to anode without ionizing the other gas molecule. Smaller gap sizes also reduce the volume of operating gas inside the electrode. This is why the traditional Paschen law follows the trend as shown by the dark solid line in the Figure 1.4 (left). The deviation from Paschen law for small gaps arises because of the field emission of effects were not taken in to account as in small gap sizes the electrode gets sufficiently high electric field that induces field emission where electron are pulled from the cathode through tunneling [36]. Shorter gaps size also increase probability of the positively charged ions collide the cathode and produces free more electrons because there will be less opportunity for recombination. Thus, this colliding effect and field emission effect reduces the breakdown voltage for the decreasing gap size. A typical modified Paschen curve can be divided into two parts with the right branch corresponding to large gaps where field emission is negligible due to secondary electron emission ($\gamma_{se}$) and the left branch controlled by field emission.

Breakdown in macroscale occurs through the critical matching of electron production and electron loss processes as shown schematically shown in Figure 1.4. The electron impact ionization process in the gas gap leads to an exponential in-

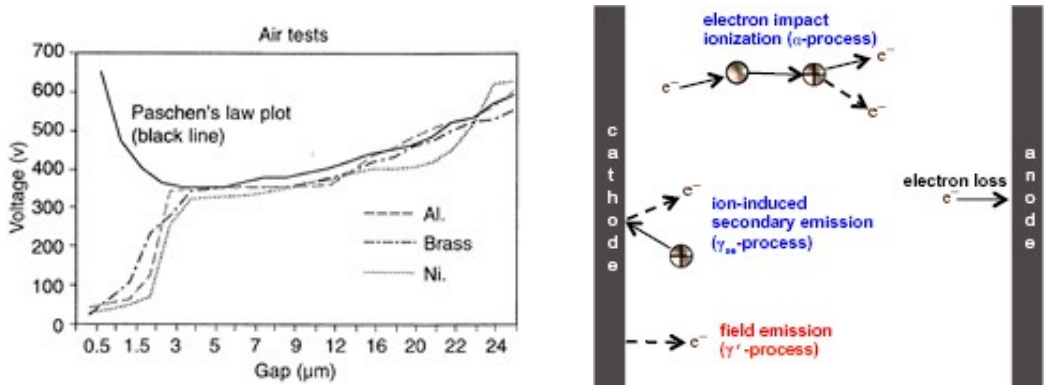


Figure 1.4: (Left) Plot of the breakdown voltage Vb as a function of the electrode gap spacing d for ambient air at atmospheric pressure using different cathodes materials. [4] (Right) Schematic showing the various processes that occur in a typical microdischarge [5]

crease of electrons and is referred to as the electron avalanche as explained by equation (1.6) and equation (1.5) . However these electrons are eventually lost to the anode and to further sustain the discharge, they must be replaced and this occurs by the secondary electron emission from the cathode. Breakdown occurs when the number of ions generated in the volume by single electron entering from the cathode is sufficient to emit a new electron from the cathode to replace it. Since, electron loss to the boundaries overwhelms electron generation either by ionization or by secondary emission from the electrodes due to bombardment unless additional energy (i.e. voltage) is added to the system. However, in the past decade, a number of experimental studies have suggested that Paschens curve does not accurately describe the processes in microscale gaps, and the breakdown voltage does not reach a minimum but continues to decrease as the gap separation decreases.

It is found that the Paschen theory predicts that the minimum breakdown voltage is about 300 V for atmospheric pressure air and also a very high breakdown voltage for microgaps. The breakdown voltage explained in equation (1.3) depends on the values of parameters such as Ap, Bp and $\gamma_{se}$. Thus, breakdown was considered impossible when dealing with voltage nearly 100V across microgaps. Various experiments shown that the glow appears even below the minimum voltage and

parameters predicted by Paschen law in the microgaps scale of various gases. A wide variety of experiments have been conducted on microscale breakdown over wide range of cathode materials, geometric configurations, gas atmospheres and gas pressure. In extreme conditions, such as vacuum or high pressure and long electron gaps, Paschen's law naturally fails as other physical mechanisms become important. Once the Paschen's law fails to explain the breakdown voltage for microscale gap size, series of studies are done starting from 1950. In 1955, Kisliuk introduce the theoretical implications of field emission playing an important role in breakdown in micron- and sub-micron-scale electrode separations. A correction need to be taken care of to explain the gas breakdown for all gap sizes by including the effect of field emission. At the first time, Torres and Dhariwal in 1999 [4] explains why the Paschen law fails to explain in microscale gap size by including the field-induce electron emission for the left branch Figure 1.4 when gap dimensions fall below 10m, with the left branch that continued to decrease as gap sizes decreases and now referred to as the modifying Paschen curve. The comparison between the experimental data by different researcher is shown in Figure 1.6 which is clearly shows that the breakdown voltage decreases with the decreases in gap sizes instead of increasing breakdown voltage for smaller gap sizes. The modified Paschen curve connects as bridge between the field emission induce breakdown at very small gaps to the traditional Paschen curve through a transitional plateau region in which both processes play a role in the breakdown. More recently D.B. Go *et.al.* explains the analytical model to describe the transition between these two situations. Researchers have considered various cathode materials, different types of gases including air, nitrogen, hydrogen, oxygen, carbon dioxide etc. in different pressures and gap sizes with similar conclusion. The large number of experimental datasets that supported the deviation from Paschen law led to the first qualitative description of the modified Paschen law which is shown schematically in Figure 1.5. The relation between the applied electric field and the number of field emitted electrons emitted per unit per unit time (in other words, the current density of field emitting electrons) is quantitatively described by the Fowler-Nordheim theory

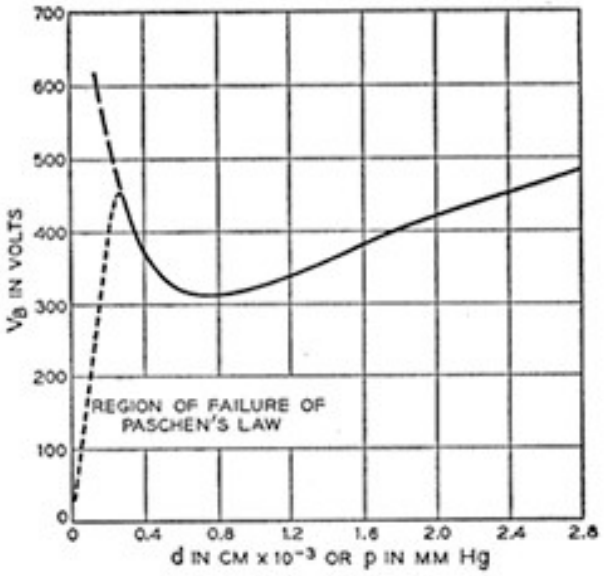


Figure 1.5: Schematic of the modified Panchen's curve plotting the breakdown voltage $V_b$ as a function of electrode gap spacing ($d$) or pressure($p$). [5]

[36], the total current density of electron is given by

$$J_{FN} = \frac{(A_{FN})\beta^2 E^2}{t^2(y)\phi} \exp(-\frac{B_{FN}\phi v(y)}{\beta E}) \tag{1.9}$$

where $A_{FN} = 1.54 \times 10^{-6} \frac{Ac^2}{J.s}$ and $B_{FN} = 6.83 \times 10^9 \frac{K_g C}{J.s}$ are Fowler-Nordheim constants, $\phi$ is the cathode work function, $\beta$ is the field enhancement factor, and E is the cathode electric field. v(y) and $t^2(y)$ were not the part of the Fowler-Nordheim equations and were corrections included in [37]. The correction term are given by,

$$v(y) = 0.95 - y^2 \tag{1.10}$$

$$t^2(y) = 1.1 \tag{1.11}$$

where $y = 3.79 \times 10^{-4} \sqrt{\frac{\beta E}{\phi}}$ is a function of electric field,work function of metal and the field enhancement factor.

The role of the field enhancement factor is worth discussing in greater detail. Field enhancement refers to the process by which a cathode experiences a higher electric field than what is applied. For example, in non-planar configurations (such

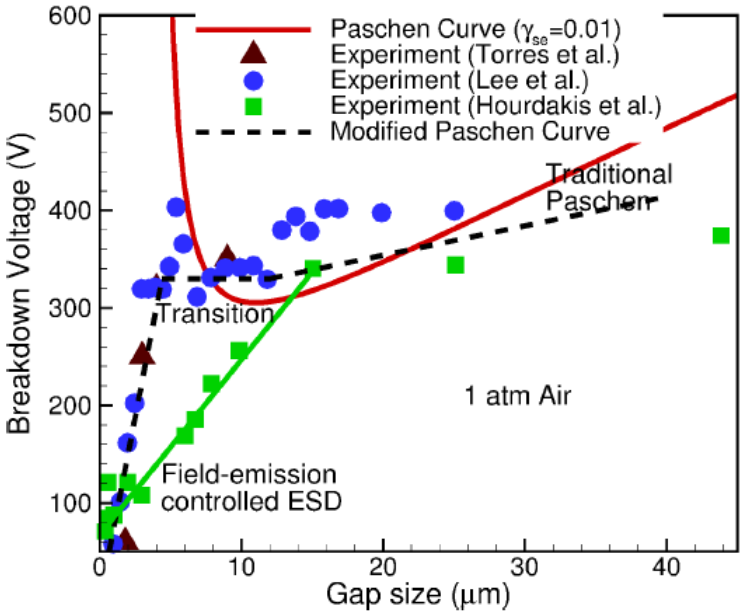


Figure 1.6: Modified Panchen curve and its experimental comparison [6]

as needle-plane), the geometry leads to a modification of the electric field experienced by the tip of the needle electrode. However, field enhancement can occur even in planar configurations (where both electrodes are planar) and is usually a result of the surface roughness that leads to local hotspots where the electric field is significantly higher than the applied electric field. In practice, experiments have observed a wide range of field enhancement factors ranging from as low as 5 to as high as 150 (for planar electrodes). In fact, if not for the influence of surface roughness and the resulting field enhancement, field emission will probably never play a role in microscale gas breakdown. As a result of field emission, an applied electric field of, say, 50 $V/\mu m$ can be enhanced to values as high as 5000 $V/\mu m$ (corresponding to a field enhancement factor $\beta$ of 100). Such a high electric field is sufficiently to lead extremely large values of Fowler-Nordheim current density when used in the above equation. During the last few years, traditional Townsend breakdown criterion resulting in the Paschen law has been modified to include the effect of field emission thereby leading to several forms of what is now commonly referred to as the modified Paschen law.

Specifically, this dissertation work trying to formulate predictive device-level

models that can describe the pre-ignition, ignition, and post-ignition characteristics of field emission-assisted microdischarges using field emission of electron. The device-level models that we have developed with more detailed simulations is compared with the different set of independent experimental datasets including different gases like carbon dioxide, hydrogen and dry air. It is worth reiterating the importance of device-level models in spite of the ability to perform detailed simulations. The primary advantage of such simplified models is the ability to obtain results in a short duration when compared to more accurate simulations that require several hours of runtime. Therefore, while detailed simulations are extremely crucial to obtain a better understanding of the microplasma device, device-level models are very useful to answer design-related questions including current vs voltage characteristics of the device. For example, most microelectromechanical systems (MEMS) involve the application of moderate voltages across gap sizes that are smaller than 5 m. It is imperative to determine the breakdown/ignition voltage of this gap to ensure that the applied voltage does not lead to plasma ignition and therefore device failure.[38, 39] The field enhancement factor is the key factor that plays an important role in the microscale gap sizes. It depends on the surface roughness of the materials [40, 26, 41]. The sharpness of the surface of materials loose more electron due to action of points thereby playing important role in microscale gas breakdown as field enhancement factor depends on the roughness of the material. In practice, experiments have observed a wide range of field enhancement factors ranging from as low as 5 to as high as 150 (for planar electrodes). In fact, if not for the influence of surface roughness and the resulting field enhancement, field emission will probably never play a role in microscale gas breakdown. As a result of field emission, an applied electric field of, say, 50 V/m can be enhanced to values as high as 5000 V/m (corresponding to a field enhancement factor, $\beta$, of 100). Various experiments have been done to determine the breakdown voltage of microgaps for various configurations. During the last few years, traditional Townsend breakdown criterion resulting in the Paschen law has been modified to include the effect of field emission thereby leading to several forms of what is now commonly referred to as the modified Paschen law. Kisliuk

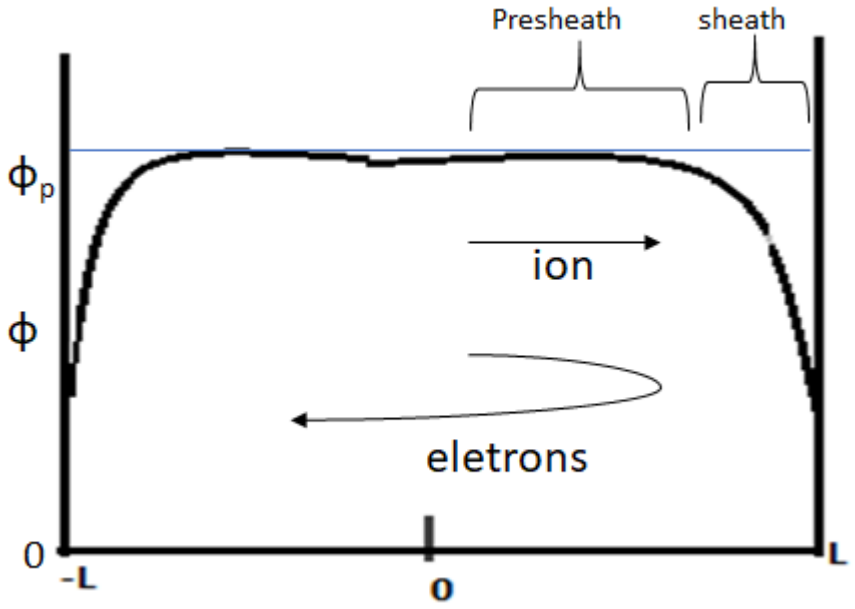


Figure 1.7: Formation of presheath and sheath region for plasma between planner walls

[42] and Germer [43] provided some evidences for the deviation of Paschen law in the earlier time and later Torres and Dhariwal [4] performed experiments to characterize breakdown in air for gap sizes varying from 500nm to 25nm concluding the results which is significantly different from those predicted by Paschen law. Radmilovic-Radjenovic et.al.[44, 45, 46] explains the modified Paschan law including field emission with series of numerical simulations using Particle-in-cell/ Monte Carlo Collisions (PIC/MCC) method. They have shown that the field emission is not significant for gap sizes grater than about 5 m.

## 1.9 Sheath Model

At the edge of the bounded plasma, a potential exists to contain the more mobile charged species. This allows the flow of positive and negative carriers to the wall to be balanced. In normal situation, the number of electrons and positive ions are equal. But as electrons are far mobile compare to positive ions there by creating an interface between the plasma and the cathode wall. This interface

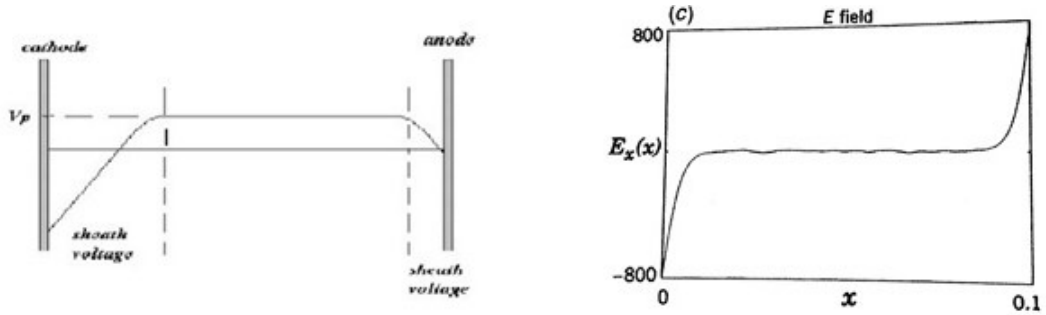


Figure 1.8: Potential and electric field curve after electron are lost

between the plasma (Quasineutral region) and the wall is called a sheath. Sheath is a thin positively charged region. The sheath has its particular importance in plasma physics because it determines the flow of heat that can cause damage. The sheath also determines the flow of ions that is used for ion implantation and other surface treatments. Electrons-ion pairs are assumed to be created homogeneously by ionization and current of ions to be the wall must have the value that maintains the density in the steady state because the assumption is made as the electron and ions arrive at the wall at equal rates which is possible for positive plasma potential as shown in the Figure 1.7 but the potential profile has steep gradient in the wall sheath but there exist the presheath region from the plasma mid plane to the sheath region which accelerates ions towards the wall.

The energy in the weak plasma is generally heating of the electrons by the source, while the ions are at near equilibrium with the background gas. The electron temperature is then typically of few volts, while the ions are cold.For $T_e \gg T_i$ which means $\sqrt{\frac{KT_e}{M_e}} \gg \sqrt{\frac{kT_i}{M_i}}$ and hence electrons starts losing at a higher rate which causes $n_e < n_i$ near the wall as shown in the Figure 1.7. The electron density would than decay with the order of a Debye length $\lambda_{De}$, to shield the electron from the wall. So, at the beginning $\phi = 0$ and E=0 but after electron are lost we see the negative potential. The electric field profile after being electron are lost at the wall is shown in the Figure 1.8.

The main focus of this task is to have better understanding about sheath model in plasma and its design in the context of field emission assisted microplasma. Plasma discharge in microscale have contributed to a new direction in plasma science and engineering during last decades with various applications in electronics [38, 39], biomedicine [47, 48], nanomaterial synthesis lighting [20], material surface processing etc. Many experimental work has been done using different cathode along with carbon nanotube (CNT) [49].

Different researchers purposed different type of sheath models. Recently Venkattraman *et. al.* [50] developed the sheath model considering with constant ionization coefficient for each gaps size in the uniform electric field and explained the sheath characteristics of microscale plasma. Microscale ionization coefficient ($\alpha$) also depends with the electric filed and this should be considered while explaining sheath model. Previously purposed sheath models are also using in linear electric field which couldn't explain the details for non-linear electric field. In this regards this dissertation explained clearly the consequence of effect of microscale ionization coefficient, present the new model called non-linear sheath model in the uniform electric field and compare its results with the existing linear sheath model and PIC-MCC data and validate the result. The discrepancies of linear sheath model are properly addressed. With the help of non-linear sheath model, other researcher will get the idea about the current voltage characteristics without actually doing long mathematical calculations. The device model presented here in this dissertation is small and easy to use in order to various plasma discharges technologies.

## 1.10 Research goals and objective

The major goals of this dissertation is to develop computational framework based on particle-in-cell with Monte Carlo collision (PIC-MCC) methods and to study the sheath characteristics of microscale plasma using current voltage characteristic of plasma which is useful for many microscale plasma devices like MEMS. We are using PIC-MCC simulation along with METHES simulation for,

- Enhancing the predictive capability of modified Paschen curve models for direct current field emission assisted (FEA) microdischarges.
- Formulating the model using METHES for ionization coefficient for different gases and compare the results with their experimental data.
- Formulating sheath models to study current vs voltage characteristics for FEA microplasma devices.

In order to achieve these goals the following are the specific objectives that will drive the research towards the final goals.

- Using existing 1D PIC/MCC code XPDP1 [51] to calculate the current density, electric field, ionization coefficient etc for electron and ions in plasma.
- Perform the data obtained from PIC/MCC numerical experiments to obtain the microscale ionization coefficient for gases such as argon, nitrogen, helium, hydrogen, carbon dioxide and some hydrocarbon and their mixture with argon and sulfur.
- Implement the empirical formula for the field enhancement factor ($\beta$) and explain the capability of model to predict the breakdown for the given physical parameter.
- Perform one-dimensional PIC/MCC simulation in a argon gas electrode and compare the data with the non linear sheath model.
- Perform one-dimensional PIC/MCC numerical experiments to obtain ion-enhancement coefficient as a function of gap size, electric field and field enhancement factor.

## 1.11 Scope of Dissertation

Microscale breakdown voltage is the key parameter affecting the ionization of plasma and hence the field enhancement factor ($\beta$). So in this regards, understanding about the ionization coefficient and field enhancement factor is one of the key focus in this work. While $\alpha$ represents the volume process in a discharge, the most important surface process in microdischarge is field emission which is characterized by the field enhancement factor $\beta$. Calculation of ionization coefficients for various gases will give the broad view of understanding plasma behavior and understanding about the field enhancement factor helps formulate the predictive capability of modifying Paschen curve in presence field emission effect on microplsma and hence predict the breakdown voltage. While $\alpha$ represents the volume process in a discharge, the most important surface process in microdischarge is field emission which is characterized by the field enhancement factor $\beta$. The state-of-the-art modified Paschen law still requires the field enhancement factor as an input parameter in order to predict breakdown voltage and unlike many other operating parameters such as pressure, gas composition, gap size, cathode material etc., there is no easy way to determine the value of $\beta$. As a result, analyses performed still use the modified Paschen law models as a tool to explain existing experimental datasets for breakdown in microgaps as opposed to a tool for predicting breakdown voltages in microgaps. Choosing the right value of $\beta$ is extremely sensitive. Particle simulations as a predictive tool to model the effect of field emission/evaporation in MEMS devices. In spite of the recent development of well-established models to describe the modified Paschen curve, there are still several fundamental questions that are unanswered.

In this regards, the chapter 2 provides the necessary theory, background and computational tools used while gathering information of present work. Chapter 3 discuss about microscale ionization coefficient ($\alpha$) for different gases and their mixtures obtained from METHES and compare the data with the existing data from the experiment. This chapter also explains the role of uniform and non-uniform electric field in the microscale ionization coefficient. Chapter 3 also provides the

importance of field enhancement factor ($\beta$) for the predictive capability of modified Paschen's law and explain the way of choosing $\beta$ while calculating breakdown voltage in the formula. Chapter 4 will talk about non-linear sheath model in the uniformly varying electric field and explains sheath characteristics of the microplasmas and compare the result of purposed model with PIC results as well as previously reported data for linear sheath model. Chapter 5 presents the summary of results and future works followed by the conclusion and references at the end of the thesis.

# Chapter 2

# Theory, Background and Computational Tools

## 2.1 Non-linear Sheath Model

The purposed work is to develop theoretical framework using similar condition used by experiments that can better explain about the sheath model using field emission concept in reference with the exiting linear sheath model by Venkattraman [6] developed a sheath model including field emission that is giving some clear understanding about sheath model in the linearly varying electric filed. The propose of this present work is to compare to the cathode fall model and improve the model using non-linearly varying electric field. The equations are derived as follows: The Poisson's equation in one dimension can be written as,

$$\frac{dE}{dx} = -\frac{\rho}{\epsilon_o} \tag{2.1}$$

where $E$ is the electric field, $\rho$ is the charge density. The negative sign arrises due to the electric field pointing in the negative x-direction. The electric field at cathode is given by,

$$E(x) = E_c \left(1 - \frac{x}{d}\right)^{\frac{1}{n}} \tag{2.2}$$

where $E_c$ is the cathode electric field and x is the distance from the cathode and d is the length of the cathode fall. $n$ represent the different values to see the behavior

of sheath in a plasma in the presences of different values of linearly varying electric field. This proposed model tends to move to linear sheath model for $n = 1$. Choosing to small value of $n$ tends the results towards the existing model and choosing higher values of $n$ causes rapid decrease electric field. Specifically n=1, 1.25 and 1.5 are taken in this dissertation and compare the results in each cases.

Equation 2.2 shows that the electric field decreases in the vicinity of anode and increases in the vicinity of cathode. Taking derivative of above equation,

$$\frac{dE}{dx} = -\frac{E_c}{nd}\left(1 - \frac{x}{d}\right)^{\frac{1}{n}-1} \tag{2.3}$$

using equation (2.1) and equation (2.2) we will get

$$\frac{E_c}{d} = \frac{\rho n\left(1 - \frac{x}{d}\right)^{\frac{1}{n}-1}}{\epsilon_o} \tag{2.4}$$

solving for the total potential we will get,

$$V_c = \int_0^{d_c} E(x)dx = \int_0^{d_c} E_c\left(1 - \frac{x}{d}\right)^{\frac{1}{n}} dx = \frac{nE_c d_c}{n+1} \tag{2.5}$$

and the charge density is written as,

$$\rho^*(x) = \epsilon_o \frac{dE}{dx} = -\frac{\epsilon_o E_c}{nd}\left(1 - \frac{x}{d}\right)^{\frac{1}{n}-1} = \rho_c\left(1 - \frac{x}{d}\right)^{\frac{1}{n}-1} \tag{2.6}$$

where $\rho_c$ is constant. Thus current density can be written as,

$$J_c^+ = \frac{j_{FN}(E_c)(e^{\alpha d} - 1)}{1 - \gamma_{se}(e^{\alpha d} - 1)} \tag{2.7}$$

where $J_{FN}$ is called Fowler-Nordheim current density and is given by (1.9), $\gamma_{se}$ is the secondary ionization coefficient and $\alpha$ is called microscale ionization coefficient and is defined as,

$$\alpha = Cpexp\left(-D\sqrt{\frac{p}{E}}\right) \tag{2.8}$$

where C and D are gas dependent constants available for inert gas and tabulated in Raizer [3]

So,

$$j_c^+ = \frac{j_{FN}(E_c)e^{\alpha d} - j_{FN}(E_c)}{1 - \gamma_{se}(e^{\alpha d} - 1)} \tag{2.9}$$

$$J_{total} = \frac{j_{FN}(E_c)e^{\alpha d}}{1 - \gamma_{se}(e^{\alpha d} - 1)} \tag{2.10}$$

and

$$\frac{J_{total}}{j_{FN}(E_c)} = \frac{e^{\alpha d}}{1 - \gamma_{se}(e^{\alpha d} - 1)} \tag{2.11}$$

The ion drift velocity at cathode depends on the background gas and the local electric field is obtained as,

$$V_{dc}^+ = \sqrt{\frac{2eKTE_c}{\pi mp\sigma_{cE}}} \tag{2.12}$$

where $\sigma_{cE}$ is the charge exchange cross section. The charge exchange cross section typically depends on the energy and drift velocity obtained should be consistent with the ion energy at which $\sigma_{cE}$ is computed thereby requiring the above equation to be solved numerically. In this work the model used the charge exchange cross section as in the PIC/MCC simulation used in Poisson equation as,

$$\frac{E_c V_{dc}^+ \epsilon_o}{ndj_c^+} - 1 = 0 \tag{2.13}$$

where $d = 2V/E_c$ and $j_c^+$ being the ion current density at the cathode, $E_c$ is the cathode electric field and $\alpha$ is the ionization coefficient in the sheath region. All quantities in equation (2.13) are expressed in terms of $E_c$ and hence this equation can be used to solve for$E_c$ for given Potential (V). Once $E_c$ is obtained, the total current density is computed and is then used to determine current-voltage characteristics of these microplasmas.

## 2.2 PIC-MCC Method

It is the technique to solve certain class of partial differential equations considering individual particles in the Lagrangian form are tracked in continuous phase space where moments of the distribution such as densities and currents are computed simultaneously on Eulerain mesh points. This method is very effective in

plasma physics for the trajectories of charged particles in self-consistent electromagnetic field computed on a fixed mesh. This is particularly important on space propulsion [52], plasma processing of materials [53], plasma aerodynamics [54], plasma medicine [12] and plasma display panels[55]. Kinetic model and fluid model are the two types of the plasma simulations and in both types of model continuity and momentum equations are used for both ions and electrons fluids to get the velocity distribution of electrons and ions. Most particularly, in this work we are using kinetic model to simulate our results as this model can be solved using traditional numerical methods by using Boltzmann equation in six-dimensional phase space.

PIC/MCC methods considers all charged electrons and positively or negatively charged ions as particles.These step by step process for the PIC/MCC is briefly summarized in the Figure 2.1. Each computational particles are considered as real particle and are moved in the electric field by updating position and velocity with Leap-frog algorithm [56] typically used in most PIC/MCC codes. The particles in each cell is then used to compute the corresponding charge density distribution to the nodes associated with the cell. Thus obtain charge density are than used to obtain the self-consistent model electric field values by solving Poisson equation.

$$\nabla^2\phi = -\frac{\rho}{\epsilon} \tag{2.14}$$

Electric fields thus obtained from the above equation are used to update the velocity of the particles and the simulation repeated until the steady state is reached. Since PIC method doesn't account for the collisions of electrons and ions with the background neutral gas, the PIC/MCC method has been used to include the collision and are computed using fundamental cross-section data as a function of collision energy where the charged particles are updated depending on the nature of collision.

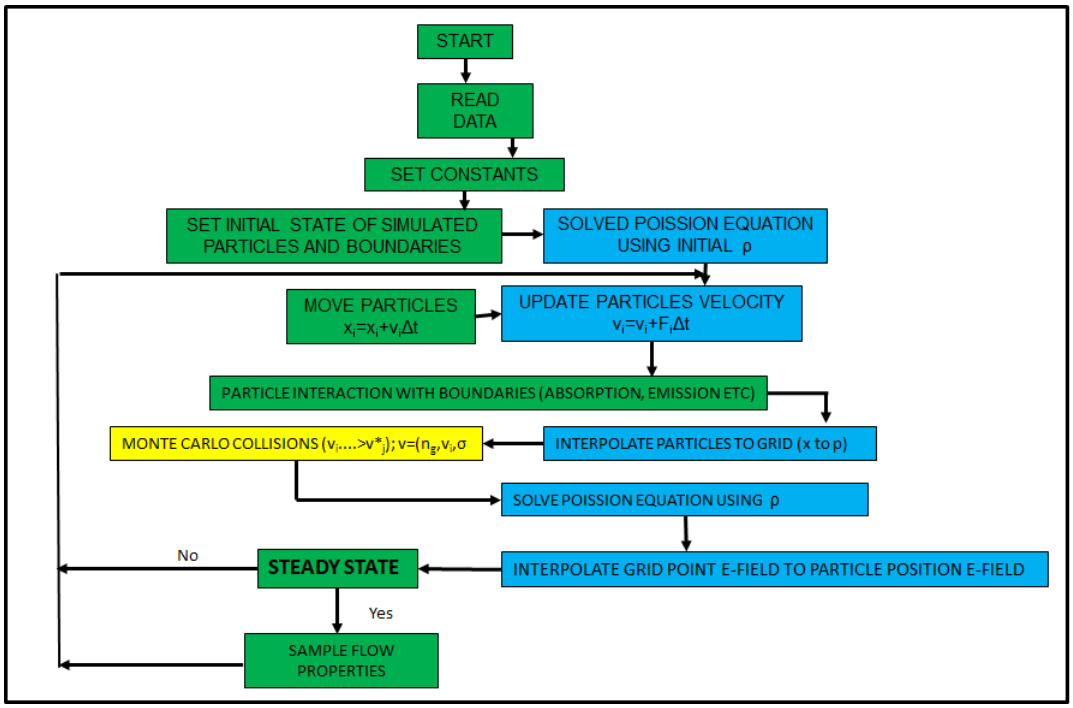


Figure 2.1: Schematic diagram involved in PIC/MCC technique

## 2.3 Zero-Dimensional Monte Carlo Code

Monte Carlo code is a random sampling techniques to get the numerical results. It is mostly used for computer simulation to obtain approximate solutions to mathematical or physical problems especially in terms of a range of values each of which has a calculated probability of being the solution. It was developed by using the simulation of some known problems and using probabilistic analog. The modern version of code was designed by Stanislaw Ulam in late 1940 while working in nuclear weapons project in Los Alamos National Laboratory. In the case of gas in the applied electric field, electron transport is important where the electrons more likely undergo collision and need to be track by using Monte Carlo simulation. PIC/MCC uses the null collision method. Null collision method [57] requires the specification of a number of collision process between a particle species and the background gas whose number density is given and could be uniform or have a spatial dependence. The collision cross-section as a function of the collision energies are also specified for the various collision processes. The collision frequency

is defined as

$$\tau_m = \frac{\lambda_m}{v} \tag{2.15}$$

$$\nu' = n_{max}(\sigma v_r)_{max} \tag{2.16}$$

where $n_{max}$ is the maximum gas number density, $(v_r)$ is the relative velocity between the two colliding particles which is approximately equal to the velocity of the ion itself and $\sigma$ is called the total collision cross section.

Monte Carlo method have been used in PIC codes to model collisional plasmas in which the ion motion is determined by mobility. kuhn *et. al.* [58] and Jelic *et. al.* [59] have compared the quantities from PIC and fluid sheath models to validate their results.

## 2.4 BOLSIG+

Transport coefficients and rate coefficients the key parameters to solve the fluid models go gas discharges that depend on the electron energy distribution function. Such coefficients are usually calculated from collision cross-section data by solving the electron Boltzmann equation (BE). The continuity equation, momentum equation as well as energy equation needs transport of electrons and ions.[60] The computer generated BE solver that can solve these types of problems is called BOBLSIG+. It is a free and user friendly computer program for the numerical solution in order to solve Boltzmann equation for electron in weakly ionized gases in uniform electric fields usually occurs in Swarm model and in various types of discharges and collisional low temperature plasma. At the first time the software was lunched and available to public in 2005. A swarm model is a fluid model that assigns a mean temperature to electrons and monitors their time evolution through the use of various collision frequencies and reaction rates in conservations equations. [61]. The main use of the BOLSIG+ is to obtain electron transport coefficient and collision rate coefficients from more fundamental cross section data which can than be used as input for fluid models.

# Chapter 3

# Microscale Ionization Coefficient and Field Enhancement Factor in Modified Paschen curve models

## 3.1 Microscale ionization of various gases

This section of this dissertation will focus on the ionization process on various gases and the careful comparison of ionization coefficient of different gases with the model that we have developed using METHES. METHES is a zero dimensional Monte Carlo collision code for the simulation of electron transport in presence of uniform electric field for the low temperature plasmas. For the given input as (E/N) where E is the electric field and N is the number density of gas, the program provides the transport coefficients, reaction rates and the electron energy distribution function. This program also supports electron scattering cross section files from the Open-access Plasma Data Exchange Project LXCat. This program is firstly designed by M. Rabie and C.M. Franck in The Power System and High Voltage Laboratories, ETH Zurich, Switzerland [62].

Numerous studies of ionization coefficient are done during last 40 years using different experiments for many different gases. There are less number of theoretical simulations have been done. Some of the simulation are done without using the

field emission effect which cannot predict the correct result in the microscale gap size. Deviation from Paschan law in small micro gaps are studied widely and explained with reason in different journal articles. The One possible mechanism responsible for deviations of Paschen law model in small gap sizes is the increase of the secondary electron emission yield due to the quantum tunneling of electrons from the metal electrodes to the gas phase as high electric fields undergoes within a small gaps and potential barrier seen by the electrons in the cathode as an ion approaches lead to the onset of ion-enhanced field emissions. The equation to determine the ionization coefficient for different gases is given by Equation (1.7) and the values of constants are shown in the Figure 1.3 from Raizer.

Most of the experiments are done with the low electric field and hence the ionization coefficient for the higher electric field is still in the process of finding. Thus to understand the ionization process for different gases for the wide range of electric field, we developed the new model using METHES and compare the best known experimental data in order to validate our results and predicts the values of $\alpha$ for higher electric field. We extracted the experimental data for Carbon dioxide, Ethylene, Helium, Hydrogen, Methane, Methane-argon mixture and Nitrogen from the different journals articles. Most of the data we found with low electric field values so we narrow down the range of electric field to match the the model is predicting the right result for the given electric field.

Electron transport in a gas with uniform electric field is always useful for various applications. One should be clear that how the electrons behaves within the electric field since electron are colliding with the neighboring other electrons in and atom or molecules. Elastic collision commonly occur while they are interacting with the electric field. Sometime if the electrons doesn't have sufficient energy, the atom or molecules used as dielectric with in the electrode will only be excited if electron knocked out the other electron to the higher energy level. If the knocking electron has sufficient energy to knock out the electron from the gas then the extra free electron is produced during the reaction. The simple representative examples for argon gas in an electric field is explain as,

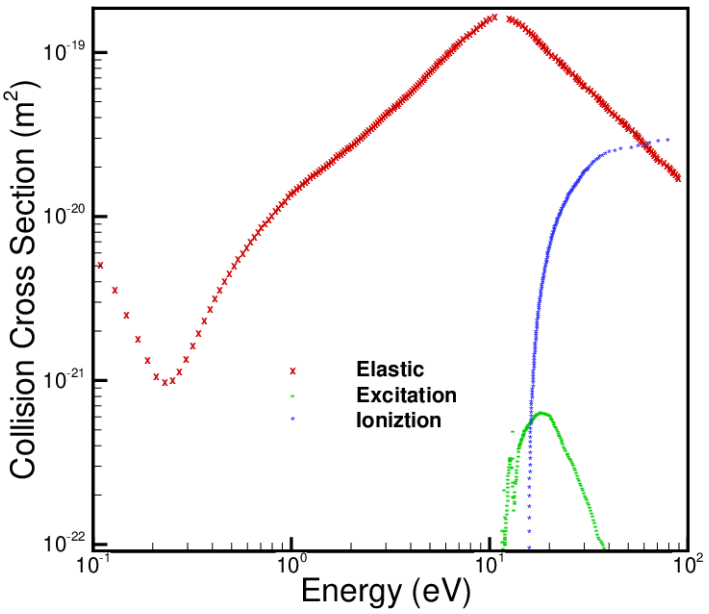


Figure 3.1: Electron-neutral cross-section for elastic, excitation and ionization collisions in an Argon electric discharge

$$e^- + Ar \rightarrow e^- + Ar \text{ (Elastic )}$$
$$e^- + Ar \rightarrow e^- + Ar^* \text{ (Excitation )}$$
$$e^- + Ar \rightarrow e^- + e^- + Ar^+ \text{ (Ionization )}$$

where $e^-$ is for electron, Ar is for Argon gas, $Ar^*$ is for excited Argon gas and $Ar^+$ is for Argon ion. The collision cross section for argon for different process is shown in the Figure 3.1

If the gas has more than two atoms taking part in the collision then there will be number of ways they react in the collision . For example, The steps involved in the Sulfur hexafluoride ($SF_6$) is shown as below and plotted as shown in the Figure 3.2

$$e^- + SF_6 \rightarrow SF_4^- + F_2, \text{ Attachment}$$
$$e^- + SF_6 \rightarrow SF_5^- + F, \text{ Attachment}$$
$$e^- + SF_6 \rightarrow SF_6^-, \text{ Attachment}$$
$$e^- + SF_6 \rightarrow e^- + SF_6, \text{ Effective}$$
$$e^- + SF_6 \rightarrow e^- + SF_6(0.095eV), \text{ Excitation}$$

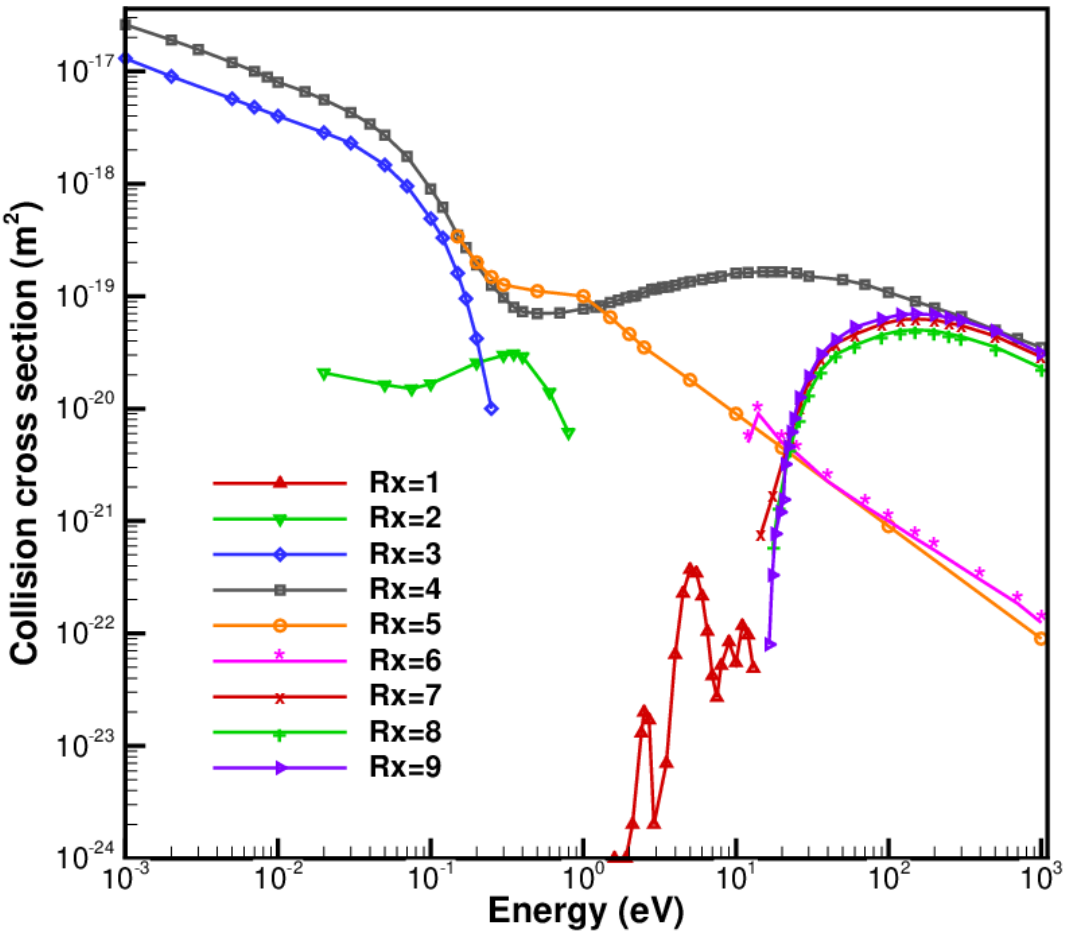


Figure 3.2: Electron-neutral cross-section for elastic, excitation and ionization collisions in an sulfur hexafluoride electric discharge

$e^- + SF_6 \rightarrow e^- + SF_6(10.0eV)$, Excitation
$e^- + SF_6 \rightarrow e^- + SF_6(11.7eV)$, Excitation
$e^- + SF_6 \rightarrow e^- + SF_6(15.0eV)$, Excitation
$e^- + SF_6 \rightarrow e^- + e^- + SF6^+$, Ionization

Thus it is seen that the the ionization coefficient for different gas are different. It also depends on the pressure and temperature of the system. In this regards, the model can explain ionization coefficient for the wide range of uniform electric field.

### 3.1.1 Microscale ionization coefficient for Hydrogen

The simulation were performed for Hydrogen gas using the reference from the cross-section data for Hydrogen provided by LXcat modified the data using METHES. The database for Hydrogen has a larger number of collision processes considered when compared to argon. The experimental data and the model data for hydrogen gas is shown in the Figure 3.3. The experimental data and the METHES data are agree with each other for intermediate range of E/N. (100-1000 Td). For the lower values higher values of E/N $\alpha/N$ scattered from the model data.It is seen that the METHES data under predicting for Hydrogen gas compared to its experimental data. similar data were predicted by Loveless *et. al.* [63] in terms of breakdown voltage vs gap distance.

Following reaction took place during the ionization process of Hydrogen gas.

$e^- + H_2 \rightarrow e^- + H_2$, Effective

$e^- + H_2 \rightarrow e^- + H_2(j0-2)(0.044eV)$, Excitation

$e^- + H_2 \rightarrow e^- + H_2(j1-3)(0.073eV)$, Excitation

$e^- + H_2 \rightarrow e^- + H_2(V1)(0.516eV)$, Excitation

$e^- + H_2 \rightarrow e^- + H_2(V2)(1eV)$, Excitation

$e^- + H_2 \rightarrow e^- + H_2(V3)(1.5eV$, Excitation

$e^- + H_2 \rightarrow e^- + H_2(B3 \quad SIG)(8.9eV)$, Excitation

$e^- + H_2 \rightarrow e^- + H_2(B1 \quad SIG)(11.3eV)$, Excitation

$e^- + H_2 \rightarrow e^- + H_2(C3PI)(11.75eV)$, Excitation

$e^- + H_2 \rightarrow e^- + H_2(A3SIG)(11.8eV)$, Excitation

$e^- + H_2 \rightarrow e^- + H_2(C1PI)(12.4eV)$, Excitation

$e^- + H_2 \rightarrow e^- + H_2(G1SIG)(13.86eV)$, Excitation

$e^- + H_2 \rightarrow e^- + H(n=2)(15.0eV)$, Excitation

$e^- + H_2 \rightarrow e^- + H_2(RYDBERG-SUM)(15.2eV)$, Excitation

$e^- + H_2 \rightarrow e^- + H(n=3)(16.6eV)$, Excitation

$e^- + H_2 \rightarrow e^- + e^- + H_2^+$, Ionization

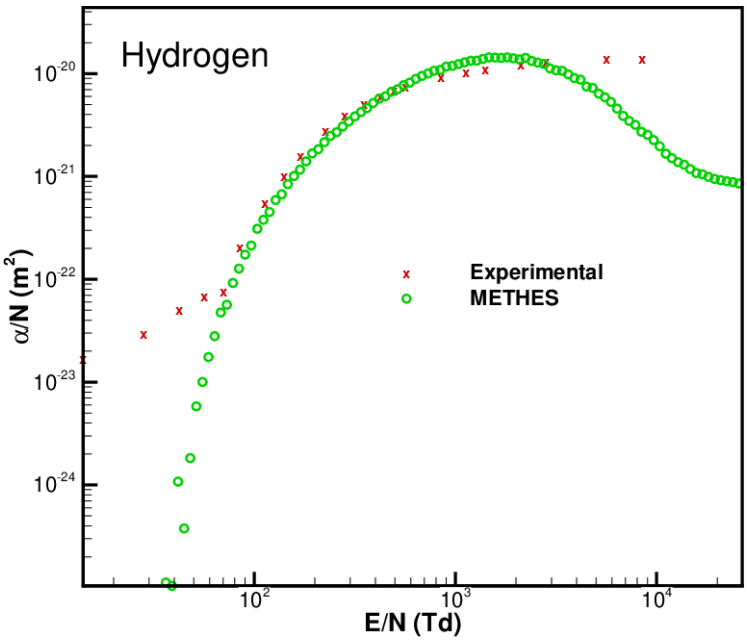


Figure 3.3: Comparison of the METHES values of $\alpha/N$ with the experimental result for Hydrogen.

### 3.1.2 Microscale ionization coefficient for Nitrogen

The simulation were performed for nitrogen which can be used as approximation for air. The experimental data and the data from the model are plotted and shown in the Figure 3.4. It is seen that both data are properly agree with each other. At the lower value of E/N, the experimental data for Nitrogen gas are also deviated from the model data as in case of hydrogen but for higher values of E/N experimental data agree well with the METHES data. The reactions takes place during the ionization process of Nitrogen is given in the Appendix A.

### 3.1.3 Microscale ionization coefficient for Helium

Most of the experiments are done using Helium gas for the understanding of ionization coefficient. Dutton *et. al.* [64] found that the spatial growth of pre-breakdown ionization coefficient values of E/N in the range from $2.24 \times 10^5$ to $11.2 \times 10^5$ Td. Compared to other gases, the experiments is done for helium for higher E/N. The experimental data set and model data for Helium is are plotted

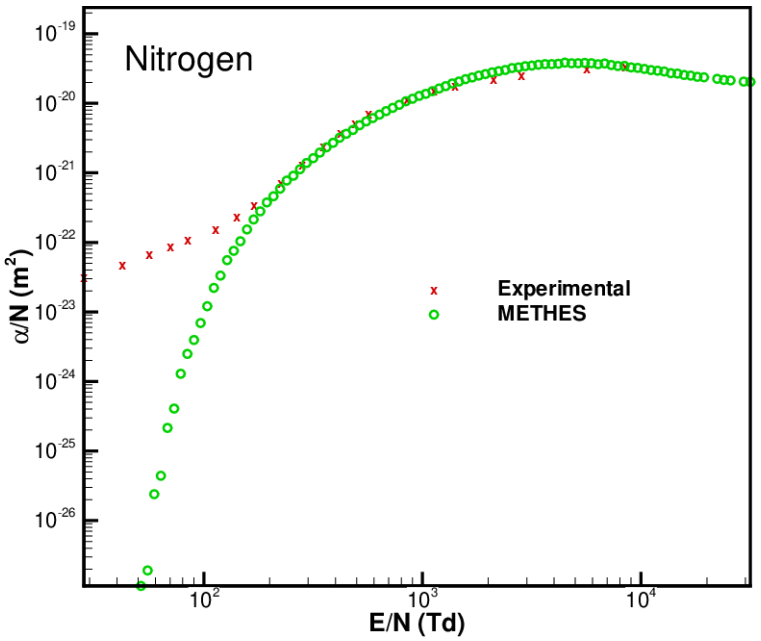


Figure 3.4: Comparison of the METHES values of $\alpha/N$ with the experimental result for Nitrogen.

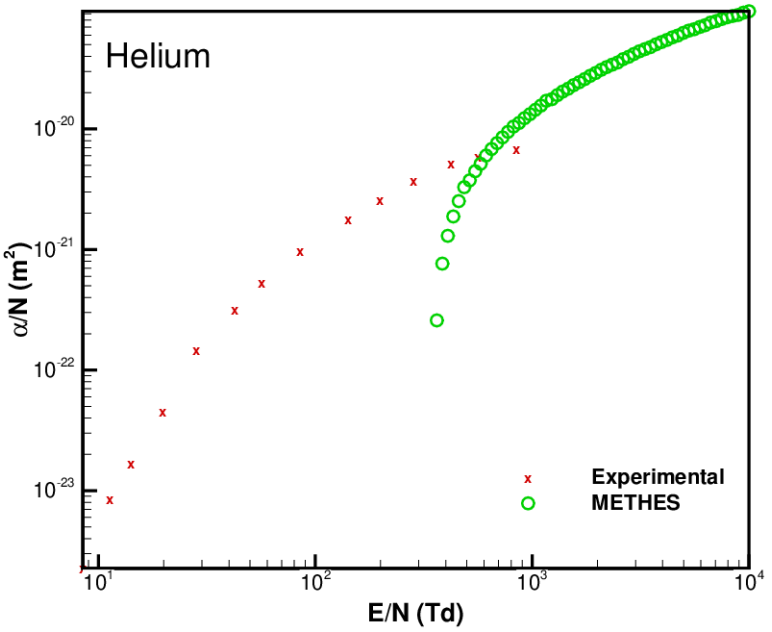


Figure 3.5: Comparison of the METHES values of $\alpha/N$ with the experimental result for Helium.

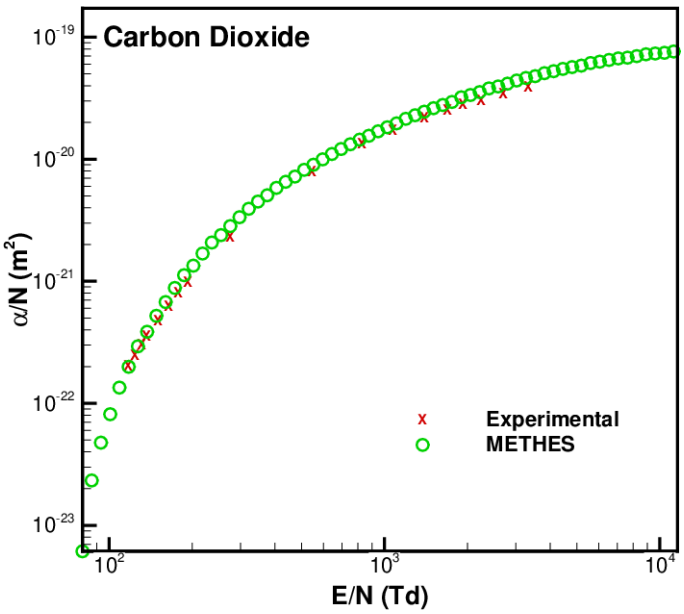


Figure 3.6: Comparison of the METHES values of $\alpha/N$ with the experimental result for Carbon Dioxide.

and shown in the Figure 3.5. Since the experimental data are only up to 1000 Td but the theoretical data are found after 950 Td. But they agree with each other for the 950 Td onwards. This is the beauty of the model that it can give $\alpha$ values for very high electric filed even it is not possible till this data by experiment. The reactions takes place during the ionization process of Nitrogen is given in the Appendix A.

### 3.1.4 Microscale ionization coefficient for Carbon Dioxide

In order to understand and validate the model a heavy gas carbon dioxide is taken and the data were compared with the experiment. It is found that the experiments are performed for Carbon dioxide the experiments for several thousand Townsend which makes us to compare our model and see its outcome for higher values of E/N. The experimental daa and model data for carbon dioxide the data are shown in the Figure 3.6. It is found that the experimental data and model data are are both agree to each other which shows that the model we have generated satisfies the previously published data even for higher Townsend. At the lower

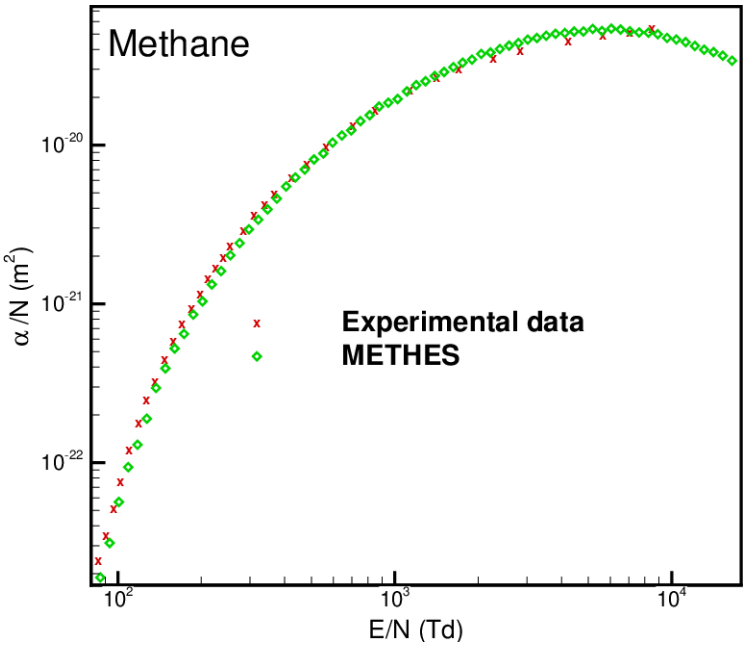


Figure 3.7: Comparison of the METHES values of $\alpha/N$ with the experimental result for Methane.

values of E/N the METHES data are well agree with the experimental data which was not seen in case of Hydrogen and Nitrogen. The reactions take place during the ionization process of Nitrogen is given in the Appendix A.

### 3.1.5 Microscale ionization coefficient for Methane and Ethylene and Propane

As carbon based materials are found excellent to work on low-voltage ionization [23], the demand is growing up day by day. Heylen *et.al.* [65] explained the experimental study of ionization coefficient and sparking voltages from methane to butane by considering the constant A and B in the Townsend ionization equation (1.7) with the limited pressure range from 0.5 - 20 Torr. Later the Townsend $\alpha$ and $\gamma$ are measured up to 400 Torr by the same researcher. Thus in order to see the validity of proposed model with the experimental data for Methane, Ethylene and Propane, the model was used and data were extracted to plot and compare the results.

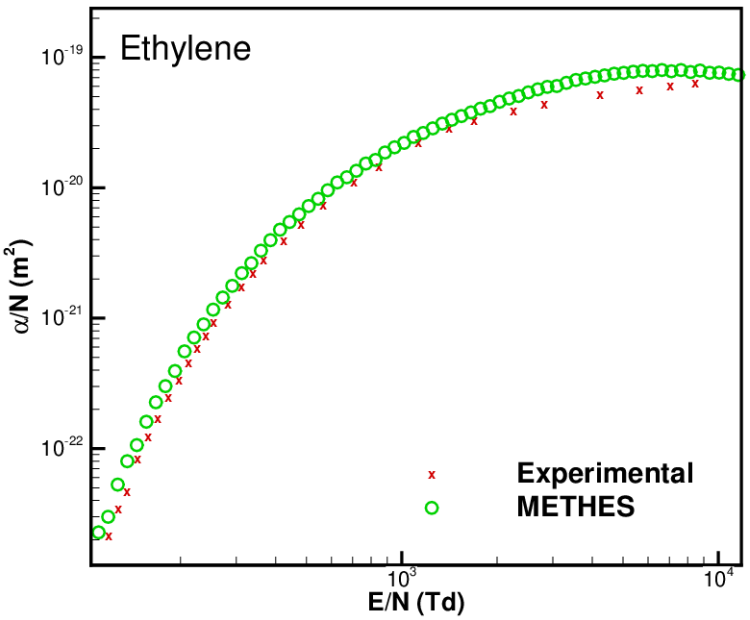


Figure 3.8: Comparison of the METHES values of $\alpha/N$ with the experimental result for ethylene.

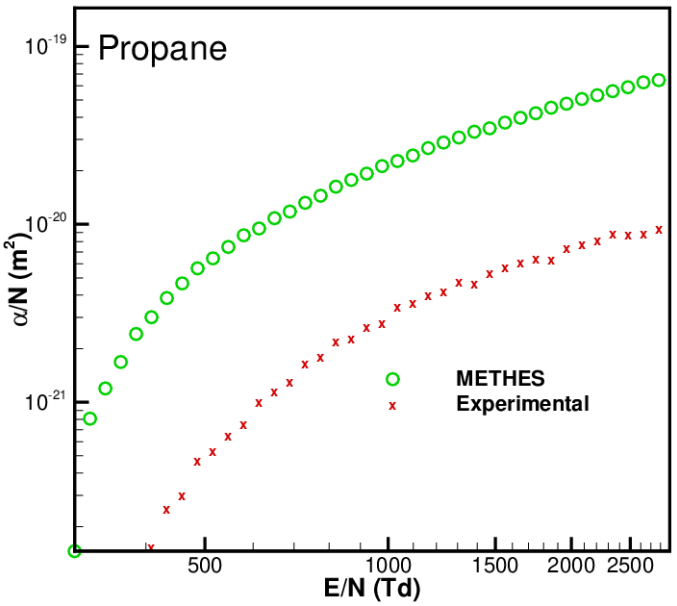


Figure 3.9: Comparison of the METHES values of $\alpha/N$ with the experimental result for Propane.

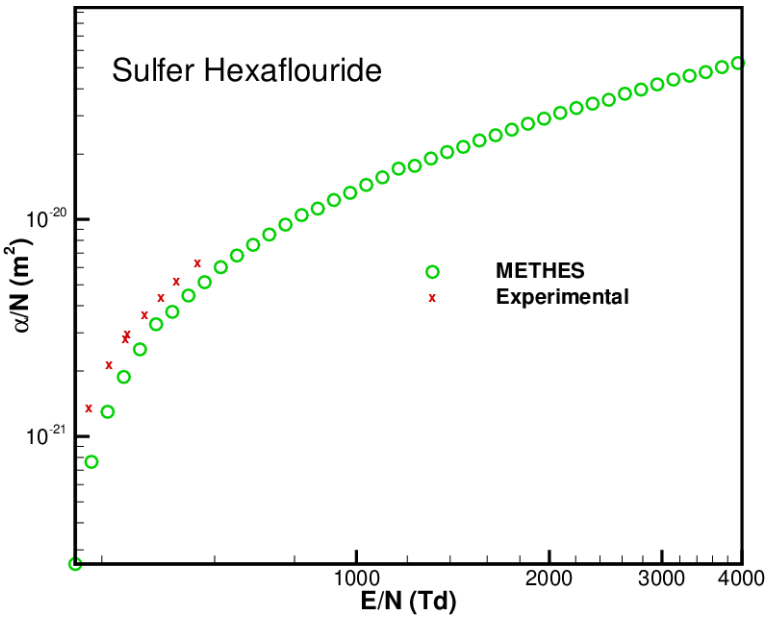


Figure 3.10: Comparison of the METHES values of $\alpha/N$ with the experimental result for Sulfur Hexaflouride.

The graph of experimental data and model data for Methane ($CH_4$) is shown in the Figure 3.7. It is found that the experimental data totally agree with the corresponding model data for all values of E/N. The graph for $\alpha/N$ vs E/N for Ethylene ($C_2H_4$) is shown in the Figure 3.8. Similarly Figure 3.9 shows graph for Propane gas. It is found from the Figure 3.9, the METHES data are off the experimental data but following the same pattern. It may be because of the experimental data are performed at low pressure and the METHES data are performed at higher pressure. The reactions takes place during the ionization process of Nitrogen is given in the Appendix A.

### 3.1.6 Microscale ionization coefficient for Sulfur Hexafluoride

Sulfur hexafluoride is one of many compounds of polyatomic molecules that have a dielectric strength higher than air or nitrogen. It has the another advantage that it may be used for higher gas pressures than most of the highly attaching gases

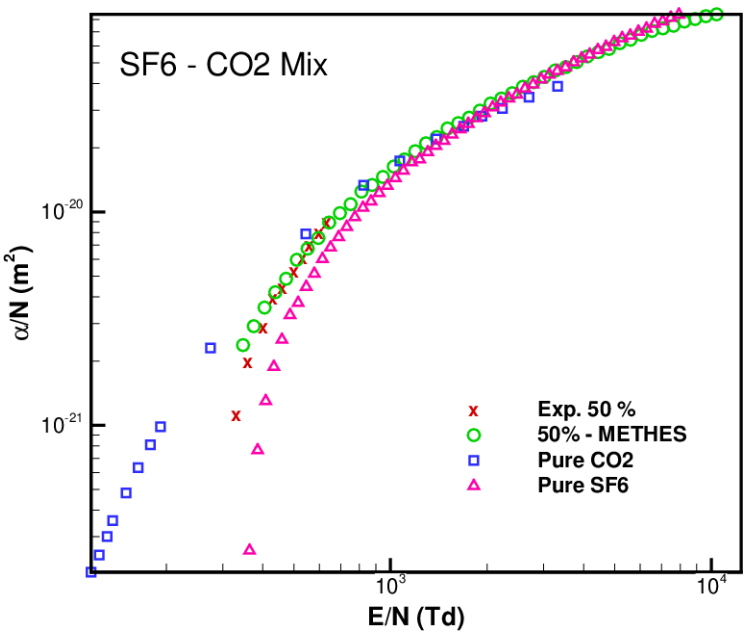


Figure 3.11: Comparison of the METHES values of $\alpha/N$ with the experimental result for mixture of Sulfur Hexafluoride and Carbon Dioxide .

because of its low critical temperature. In this context, $SF_6$ is given importance as a good dielectric in microscale breakdown. Wide varieties of experiments are done to get the ionization coefficient of $SF_6$ as a function of E/p. Bhalla *et. al.* has published their experimental data for ionization coefficient of $SF_6$ as a function of E/p [66].The graph of both experimental data and METHES data are plotted as shown in the Figure 3.10. The experimental data are slightly higher than the METHES data but they are following with the same pattern. It may be because of the experimental data of $SF_6$ were performed at very low pressure.

### 3.1.7 Microscale ionization coefficient in Mixture form

It is found from the study that the dielectric strength can be increased if we use materials in mixture form. If we use them in mixture form, it will contains more Polyatomic molecules with in the small gap size there by increasing the collision rate with in the electrode and hence increase the ionization process. Experimental study shows that the mixtures forms of materials are giving excellent results. The

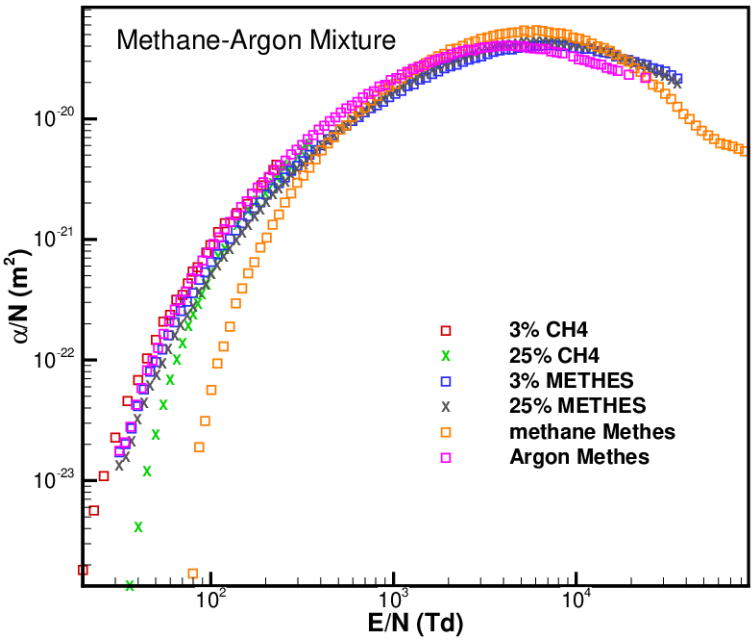


Figure 3.12: Comparison of the METHES values of $\alpha/N$ with the experimental result for Methane-Argon Mixture.

Sulfur hexafluoride ($SF_6$) and carbon dioxide ($CO_2$) gas were mixed in the ratio 1:1 in order to get the results from METHES. The experimental data of $SF_6$ and $CO_2$ are also also extracted keeping the ratio 1:1 in order to study ionization coefficient. The pure form of carbon dioxide and sulfur hexafluoride are also plotted in order to have the comparative study. The combined graph is shown in the Figure 3.11. It is found that from the Figure 3.11, the ionization coefficient for the mixture lies in between the ionization coefficient of their pure forms.

To study further about the ionization coefficient in the mixture form, Methane-Argon mixture is studied for various concentration. The experimental data for 3% Methane and 25% Methane in a Methane-Argon mixture were extracted and their corresponding METHES data are computed and plotted together and shown in the Figure 3.12. The individual METHES data for Methane and Argon are shown in the Figure 3.12. It is seen that the Methane METHES data were computed only up to 98 Td and Argon METHES data were computed for small value of E/N but the experimental data for the mixture provides the excellent result as we can see

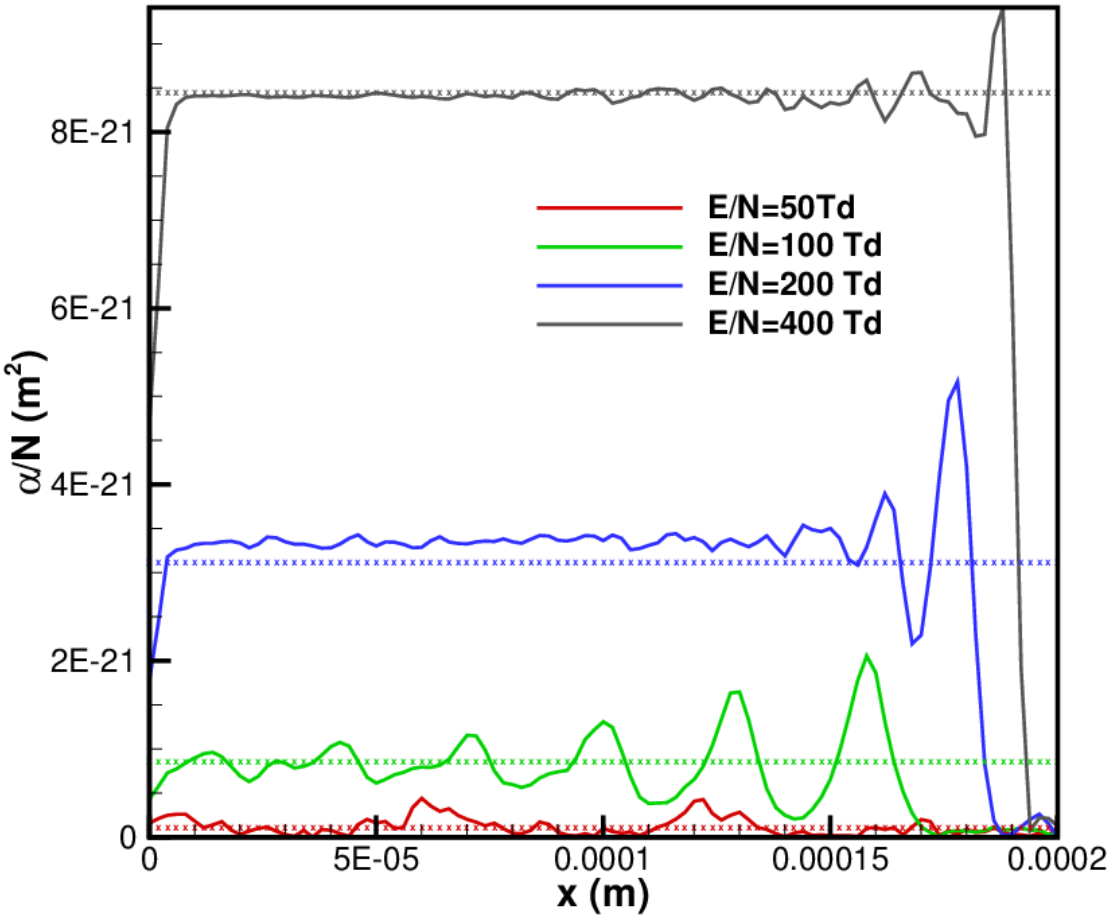


Figure 3.13: Comparison of the Ar-METHES data of $\alpha/N$ with PIC results in the uniform electric field for E/N=50 Td, 100 Td, 200 Td and 400 Td.

clearly from the Figure 3.12 that the mixture form gives the values up to nearly 1 Td.

## 3.2 Ionization coefficient of argon gas electrode in uniform electric field

In order to validate our the model, the data obtained for argon gas electrode from the PIC-MCC in the uniform electric field are considered. With the given data from PIC-MCC, $\alpha/N$ and E/N are calculated and plotted as shown in the solid

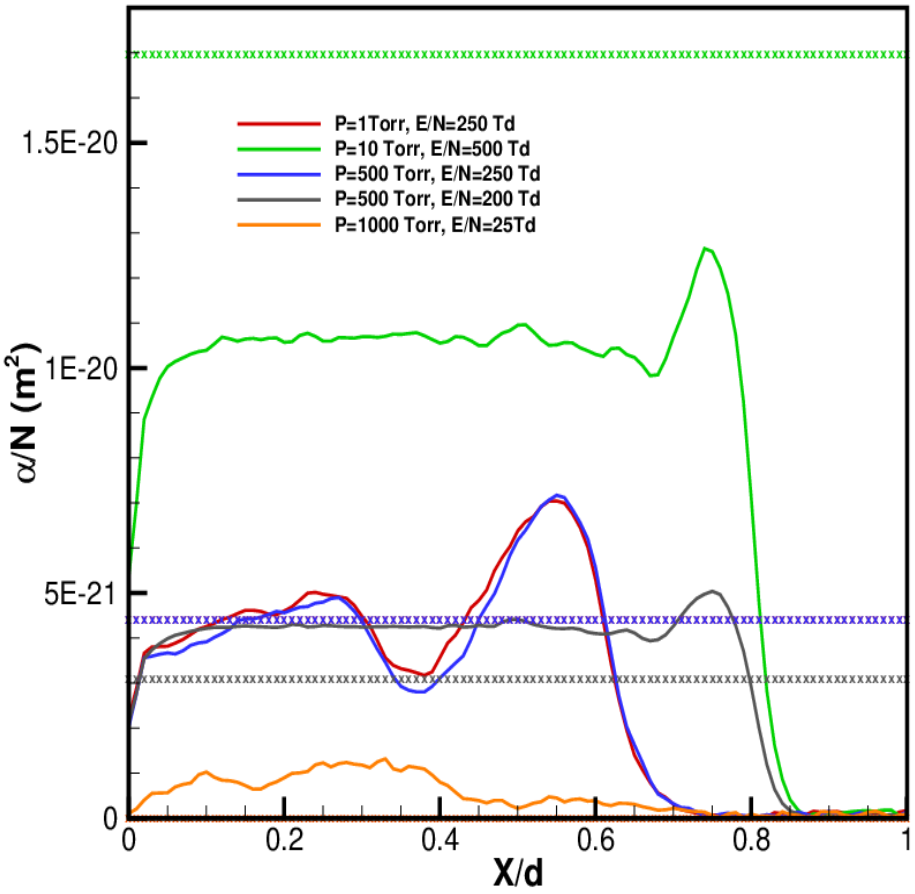


Figure 3.14: Comparison of the Ar-METHES data of $\alpha/N$ with PIC results in the uniform electric field for different pressure 1Torr, 10 Torr, 100 Torr, 500Torr and 1000Torr.

lines in the Figure 3.13. The $\alpha/N$ for argon gas obtained from the METHES for are $1.14\times10^{-}22m^2, 8.6\times10^{-}22m^2, 3.12\times10-^{21}m^2$ and $8.46\times10^{-21}m^2$ respectively for E/N= 50, 100, 200 and 400 Td. All the data were performed at pressure 124.21 Torr and gas temperature= 0.026 eV (301.6K). The $\alpha/N$ values obtained from the METHES are shown as a dotted lines in the Figure 3.13. It is seen from the graph that the data are properly matching with the PIC data for their respective E/N values. The oscillation in the PIC result is seen for smaller values of E/N is due the lower value of ionization coefficient. The oscillation is more smoother for the 200 Td and 400 Td.

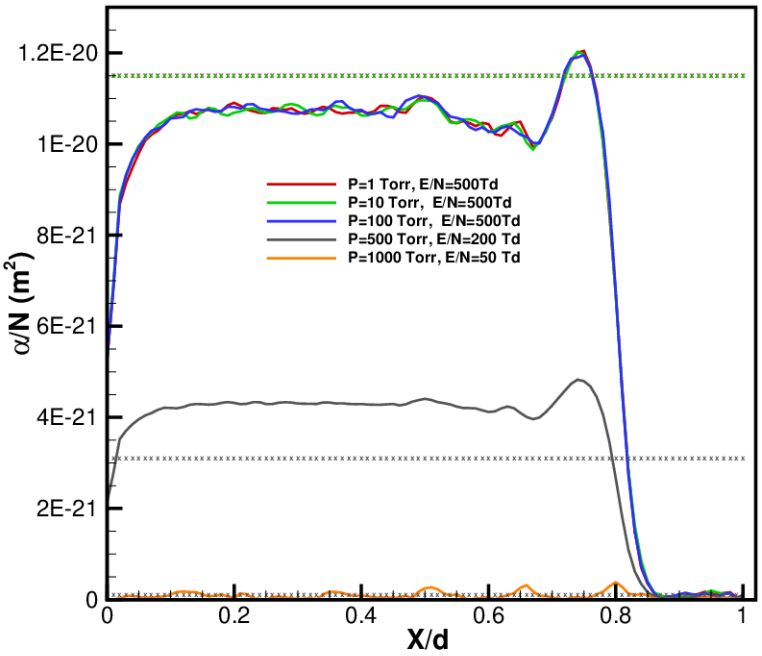


Figure 3.15: Comparison of the Ar-METHES data of $\alpha/N$ with PIC results in the uniform electric field for different pressure 1Torr, 10 Torr, 100 Torr, 500Torr and 1000Torr

Another data from the PIC-MCC in the uniform electric field is also taken for different pressure. $\alpha/N$ and E/N are also calculated and plotted as shown in the Figure 3.14. The experimental values for E/N =25 Td, 200 Td, 250 Td and 500 Td are obtained from the argon METHES plot and found as $1.9 \times 10^{-23} m^2$ , $3.12 \times 10^{-21} m^2$ , $4.41 \times 10^{-21} m^2$ and $1.08 \times 10^{-20} m^2$ respectively. The data for 250 Torr are in the same pattern but they are not properly lie on same line because the data for 1 Torr was taken for potential difference of 40V with gap size $5 \times 10^{-3} m$ but the data for 500Torr was taken for potential difference of 80V with the gaps size of $2.5 \times 10^{-5} m$. The $\alpha/N$ for 25 Td is very small and doesn't properly fit with the PIC-MCC data because the smaller value of E/N is almost zero and applied potential is not sufficient to ionize the gas. The ionizing potential of Argon is 15.6V [67].

Figure 3.15 shows the plot for different PIC-MCC data obtained for the different pressure but the same applied potential difference of 80 V and gas temperature

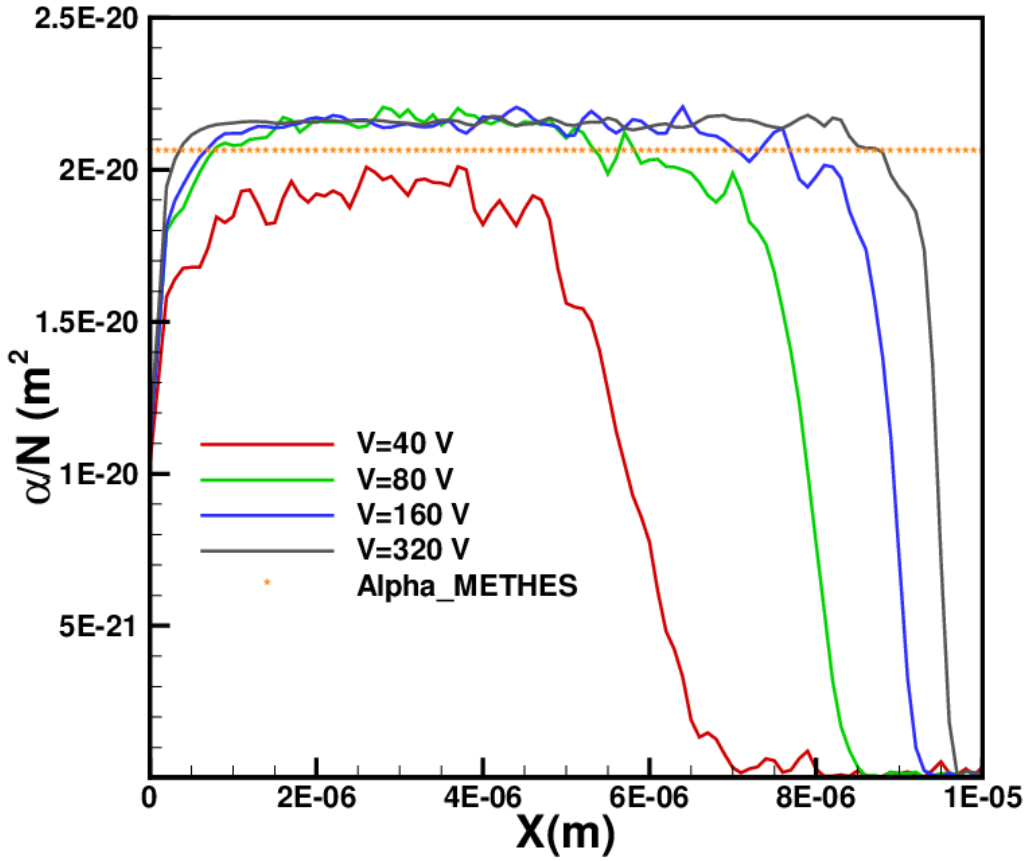


Figure 3.16: Comparison of the Ar-METHES data of $\alpha/N$ with PIC results in the uniform electric field for constant E/N=2000 Td.

of 0.026 eV (301.6K) with varying gap sizes. The gap sizes along the x-axis are normalized in order to make them in same scale. The E/N for pressure 1Torr, 10 Torr and 100 Torr is same as they were operated at same applied potential but different gap sizes $5 \times 10^{-3}m$, $5 \times 10^{-4}m$ and $5 \times 10^{-5}m$ respectively. Since $E/N = \frac{V}{d}/\frac{P}{kT}$ where V is the applied potential, d is the gap size, P is the pressure, k is the Boltzmann constant and T is the temperature, the E/N values are same eventhough they are taken for different pressure.

In order to further validate the model, we have used the PIC-MCC data taken at different applied potential and pressure but same gap sizes to make the constant E/N =2000Td. The for different applied potentials is shown in the Figure 3.16. The solid curve are for different applied potential with different pressure

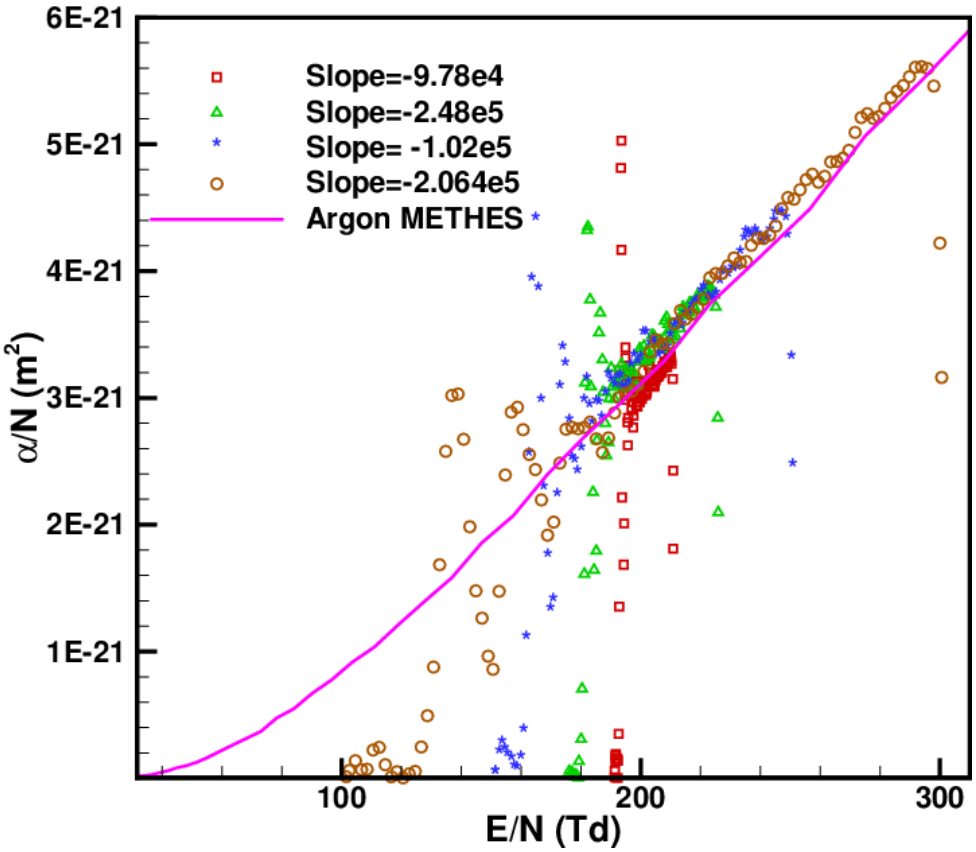


Figure 3.17: Comparison of the Ar-METHES data of $\alpha/N$ with PIC results in the non-uniform electric field

but constant gap size. The $\alpha/N$ value for argon from METHES simulation is $2.05 \times 10^{-20} m^2$ for E/N=2000Td. All the data were operated at same gas temperature 0.026 eV and same gap size $10^{-5}$ m.

## 3.3 Microscale ionization coefficient for Argon electrode in presence of non-uniform electric field

In order to understand further for METHES model works well for the non-uniform electric field, the PIC-MCC data for non uniform field is used and cor-

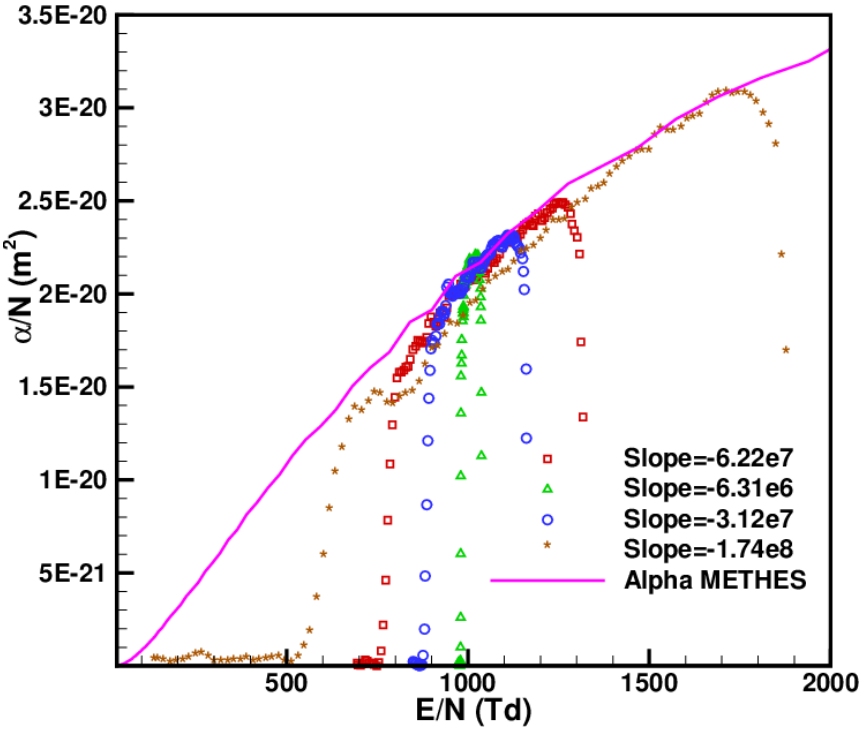


Figure 3.18: Comparison of the Ar-METHES data of $\alpha/N$ with PIC results in the non-uniform electric field

responding values of $\alpha/N$ and E/N are calculated. The argon METHES data is also plotted together with the PIC-MCC data and shown in the Figure 3.17. The slope in the figure means the $\frac{d(E/N)}{dx}$ and its unit is Td/m. The data from Zero dimensional METHES for Argon gas and the data from 1-Dimensional PIC-MCC are plotted as shown in the Figure 3.17. Oscillation in the smaller values of E/N are seen but becomes narrower and small for higher values of E/N. It is because, for smaller values of E/N, the potential is about 0-15 V where $\alpha/N = 0$, which means the elections are not ionized but as soon as the voltage increases and becomes equal to ionizing potential, the electrons get excited and hence we see sudden fluctuation in the alpha/N. But for higher E/N the electrons are already gets excited and continuous ionization occurs which stabilizes the $\alpha/N$ values and no such fluctuation occur.

Another PIC-MCC data also considered for higher values of E/N. The $\alpha/N$

and E/N are also calculated and plotted with argon METHES data and shown in the Figure 3.18. It is seen from the graph that $\alpha/N$ values are with the best fit with in for higher E/N and smaller slope of $\frac{d(E/N)}{dx}$. The sudden drop of $\alpha/N$ is seen from in the graph and is possible at the cathode and anode ends.

## 3.4 Field enhancement factor and its empirical dependence on $C_1$ and $C_2$ in modified Paschen's curve

Microelectromechanical systems (MEMS) have been great importance and interest over the last two decades. Thus, microscale breakdown phenomena should be consider very carefully. As these breakdown phenomena takes place in small gap size, electron can easily tunnel from cathodes to anode and in order to have continuous emission of electron, electric field should be applied across the electrode. It is found that field enhancement factor ($\beta$) is an important parameter that play an important role while working on the microscale gap size. Many studies found that $\beta$ is the factor that should be taken into consideration in the field emission effect of electron in a plasma. As it is discussed earlier that the state of art of this work is to predict the breakdown voltage for the different electrode once their physical parameter are known by formulating the new empirical model in terms of field enhancement factor ($\beta$). Choosing right value of $\beta$ is extremely sensitive. The present work explains carefully the sensitivity of $\beta$ while predicting breakdown voltage of micro-devices.

We are reporting the result to determine the effective field enhancement factor and its dependence on electric field for various gases. Many experimental studies are done by considering electrode materials like Nickel (Ni), Aluminum (Al), Iron (Fe), Silver(Ag) [68], Molybdenum (Mo) [69], Copper (Cu) [4], Titanium (Ti) [24], Tungsten (W), Silicon (Si), Ruthenium (Ru) and other alloys form like Platinum-chromium (Pt-Cr), Gold-Chromium (Au-Cr) [70]. Different gases like Argon (Ar), Helium (He), Nitrogen ($N_2$), Hydrogen ($H_2$), Oxygen ($O_2$), Carbon dioxide ($CO_2$),

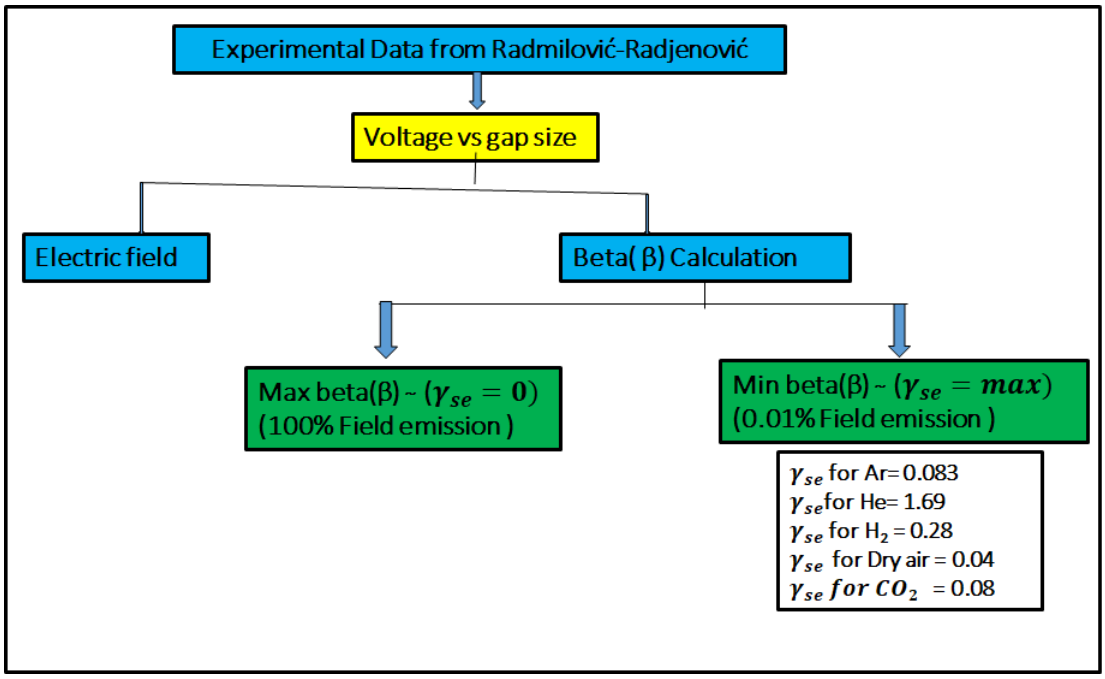


Figure 3.19: Method involving while extracting $\beta$

Methane ($CH_4$) etc are used as dielectric inside the electrode. The electrode system is configured in different orientations and pressure are changes in order to get best possible result to explain the modified paschen curve. Among many experimental data, we consider the experimental dataset from $Radmilovic - Radjenovic$ et. al [71] as their data set consist of breakdown voltages for a wide range of gaps size from 1 $\mu m$ to 100 $\mu m$. This data we considered also have lots of option to choose for different gases used withing the electrode. We have reported for four different gases including argon, dry air, carbon dioxide and hydrogen and do one by one analysis for each gases.

In order to proceed the result, the experimental data from Radmilovi-Radjenovic *et. al.* [69] were used for analysis. The dataset involves argon microscale gas breakdown at a wide range of pressures and gap sizes and hence is a pretty comprehensive dataset for comparing with theoretical models. The breakdown voltages and corresponding gap sizes were extracted using an online tool called web digitizer and the corresponding breakdown electric field ($E_{bd}$) were computed. Comparison of mea-

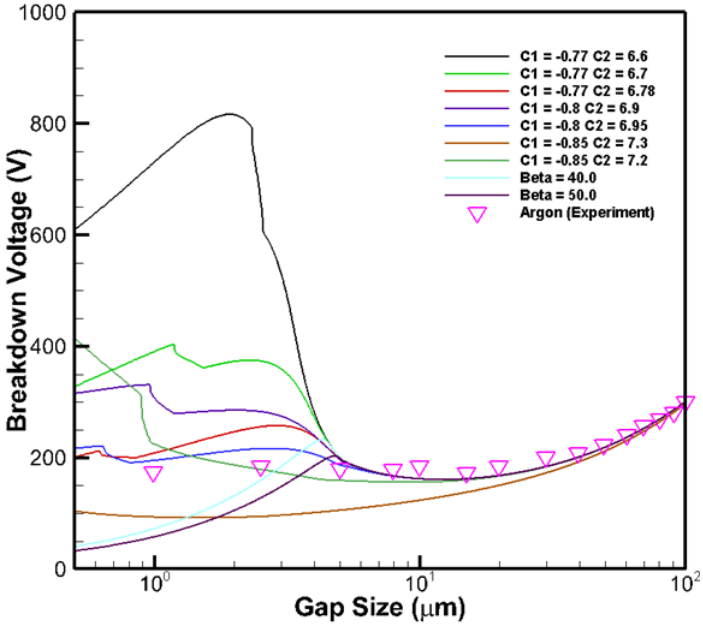


Figure 3.20: Comparison of experimental data for Ar with modified Pachan law model for the different values of $C_1$ and $C_2$

sured breakdown voltage data in conjunction with a modified Paschen law model is used to obtain a range of possible $\beta$ and $\gamma_{se}$ values that can explain experimental data. The modified Paschen law model proposed by Venkattraman and Alexeenko was used to extract the minimum and maximum values of $\beta$. $\beta_{min}$ and $\beta_{max}$ are based on the relative contribution of secondary electron emission. for example $\gamma_{se}$ is considered as 0.01% and 100% respectively for $\beta_{max}$ and $\beta_{min}$. If $\gamma_{se}$ is nearly zero than it is 100% field emission where we get the $\beta_{max}$ and if $\gamma_{se}$ is maximum then there is zero field emission and hence we get $\beta_{min}$. Thus, to get the maximum $\beta$, $\gamma_{se}$ is set to be almost zero (0.001) in the present calculations and to get the minimum $\beta$, $\gamma_{se}$ is set to be 100% which makes completely the effect of secondary electron emission. The minimum $\gamma_{se}$ used for different gases is shown in the Figure 3.19. With the calculated values of $\beta_{max}$ and $\beta_{min}$, the corresponding maximum and minimum values of breakdown voltages are calculated using the algorithm we have developed in python script to compare with the experimental result calculated by Radmilovi-Radjenovic *et. al.* [71]

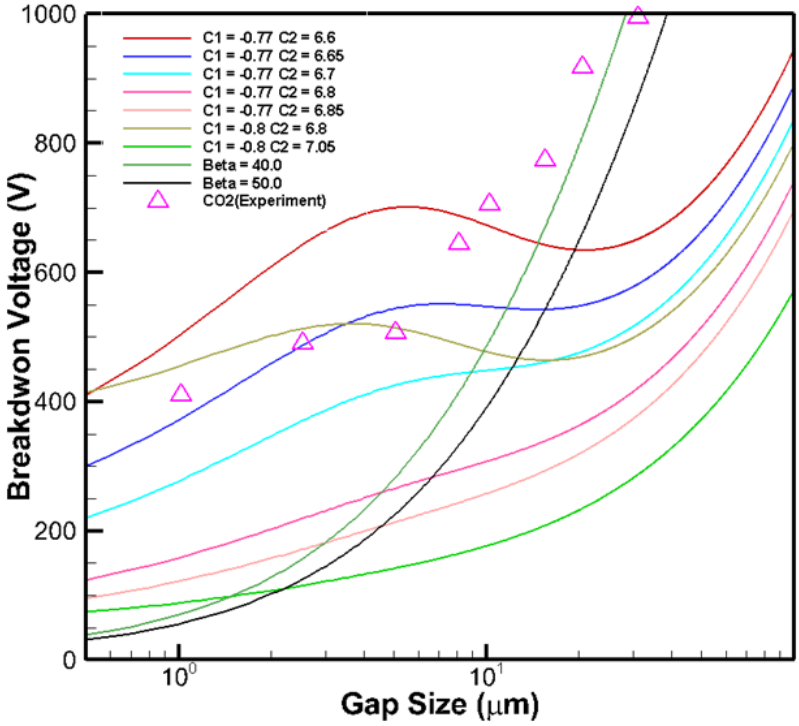


Figure 3.21: Comparison of experimental data for $CO_2$ with modified Pachan law model for the different values of $C_1$ and $C_2$

Thus obtained data are further analyzed and plot the graph to show the dependence of electric field with field enhancement factor. The graph is shown as in Figure 3.25 . The minimum and maximum values of $\beta$ were calculated by controlling the influence of field emission. Specifically, for $\gamma_{se} = 0$ the maximum field emission is observed thereby corresponding to the maximum possible $\beta$ value. Similarly, the minimum possible value of $\beta$ is obtained when secondary electron emission dominates and field emission contributes little to the breakdown. It is seen from the Figure 3.25, that the $\beta$ decreases with the increasing electric field. as reported in Buendia et.al [72].

We proposed the empirical formula as in the equation (3.1).

$$ln\beta_{eff} = C_1 lnE_{bd} + C_2 \tag{3.1}$$

where $C_1 = -0.773$ and $C_2 = 6.76$. The conclusions were based on a proce-

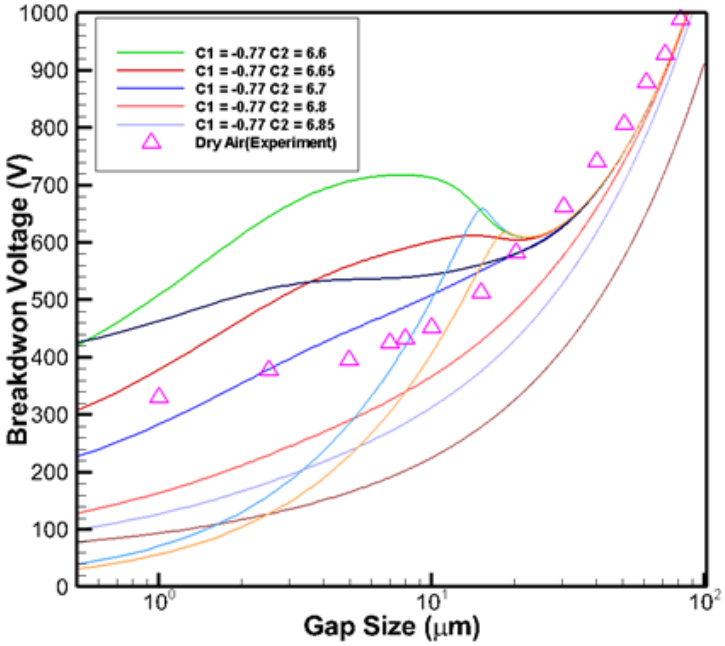


Figure 3.22: Comparison of experimental data for Dry air with modified Pachan law model for the different values of $C_1$ and $C_2$

dure by which the breakdown voltage for given operating conditions (pressure, gap size etc.) was used in conjunction with the modified Paschen law model described earlier to determine the value of $\beta$. Values of $\beta$ determined based on this process were correlated with the electric field at breakdown and a curve-fit was used to determine the values of $C_1$ and $C_2$. Interestingly though, the empirical model for $\beta$ was not used in modified Paschen law models to predict breakdown voltages at other conditions. The current work expands on this work significantly by considering a larger number of datasets and also analyzing the potential influence of uncertainties in $C_1$ and $C_2$ by determining the sensitivity of the empirical model for $\beta$.

We also analyze the importance of parameter$C_1$ and $C_2$ purposed by Bauendia *et. al.* [72] for the different field enhancement factor and plotted the graph for breakdown voltage vs gap sizes as shown in Figure 3.20 - Figure 3.23. $\beta$= 40 and $\beta$=50 are chosen to show up for the modified Paschen curve explained by Torres

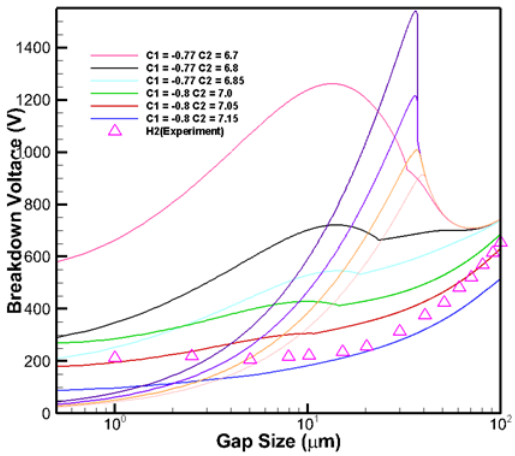


Figure 3.23: Comparison of experimental data for $H_2$ with modified Pachan law model for the different values of $C_1$ and $C_2$

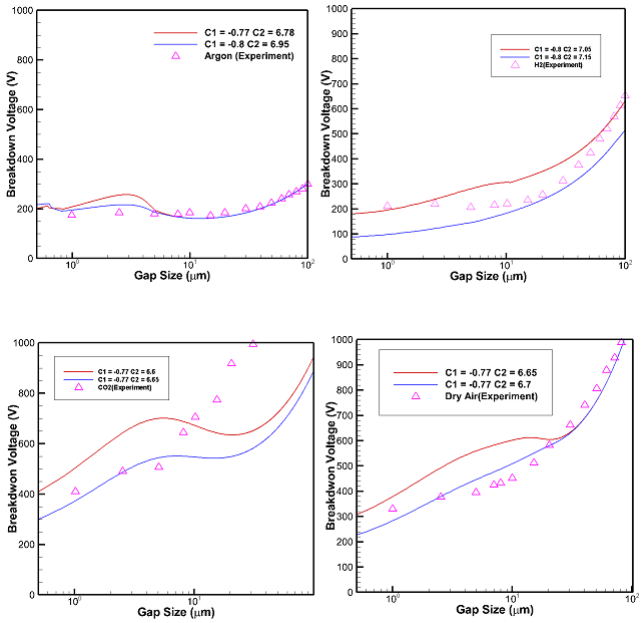


Figure 3.24: Comparison of experimental breakdown voltage with predictions of the modified Paschen law model using different values of $C_1$ and $C_2$ closed to experimental data

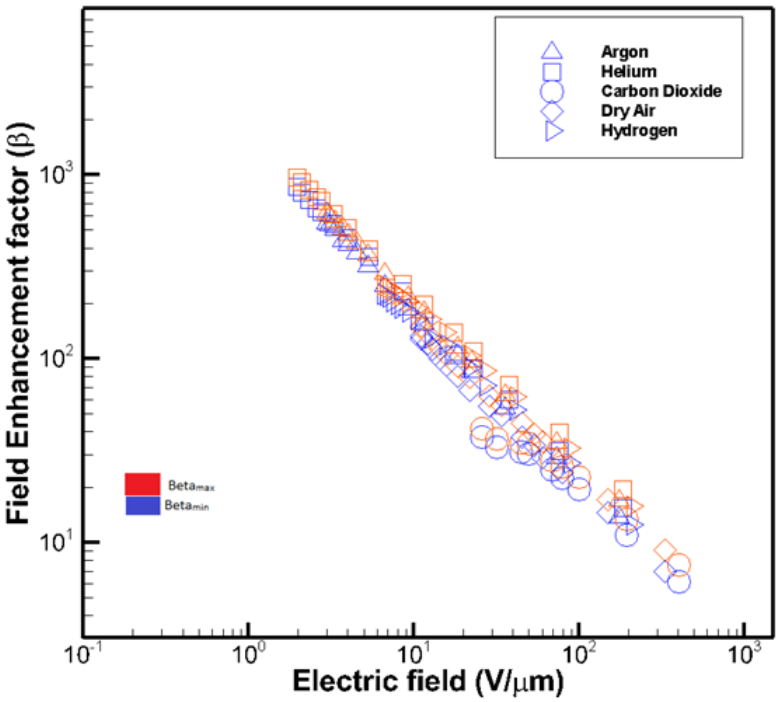


Figure 3.25: Field enhancement factor $\beta$ vs electric field for different gases.

J-M and Dhariwal.

It is clear from the graph that for the smaller change in values of $C_1$ and $C_2$ field enhancement factor changes highly which has the direct impact in the breakdown voltage. The maximum and minimum $\beta$ values are chosen which are closed to experimental values of breakdown voltage for further analysis. The experimental data along with the different values of $C_1$ and $C_2$ are shown in the Figure 3.20 - Figure 3.23. The values of $C_1$ and $C_2$ for which the breakdown voltage gives the approximate results can used for further analysis.

Figure 3.20 - Figure 3.23 clearly indicated that the values of $C_1$ and $C_2$ chosen using equation (3.1) with the best fitting values to plot the line for $\beta$ vs electric field. To fit these minimum values and maximum values we use the empirical formula in equation (3.1) to get the range of beta values. With those values of $C_1$ and $C_2$. we have plotted the curve between breakdown voltage and gap sizes using our python model that we built and shown in Figure 3.26 .

Thus, It is seen that the $C_1$ and $C_2$ selection in the empirical formula are very

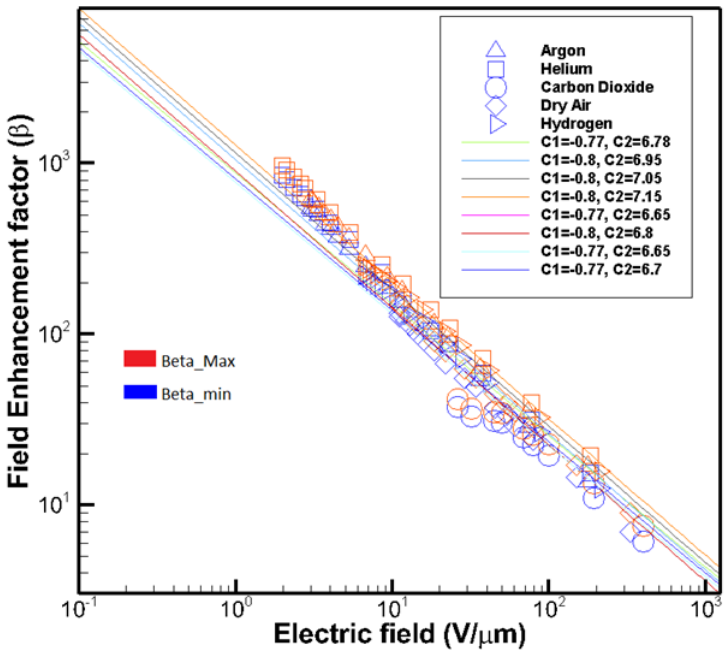


Figure 3.26: Field enhancement factor ($\beta$) with electric field for all different gases with fitted $C_1$ and $C_2$

important. Slight change in those parameter can be greatly affected $\beta$ . Thus $\beta$ being the non-intuitive parameter limits the predictive capability of modified Paschen law models. Comparison with $\beta$ of experimental data indicates the importance of accounting the dependence of $\beta$ on electric field. The minimum and maximum field enhancement factors along with the corresponding curve fit for given values of $C_1$ and $C_2$ are shown in the Figure 3.26. The graph of $\beta$ vs electric field can thus used to calculated the range of breakdown voltages. Thus, calculating $\beta$ in this way helps to find the range of breakdown voltages within which it is safe to operate those micro-devices with out breaking it with the given operating conditions. This is truly be useful for experimental set up as one can use the information from the graph and use suitable voltage for their breakdown.

# Chapter 4

# Non-Linear Sheath Model Results and Comparison with PIC-MCC

The results presented below will discuss the comparative study for pre and post- breakdown current-voltage characteristics followed by PIC-MCC simulations to obtain the microplasma properties and their spatial variation. The PIC/MCC data at different pressures are shown using square symbol. While representing the graph the blue curve represent the ion and red curve represent for electron and different types of notation are used to represent for the different values of n as indicated in equation (2.2).

## 4.1 Non-linear sheath model

To understand and compare the relation between the developed model with the existing PIC/MCC data, the graph between electric field, current density and their ionization coefficient with respect to the gap sizes at different pressure are plotted. We are using the n= 1, 1.25 and 1.5 for the further understanding about the model. Number density vs gap sizes are also plotted to know about the variation of number density of ion and electron in the sheath width . Thus obtained results are also validated with the PIC-MCC simulations performed using one-dimensional XPDPI code [51] which were originally developed at the University of California, Berkely. For these simulations, the computational domain was divided into 400

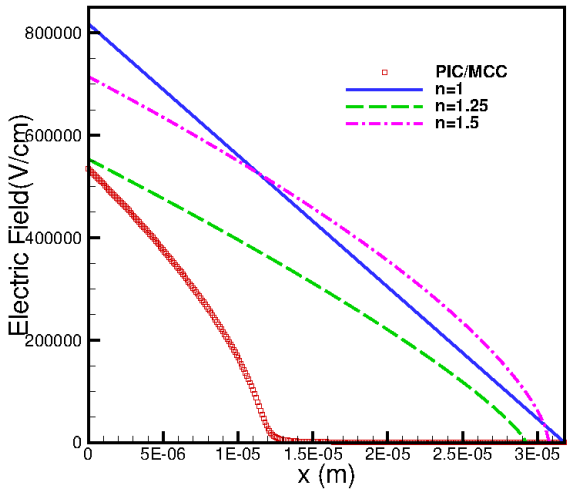


Figure 4.1: Spatial variation of electric field for different n-values and comparison with PIC/MCC result in an argon gap of size 1 mm operating at a total current density of $2 \times 10^5 A/m^2$ and a pressure of 100 Torr, at temperature 300K. The field emission parameters were $\beta = 30$ and $\gamma_{se} = 0.05$, $\phi = 5eV$.

cells resulting in a cell size of 0.0125 $\mu m$ which ensured that the cell size was smaller than the Debye length even for an electron number density of $5 \times 10^{23} 1/m^3$ which is greater than the number densities encountered in all the simulations presented. The timestep was taken as 0.01 ps, which ensures that an average electron does not cross more than one cell in one timestep. The ratio of real to simulated particles was varied depending on the case to ensure that the total number of simulated particles did not exceed $0.1 \times 10^6$. The results presented were obtained by time-averaging over 500000 timesteps after the simulation reached steady state. Several constant current density simulations were performed ranging from a current density of $4 \times 10^5 A/m^2$ to $4.1 \times 10^6 A/m^2$ for $\beta$ values of 30, 55, and 70.

## 4.2 Spatial variation of current voltage characteristics at pd=1

The graph between electric field vs gap sizes for total current density $2 \times 10^5 A/m^2$ and a pressure of 100 Torr, at temperature 300K with the field emission

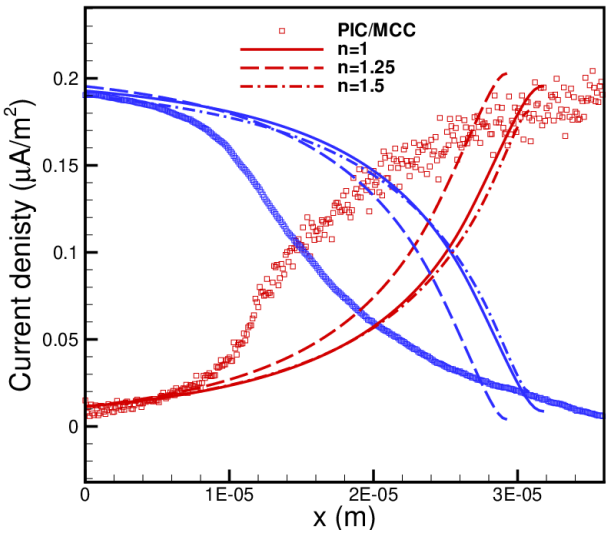


Figure 4.2: Spatial variation of Current density for different n-values and comparison with PIC/MCC result in an argon gap of size 1 mm operating at a total current density of $2 \times 10^5 A/m^2$ and a pressure of 100 Torr, at temperature 300K. The field emission parameters were $\beta = 30$ and $\gamma_{se} = 0.05$, $\phi = 5eV$.

parameters were $\beta = 30$ and $\gamma_{se} = 0.05$, $\phi = 5eV$ or the argon gas is shown in the Figure 4.1. It is found that the electric field value for n=1.25 is close to the PIC/MCC data at the cathode when x=0. As the gap size increasing, the electric field drop down to zero. The sheath thickness reported as $31\mu m$ for n=1 which is in agreement with the purposed value of sheath thickness by Venkattraman et. al. [6]. The sheath thickness are about $29\mu m$ and $30\mu m$ for n=1.25 and n=1.5 respectively. The sheath thickness has slightly increases for n=1.5 instead of decreasing. It may be because of the electric field is comparatively higher for n=1.5 compared to n=1.25 as shown in the Figure 4.1.

To understand further the effect of pressure for different values of n, the graph for ion current density and electron current density with gap sizes are plotted for the total current density of $2 \times 10^5 A/m^2$ and compare the result with PIC/MCC. The red color lines are for the electron current density and blue color lines are for the ion current density. For PIC/MCC the green symbols are used to represent for the ion current density. The Figure 4.2 shows the current density for different n at pressure 100 Torr with the corresponding PIC/MCC result. At x=0 both model

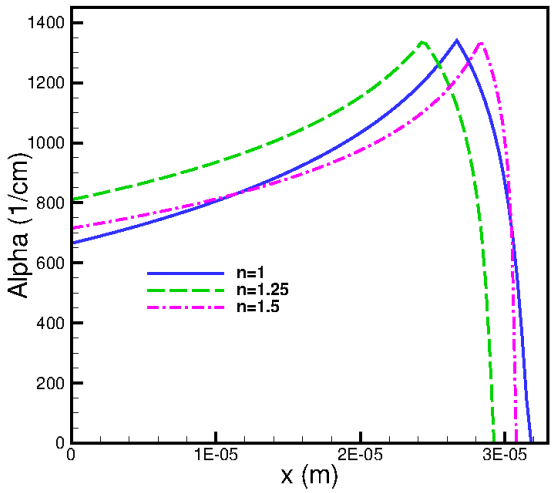


Figure 4.3: Spatial variation of Ionization coefficient ($\alpha$) for different n-values and comparison with PIC/MCC result in an argon gap of size 1 mm operating at a total current density of $2 \times 10^5 A/m^2$ and a pressure of 100 Torr, at temperature 300K. The field emission parameters were $\beta = 30$ and $\gamma_{se} = 0.05$, $\phi = 5eV$.

data and PIC/MCC data are in agreement which support that the current model we have developed providing the promising result. But as the gap sizes increases, the current density lines are pushed off further apart. It may be possible because of the sheath thickness reported for the model is higher than the sheath thickness from the PIC. Similar values of sheath thickness are also reported by [50].

The spatial variation of ionization coefficient($\alpha$) for different n-values and comparison with PIC/MCC result in an argon gap of size 1 mm operating at a total current density of $2 \times 10^5 A/m^2$ and a pressure of 100 Torr, at temperature 300K. The field emission parameters were $\beta = 30$ and $\gamma_{se} = 0.05$, $\phi = 5eV$ are also plotted.

## 4.3 Spatial variation of current-voltage characteristics at pd=3

To understand the details about the relation between electric field with pressure, the simulation is also done for p=300 Torr and and the data are analyzed

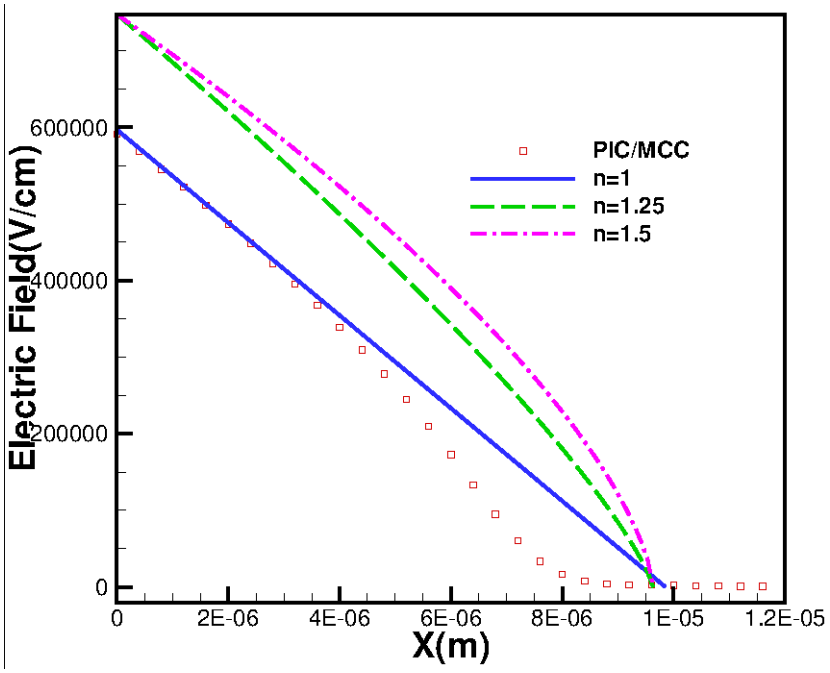


Figure 4.4: Spatial variation of electric field for different n-values and comparison with PIC/MCC result in an argon gap of size 1 mm operating at a total current density of $2 \times 10^5 A/m^2$ and a pressure of 300 Torr, at temperature 300K. The field emission parameters were $\beta = 30$ and $\gamma_{se} = 0.05$, $\phi = 5eV$.

. It is found from the Figure 4.4 that the sheath thickness decreases to $10\mu m$ whereas the thickness reported for PIC/MCC simulation is about $8\mu m$ which shows that with increase in pressure the thickness come close to the value reported by PIC/MCC simulation. The electric field for n=1 is exactly matching with the PIC data however the electric field for n=1.25 is $75V/\mu m$ which is about $15V/\mu m$ higher than the predicted value by PIC simulation. The sheath thickness from the model is slightly higher than the PIC result

The current density plot at pressure 300 Torr is shown in the Figure 4.5 The data predicted by the model are in agreement with PIC/MCC data at 300 Torr pressure. The cathode current density at x=0 is reported as $0.23\mu A/m^2$ which is about $0.03\mu A/m^2$ higher than the PIC/MCC result. It is possible because the electric field for n=1.25 is higher than the PIC/MCC result as shown in the Figure 4.4. It is also conformed that the sheath thickness is less than the sheath thickness

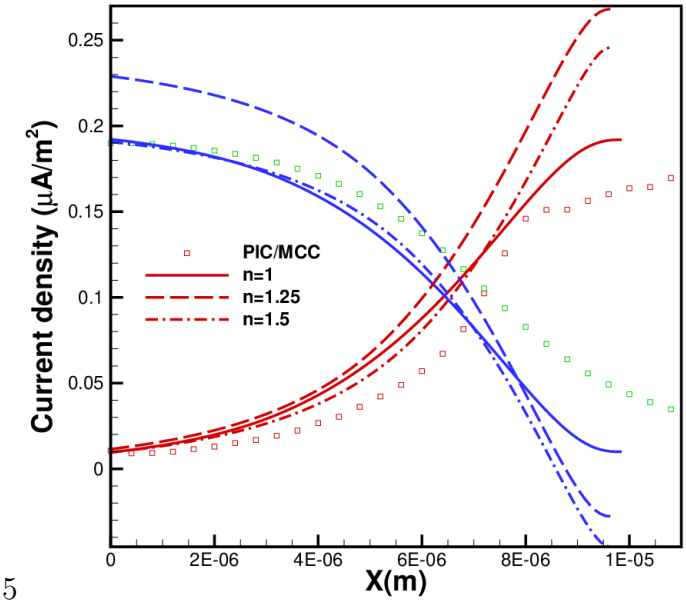


5

Figure 4.5: Spatial variation of Current density for different n-values and comparison with PIC/MCC result in an argon gap of size 1 mm operating at a total current density of $2 \times 10^5 A/m^2$ and a pressure of 300 Torr, at temperature 300K. The field emission parameters were $\beta = 30$ and $\gamma_{se} = 0.05$, $\phi = 5eV$.

predicted by PIC/MCC which validates the results from the PIC an model are with the agreement with each other.

## 4.4 Spatial variation of current-voltage characteristics at pd=5

The similar simulation is also done for pressure p= 500 Torr keeping the field emission parameter $\beta = 30$ and $\gamma_{se} = 0.05$ and $\phi = 5eV$ and the Figure 4.7. At pressure 500 Torr the electric field is closely matching with the reported PIC/MCC result for n=1.25 at the cathode but is about $70V/\mu m$ and $78V/\mu m$ are reported for n=1 and n=1.5 which are about $3V/\mu m$ and $13V/\mu m$ higher than the predicted PIC result. It is obvious to have higher electric field. The sheath thickness decreases even further to $62\mu m$ and it lies within the sheath thickness of PIC/MCC. The sheath thickness for PIC is about $68V/\mu m$ which is greater than the sheath

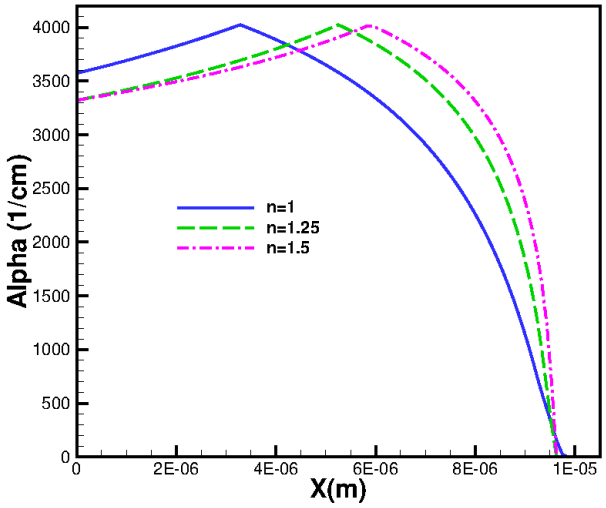


Figure 4.6: Spatial variation of Ionization coefficient ($\alpha$) for different n-values and comparison with PIC/MCC result in an argon gap of size 1 mm operating at a total current density of $2 \times 10^5 A/m^2$ and a pressure of 300 Torr, at temperature 300K. The field emission parameters were $\beta = 30$ and $\gamma_{se} = 0.05$, $\phi = 5eV$.

thickness for n=1, n=1.25 and n=1.5.

The current densities vs gap sizes plot at pressure 500 Torr is shown in the Figure 4.8.It is observed that the current density for n=1is about 0.28 $\mu A/m^2$ which is about 0.1 $\mu A/m^2$ higher than the PIC/MCC data. For further increase of n, the total electron current density goes too high to maintain the corresponding negative ion current density. As the ion current density goes more negative for the higher values of n at $\beta$=30, the model needs considers higher values of $\beta$ which is explained in the next section.

## 4.5 Spatial variation of current-voltage characteristics at pd=7

It is seen from the previous study that higher the pressure greater is the possibility that the electric field goes within the values reported PIC. For further understanding, the simulation is done with p=700 Torr which is approximately

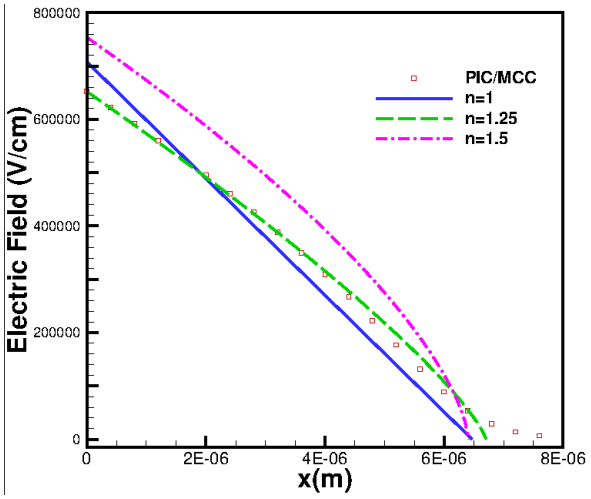


Figure 4.7: Spatial variation of electric field for different n-values and comparison with PIC/MCC result in an argon gap of size 1 mm operating at a total current density of $2 \times 10^5 A/m^2$ and a pressure of 500 Torr, at temperature 300K. The field emission parameters were $\beta = 30$ and $\gamma_{se} = 0.05$, $\phi = 5eV$.

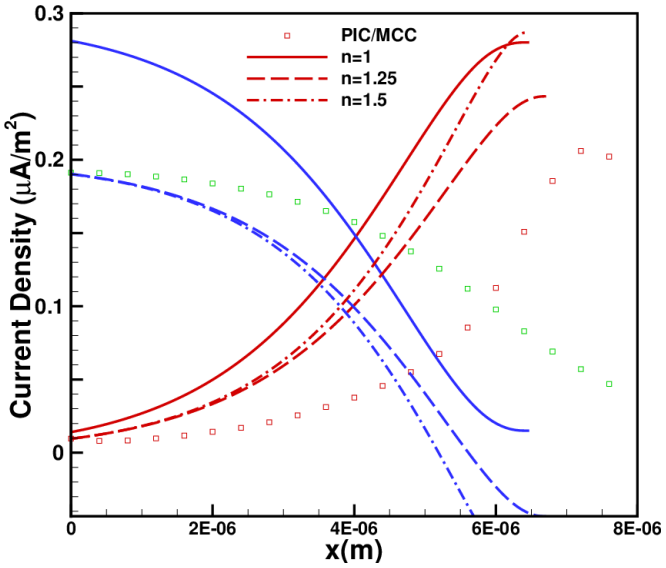


Figure 4.8: Spatial variation of Current density for different n-values and comparison with PIC/MCC result in an argon gap of size 1 mm operating at a total current density of $2 \times 10^5 A/m^2$ and a pressure of 500 Torr, at temperature 300K. The field emission parameters were $\beta = 30$ and $\gamma_{se} = 0.05$, $\phi = 5eV$.

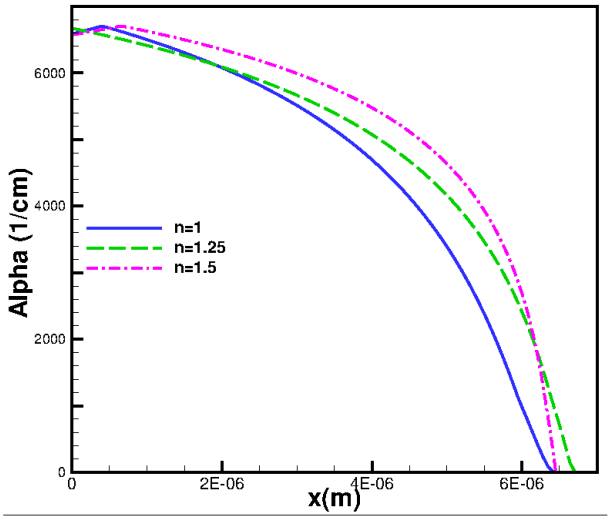


Figure 4.9: Spatial variation of Ionization coefficient ($\alpha$) for different n-values and comparison with PIC/MCC result in an argon gap of size 1 mm operating at a total current density of $2 \times 10^5 A/m^2$ and a pressure of 500 Torr, at temperature 300K. The field emission parameters were $\beta = 30$ and $\gamma_{se} = 0.05$, $\phi = 5eV$.

the atmospheric pressure and compare the model data with PIC/MCC data for p=700 Torr and is shown in the Figure 4.10. The cathode electric field drop down for n=1.25 and n=1.5. The sheath thickness for PIC-MCC data is reported as about 6 $\mu m$ and for n=1 it is reported as approximately 5.9 $\mu m$. For n=1.25 and n=1.5 the sheath thickness drop down quickly to 4.2 $\mu m$ for n=1.25 and 3.8 $\mu m$ for n=1.5. This shows that with the increases in pressure further from 700 Torr, the electric field drop down very quickly to zero with very small sheath thickness.

It is observed from the graph of Electric field vs gap sizes that the sheath thickness goes on decreasing to about 6.5$\mu m$. The cathode electric field decreases with increase in the value of n. The sheath thickness also goes on decreasing with the increase n. It is also observed from the Figure 4.10 that the sheath thickness are about 5.6$\mu m$, 4.3$\mu m$ and 3.8$\mu m$ respectively for n=1, 1.25 and 1.5. Since all electric field values and sheath thickness are within the range of PIC, the result are potentially in agreement with the PIC/MCC data and its expectation.

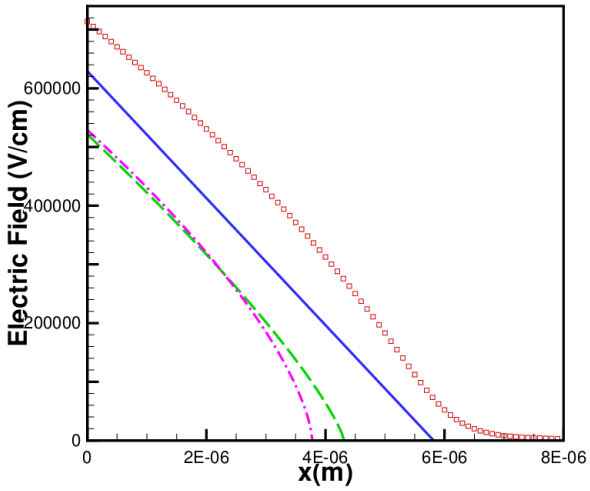


Figure 4.10: Spatial variation of electric field for different n-values and comparison with PIC/MCC result in an argon gap of size 1 mm operating at a total current density of $2 \times 10^5 A/m^2$ and a pressure of 700 Torr, at temperature 300K. The field emission parameters were $\beta = 30$ and $\gamma_{se} = 0.05$, $\phi = 5eV$.

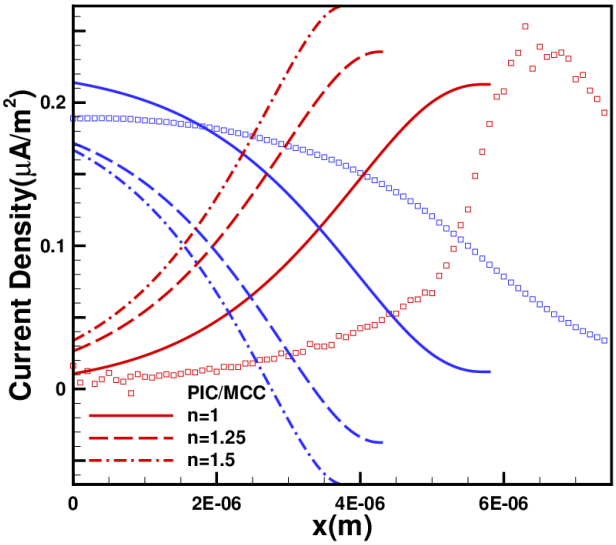


Figure 4.11: Spatial variation of Current density for different n-values and comparison with PIC/MCC result in an argon gap of size 1 mm operating at a total current density of $2 \times 10^5 A/m^2$ and a pressure of 700 Torr, at temperature 300K. The field emission parameters were $\beta = 30$ and $\gamma_{se} = 0.05$, $\phi = 5eV$.

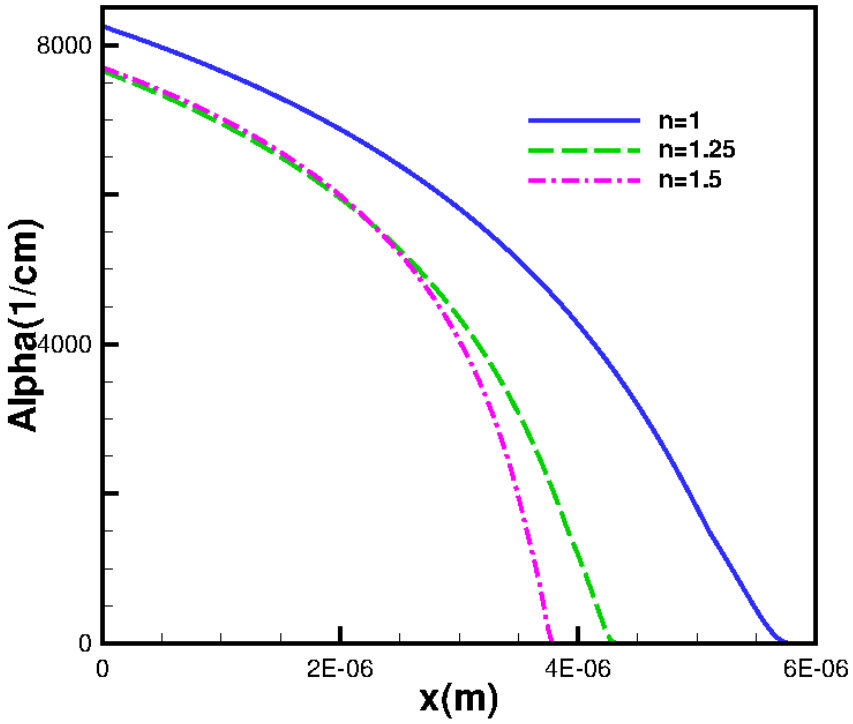


Figure 4.12: Spatial variation of Ionization coefficient ($\alpha$) for different n-values and comparison with PIC/MCC result in an argon gap of size 1 mm operating at a total current density of $2 \times 10^5 A/m^2$ and a pressure of 700 Torr, at temperature 300K. The field emission parameters were $\beta = 30$ and $\gamma_{se} = 0.05$, $\phi = 5eV$.

The plot for the ion current density and electron current density with respect to the gap size(x) is shown in the Figure 4.11. With the increases of n values, the ion current becomes more negative and electron current becomes more positive as in the graph to maintain the constant current density of $2 \times 10^5 A/m^2$.

The variation of ionization coefficient for different values of n and with respect to their gap sizes is shown in the Figure 4.12 for pressure For p=100 Torr,

## 4.6 Comparison of model when pressure ($p$)=10 Torr and $\beta = 1000$

Linear sheath model predicted previously explain and discuss the variation of microplasma properties for different total current density using the average value

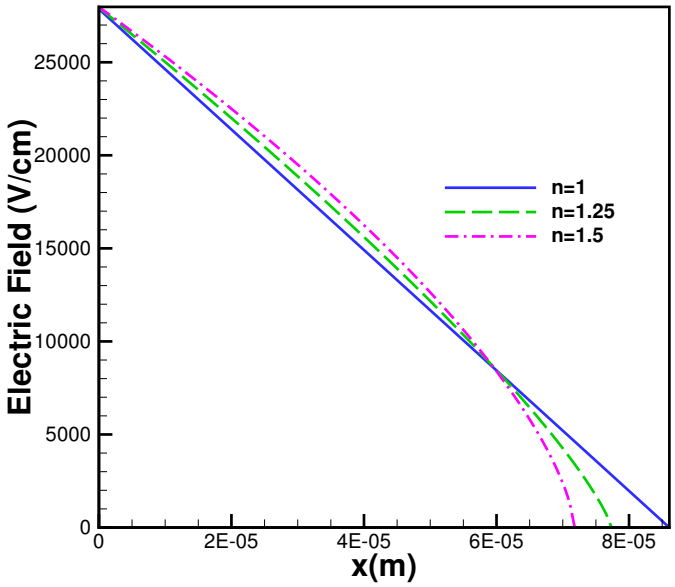


Figure 4.13: Spatial variation of Electric field for different n-values 1 mm operating at a total current density of $2000 A/m^2$ and a pressure of 10 Torr at temperature 300K and the field emission parameters were $\beta = 1000$ ,$\gamma_{se} = 0.1$, $\phi = 5eV$.

of ionization coefficient ($\overline{\alpha}$). Thus the variation of electric field and current density at a particular gap size while determining the microplasma properties can not be well explained.[6]. In order to over come this problem, we are using the ionization coefficient for each individual electric field and calculated the current density and the variation of electric field and current density are plotted.

In order to validate the result predicted by model and to estimate microplasma properties that are not predicted by model [6] the simulation were performed for 1mm argon gap electrode operating at the total current density of $2 \times 10^5 A/m^2$ and pressure of of 10 Torr at temperature 300K and the field emission parameters were $\beta = 1000$ ,$\gamma_{se} = 0.1$, $\phi = 5eV$. Thus obtained results are also validated with the PIC-MCC simulations performed using one-dimensional XPDPI code [51] which were originally developed at the University of California, Berkely. The algorithm is later modified to include the effect of field emission from the cathode [34] where field emitted electrons were performed using the algorithm similar to the

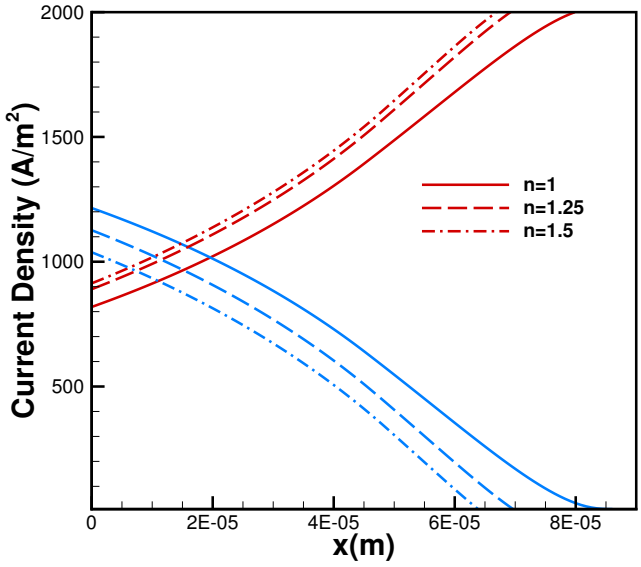


Figure 4.14: Spatial variation of current density for different n-values 1 mm operating at a total current density of $2000 A/m^2$ and a pressure of 10 Torr at temperature 300K and the field emission parameters were $\beta = 1000$ ,$\gamma_{se} = 0.1$, $\phi = 5eV$.

secondary electron emission while destining their model. The data were compared and presented as follows.

The electric field variation with respect to gap sizes is shown in the Figure 4.13. The PIC-MCC simulation predicted an electrode voltage of about 160V. But our model predicted about 120V which is 40V less than the predicted by PIC-MCC result and about 2.8 V/$\mu m$ which agree with the predicted model. The electric field value is about 0.6V/$\mu m$ more than the predicted value. It should be worth noted that the electric field predicted by our model is closed to the values reported by Venkattraman et.al[6]. Since the electric field is non-linearly varying with the gap sizes, the decrease in electric filed is linear as x approaches to zero ie near the cathode but later the electric field drop down quickly making steeper curve and approaches to zero with x increases. It is found that the sheath thickness is about 0.85 $\mu m$ for linearly varying electric field (n=1) and decreases as the value of n increases as 0.78 $\mu m$ for n=1.25 and 0.7$\mu m$ for n=1.5 as shown in the Figure

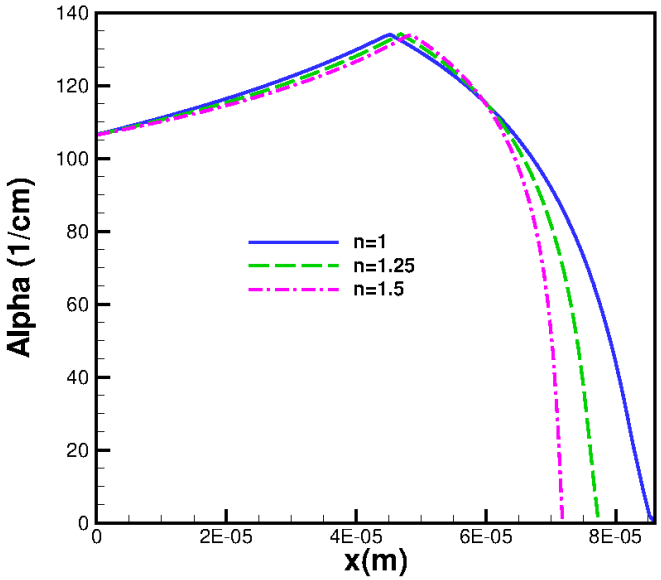


Figure 4.15: Spatial variation of ionization coeficient for different n-values 1 mm operating at a total current density of $2000 A/m^2$ and a pressure of 10 Torr at temperature 300K and the field emission parameters were $\beta = 1000$ ,$\gamma_{se} = 0.1$, $\phi = 5eV$.

4.13. The decrease in sheath thickness followed the trend and is obvious as we know that the higher cathode electric field and the resulting higher field emission current density offset the decrease in cathode fall thickness thereby producing the required current density which is higher than the previous case.

The current density vs x graph is shown in Figure 4.14 for the current density source of $2 \times 10^3 A/m^2$. It is seen from the graph that lowering the electric field will lower the current density of electron and thereby decreasing the cathode fall thickness. It can be seen that the total current density is constant across the gap indicating charge conservation. The proposed model takes as input, parameters such as pressure,$\gamma_{se}$ gas, the field emission parameters $\beta$ and $\phi$, and gap size. All parameters were taken to be exactly same as used in the PIC/MCC simulations. In other words, the results presented below evaluate the performance of the proposed model as a predictive tool.

The variation of ionization coefficient for different values of n is shown in the Figure 4.15. It is seen from the Figure that the ionization coefficient for n=1 shows

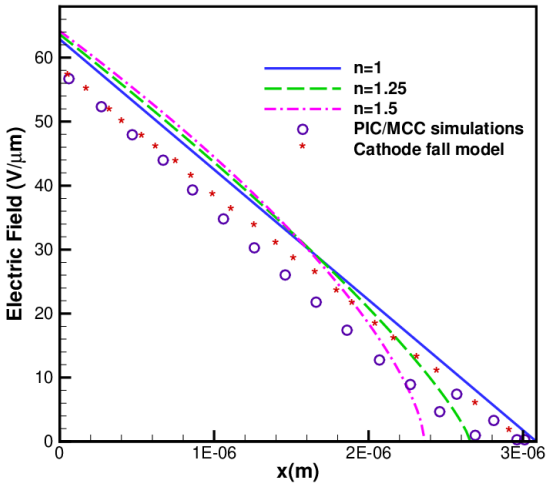


Figure 4.16: Spatial variation of electric field for different n-values with 5 $\mu m$ electrode operating at a total current density of $4.7 \times 10^5 A/m^2$ and a pressure of of 760 Torr at temperature 300K and the field emission parameters were $\beta = 55$ ,$\gamma_{se} = 0.05$, $\phi = 5.15eV$.

the higher sheath thickness ob about $0.8\mu m$ and the sheath thickness decreases as the electric field decreases with the values of n. Maximum ionization coefficient is about 135 1/cm is reported as shown is the Figure 4.15.

## 4.7 Comparison of model when Pressure=760 Torr and $\beta$=55

The predicted model is also used to legitimate the results with the previously existing model called cathode fall model proposed by Venkattraman *et. al.* [50] and carefully analyzed the data with PIC and the existing model. Cathode fall model was purposed for a 5 $\mu m$ argon microplasma and compared with PIC-MCC simulations. The field emitting cathode parameters were taken as $\beta = 55$ and $\phi = 5.15eV$, The secondary electron emission coefficient ($\gamma_{se}$) was taken as 0.05. The Figure 4.17 shows the electron current density and ion current density profiles from the PIC/MCC simulation at a total current density of $4.7 \times 10^5 A/m^2$ for different values of n. To compare the developed model with the existing model,

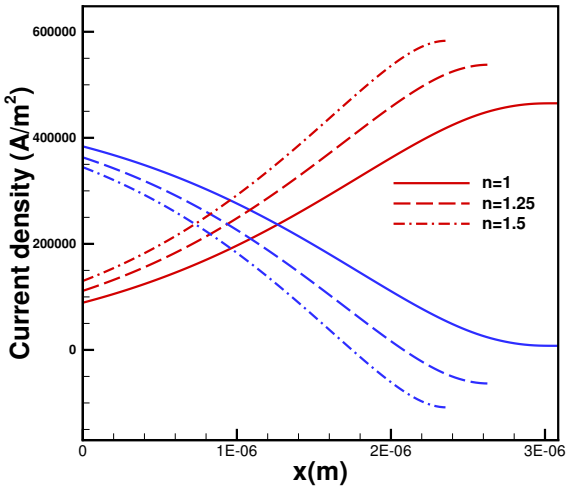


Figure 4.17: Spatial variation of current density for different n-values with 5 $\mu m$ electrode operating at a total current density of $4.7 \times 10^5 A/m^2$ and a pressure of 760 Torr at temperature 300K and the field emission parameters were $\beta = 55$ ,$\gamma_{se} = 0.05$, $\phi = 5.15eV$.

the input parameter such as $\gamma_{se}$, gas field emission parameters such as $\beta$ and $\phi$ and gap size are considered as same as in the PIC/MCC simulations.

The electric field variation with gap sizes for 5 $\mu m$ electrode operating at a total current density of $4.7 \times 10^5 A/m^2$ and a pressure of of 760 Torr at temperature 300K and the field emission parameters were $\beta = 55$ ,$\gamma_{se} = 0.05$, $\phi = 5.15eV$ is shown in the Figure 4.16. The PIC/MCC simulation predict the cathode electric field (at x=0) as about 60 $V/\mu m$ where as for n=1, our model predict the electric field is about 64 $V/\mu m$ which is about 4 $V/\mu m$ higher than the predicted result. The slope of electric field goes to zero as opposed to the sharp change assumed by the model. The cathode electric field predicted by the model agrees very well with the PIC/MCC simulation and the existing model [50].

Figure 4.16 present the results for a current density source of $4.7 \times 10^5 A/m^2$ also shows the good agreement between the old model and simulations. It is considered in the cathode fall model that the model assumes constant ion number density in the cathode fall region. The higher cathode electric field and the resulting higher

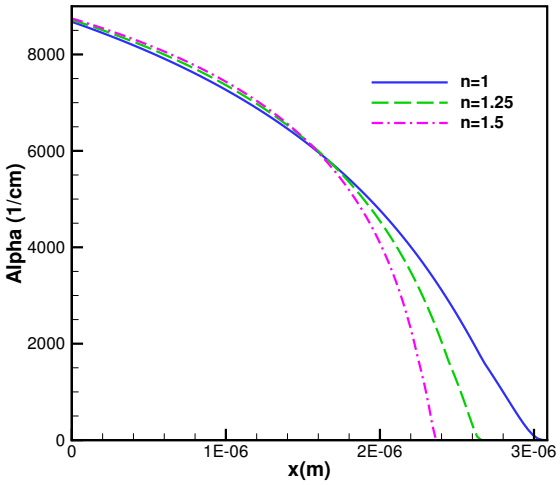


Figure 4.18: Spatial variation of ionization coefficient for different n-values with 5 $\mu m$ electrode operating at a total current density of $4.7 \times 10^5 A/m^2$ and a pressure of 760 Torr at temperature 300K and the field emission parameters were $\beta = 55$ ,$\gamma_{se} = 0.05$, $\phi = 5.15eV$.

field emission current density offset the decrease in cathode fall thickness thereby producing the required current density which is higher than the previous case as mentioned in the section 4.5.

The variation of ionization coefficient for total current density $4.7 \times 10^5 A/m^2$ is shown in the Figure 4.18. The ionization coefficient at the cathode is about 8700 1/cm and smoothly dropping down as the electric field variation as in the Figure 4.16. The sheath thickness also decreases from about $30\mu m$ for n=1 to $24\mu m$ for n=1.5.

The data are again validated with the total current density of $9 \times 10^5 A/m^2$ and a pressure of of 760 Torr at temperature 300K and the field emission parameters were $\beta = 55$ ,$\gamma_{se} = 0.05$, $\phi = 5.15eV$ for a argon gas in 5 $\mu m$ gap size. The electric field profile is shown in the Figure 4.19 are at potential of about 69V which is slightly higher than the predicted data from PIC/MCC and cathode fall model [50]. The PIC/MCC reported their potential about 62 V and Venkattramann et. al. reported the potential of 55 V.

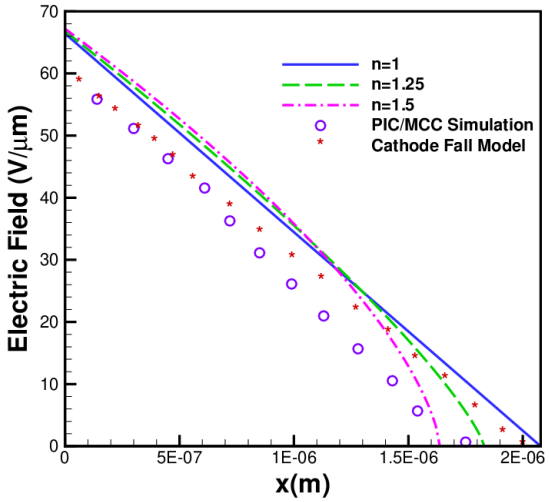


Figure 4.19: Spatial variation of electric field for different n-values with 5 $\mu m$ electrode operating at a total current density of $9 \times 10^5 A/m^2$ and a pressure of 760 Torr at temperature 300K and the field emission parameters were $\beta = 55$ ,$\gamma_{se} = 0.05$, $\phi = 5.15eV$.

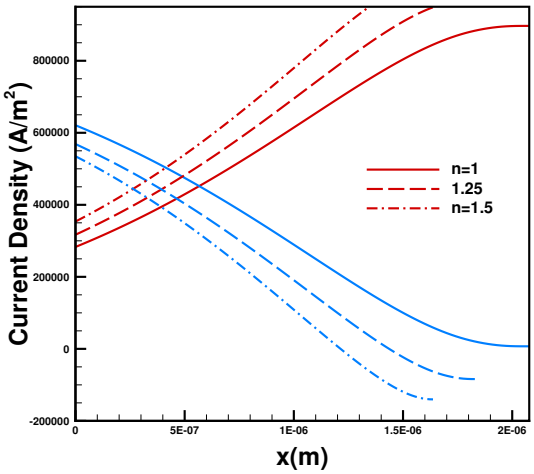


Figure 4.20: Spatial variation of current density for different n-values with 5 $\mu m$ electrode operating at a total current density of $9 \times 10^5 A/m^2$ and a pressure of 760 Torr at temperature 300K and the field emission parameters were $\beta = 55$ ,$\gamma_{se} = 0.05$, $\phi = 5.15eV$.

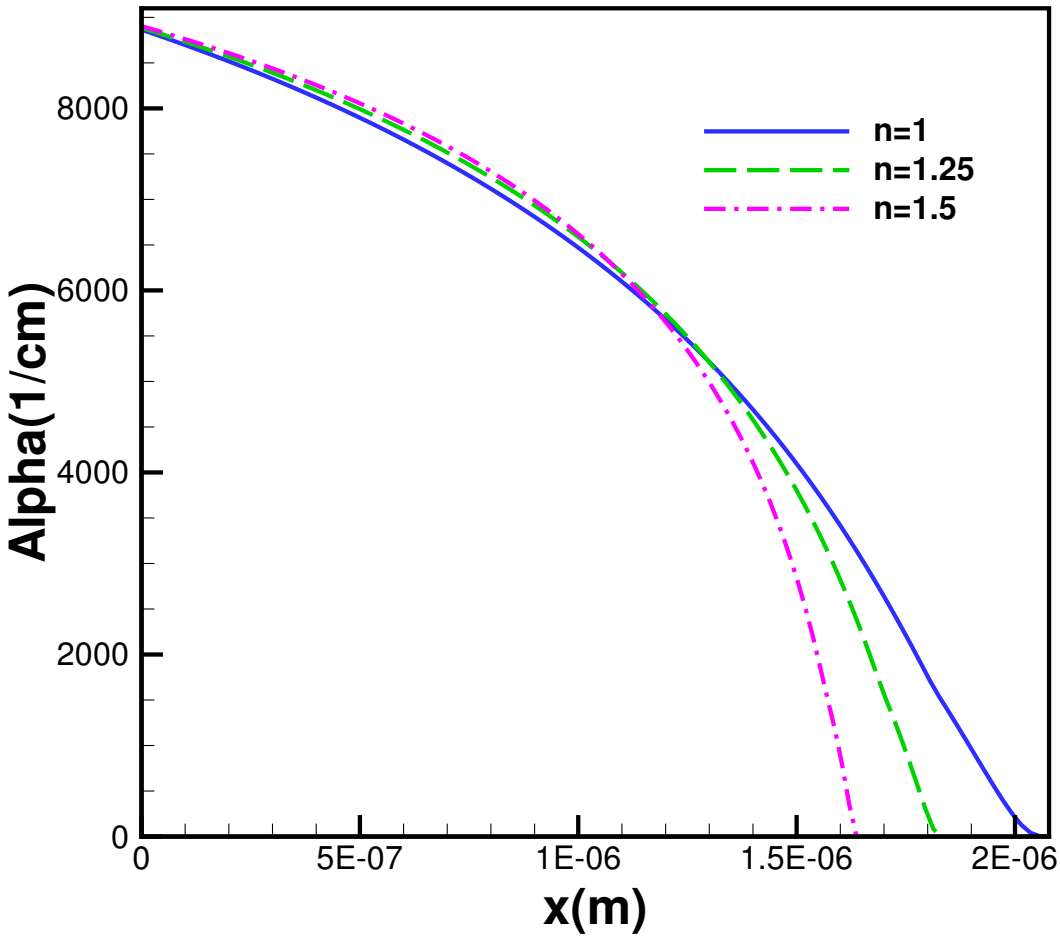


Figure 4.21: Spatial variation of ionization coefficient for different n-values with 5 $\mu m$ electrode operating at a total current density of $9 \times 10^5 A/m^2$ and a pressure of of 760 Torr at temperature 300K and the field emission parameters were $\beta = 55$ ,$\gamma_{se} = 0.05$, $\phi = 5.15eV$.

# Chapter 5

# Summary and future works

Microscale ionization coefficient for small gap size and broad range of E/N has been calculated using 0-D Monte Carlo simulations for different gases. Microscale ionization coefficients are also calculated for different gases and mixtures. The data were compared with the existing experimental data for various gases like hydrogen, helium, Nitrogen, Argon sulfur hexa-fluoride the other composite mixtures. It is found that the calculated values of $\alpha/N$ are with best fit with the experimental data. Experimental data of Microscale ionization coefficient for hydrogen and nitrogen are deviated from the METHES data in very small value of E/N but following the pattern for higher E/N. These small discrepancy observed at low E/N values possibly due to accuracy of cross sections. In case of carbon dioxide gas, helium, Methane, Ethylene both data perfectly matched with each other. This shows the METHES is well designed model to predict the ionization coefficient for wide range of E/N values which is still under investigation using experiment.The influence of applied voltage on the ionization coefficient was evaluated. Applied voltages that are only few times the ionization potential were shown to produce oscillations in the ionization coefficient profile before converging to the value predicted by 0-D simulations.

Experimental data of the microscale ionization coefficient for propane are less than the METHES data where as in case of sulfur hexafluoride the it is just opposite. The microscale ionization coefficients for mixture form are also taken into consideration in order to check the validity of the model and found that METHEs

data are properly valid and well understood even in the small scale E/N. The model also testify by comparing the Argon-METHES data with the PIC-MCC result obtained for uniform as well non-uniform electric field. It is found that E/N values are best fit for different values of E/N data.

To understand the modified Paschen's curve and the role of field enhancement factor ($\beta$) was studied. Experimental values of breakdown voltage and gaps sizes data were extracted, the values of field enhancement factor ($\beta$) are calculated and analyzed for different gases: argon, hydrogen, Carbon-Dioxide and dry air. The empirical relation between the field enhancement factor and electric field with the constant $C_1$ and $C_2$ are studied and the results were analyzed in order to understand the sensitivity of the constants $C_1$ and $C_2$ used in the empirical formula. The maximum and minimum range of ($\beta$) values are calculated and hence range of breakdown voltages were calculated which provides the limits of voltages that can be applied without breaking microscale electrical devices like MEMS.

Particle simulations were used to study the influence of field emission while understanding the importance of field enhancement factor. Field emission which refers to the emission of electrons from the cathode at very high electric fields was shown to be the driving mechanism to produce self-sustaining microdischarges in microscale gaps. The traditional Paschen theory does not describe field emission induced breakdown in microscale gaps but the present model take care of it and clearly explained the influence of field emission within the microscale gaps.

Non-linear sheath model for the modified Paschen curve was formulated and PIC/MCC simulations were done to provide the closure by determining the relevant parameters for microscale gaps. The post-breakdown conditions of field emission driven microplasma were studied theoretically and numerically using PIC/MCC simulations. A non-linear sheath model was used to obtain equations for electric field, cathode fall thickness, potential etc. The purposed model was compared with the results obtained using PIC/MCC simulations for different pressures and check the data are closely analyzed. Ionization coefficients, current densities and electric field were carefully studied. The model was also used to see the if they can be compared with the existing cathode fall model. Since the ionization coefficient in

the non-linear model varies non-linearly with the electric field, non linear sheath model is more relevant model to talk about the current-voltage characteristics of microscale plasma.

The mathematical model thus developed is also compared with the existing cathode fall model and PIC results using the similar conditions used previously.It is found that the formulated models were shown to predict breakdown voltages and other relevant parameters agreed well with those predicted by actual PIC/MCC simulations.

Since the model is designed for direct current (DC), same work can be designed for RF discharge and is considered as future plan.

# Appendix A

# List of Reactions during Micro scale Ionization process

## A.1 Nitrogen

$e^- + N_2 \rightarrow e^- + N_2$, Elastic

$e^- + N_2 \rightarrow e^- + N_2(VIB \quad V1)$, Excitation

$e^- + N_2 \rightarrow e^- + N_2(VIB \quad 2V1)$, Excitation

$e^- + N_2 \rightarrow e^- + N_2(VIB \quad 3V1)$, Excitation

$e^- + N_2 \rightarrow e^- + N_2(VIB \quad 4V1)$, Excitation

$e^- + N_2 \rightarrow e^- + N_2(VIB \quad 5V1)$, Excitation

$e^- + N_2 \rightarrow e^- + N_2(VIB \quad 6V1)$, Excitation

$e^- + N_2 \rightarrow e^- + N_2(VIB \quad 7V1)$, Excitation

$e^- + N_2 \rightarrow e^- + N_2(VIB \quad 8V1)$, Excitation

$e^- + N_2 \rightarrow e^- + N_2(VIB \quad 9V1)$, Excitation

$e^- + N_2 \rightarrow e^- + N_2(VIB \quad 10V1)$, Excitation

$e^- + N_2 \rightarrow e^- + N_2(VIB \quad 11V1)$, Excitation

$e^- + N_2 \rightarrow e^- + N_2(VIB \quad 12V1)$, Excitation

$e^- + N_2 \rightarrow e^- + N_2(VIB \quad 13V1)$, Excitation

$e^- + N_2 \rightarrow e^- + N_2(VIB \quad 14V1)$, Excitation

$e^- + N_2 \rightarrow e^- + N_2(VIB \quad 15V1)$, Excitation

$e^- + N_2 \rightarrow e^- + N_2(A3SIG \quad V = 0 - 4)$, Excitation

$e^- + N_2 \rightarrow e^- + N_2(B \quad 3PI \quad V = 0 - 3)$, Excitation

$e^- + N_2 \rightarrow e^- + N_2(W3DEL \quad V = 0 - 5)$, Excitation

$e^- + N_2 \rightarrow e^- + N_2(A3SIG \quad V = 0 - 10 - 21)$, Excitation

$e^- + N_2 \rightarrow e^- + N_2(B \quad 3PI \quad V = 4 - 16)$, Excitation

$e^- + N_2 \rightarrow e^- + N_2(W3DEL \quad V = 6 - 10)$, Excitation

$e^- + N_2 \rightarrow e^- + N_2(A \quad 1PI \quad V = 0 - 3)$, Excitation

$e^- + N_2 \rightarrow e^- + N_2(B!3SIG \quad V = 0 - 6)$, Excitation

$e^- + N_2 \rightarrow e^- + N_2(A!3SIG \quad V = 0 - 6)$, Excitation

$e^- + N_2 \rightarrow e^- + N_2(W3DEL \quad V = 11 - 19)$, Excitation

$e^- + N_2 \rightarrow e^- + N_2(W \quad 1DEL \quad V = 0 - 5)$, Excitation

$e^- + N_2 \rightarrow e^- + N_2(A \quad 1PI \quad V = 4 - 15)$, Excitation

$e^- + N_2 \rightarrow e^- + N_2(B!3SIG \quad V = 7 - 18)$, Excitation

$e^- + N_2 \rightarrow e^- + N_2(A!3SIG \quad V = 7 - 19)$, Excitation

$e^- + N_2 \rightarrow e^- + N_2(W \quad 1DEL \quad V = 6 - 18)$, Excitation

$e^- + N_2 \rightarrow e^- + N_2(C \quad 3PI \quad V = 0 - 4)$, Excitation

$e^- + N_2 \rightarrow e^- + N_2(E \quad SIG)$, Excitation

$e^- + N_2 \rightarrow e^- + N_2(A!!1SIG \quad V = 0 - 1)$, Excitation

$e^- + N_2 \rightarrow e^- + N_2(B \quad 1PI \quad V = 0 - 6)$, Excitation

$e^- + N_2 \rightarrow e^- + N_2(C!1SIG \quad V = 0 - 3)$, Excitation

$e^- + N_2 \rightarrow e^- + N_2(G \quad 3PI \quad V = 0 - 3)$, Excitation

$e^- + N_2 \rightarrow e^- + N_2(C3 \quad 1PI \quad V = 0 - 3)$, Excitation

$e^- + N_2 \rightarrow e^- + N_2(F \quad 3PI \quad V = 0 - 3)$, Excitation

$e^- + N_2 \rightarrow e^- + N_2(B!1SIG \quad V = 0 - 10)$, Excitation

$e^- + N_2 \rightarrow e^- + N_2(B \quad 1PI \quad V = 7 - 14)$, Excitation

$e^- + N_2 \rightarrow e^- + N_2(O3 \quad 1PI \quad V = 0 - 3)$, Excitation

$e^- + N_2 \rightarrow e^- + N_2(B!1SIG \quad V = 10 - H)$, Excitation

$e^- + N_2 \rightarrow e^- + N_2(SUM \quad SINGLETS)$, Excitation

$e^- + N_2 \rightarrow e^- + e^- + N_2^+$, Ionization

## A.2 Methane

$e^- + CH_4 \rightarrow CH_2 + CH_2$, Attachment

$e^- + CH_4 \rightarrow e^- + CH_4$, Elastic

$e^- + CH_4 \rightarrow e^- + CH_4(V24)(0.162eV)$, Excitation

$e^- + CH_4 \rightarrow e^- + CH_4(V13)(0.361eV)$, Excitation

$e^- + CH_4 \rightarrow e^- + CH_4^*(9eV - dissoc)$, Excitation

$e^- + CH_4 \rightarrow e^- + CH_4^*(10eV - dissoc)$, Excitation

$e^- + CH_4 \rightarrow e^- + CH_4^*(11eV - dissoc)$, Excitation

$e^- + CH_4 \rightarrow e^- + CH_4^*(12eV - dissoc)$, Excitation

$e^- + CH_4 \rightarrow e^- + e^- + CH_4^+$, Ionization

$e^- + CH_4 \rightarrow e^- + e^- + H + CH_3^+$, Ionization

## A.3 Carbon Dioxide

$e^- + CO_2 \rightarrow CO + O^-$, Attachment

$e^- + CO_2 \rightarrow e^- + CO_2$, Elastic

$e^- + CO_2 \rightarrow e^- + CO_2(0.083eV)$, Excitation

$e^- + CO_2 \rightarrow e^- + CO_2(0.167eV)$, Excitation

$e^- + CO_2 \rightarrow e^- + CO_2(0.252eV)$, Excitation

$e^- + CO_2 \rightarrow e^- + CO_2(0.291eV)$, Excitation

$e^- + CO_2 \rightarrow e^- + CO_2(0.339eV)$, Excitation

$e^- + CO_2 \rightarrow e^- + CO_2(0.422eV)$, Excitation

$e^- + CO_2 \rightarrow e^- + CO_2(0.505eV)$, Excitation

$e^- + CO_2 \rightarrow e^- + CO_2(2.5eV)$, Excitation

$e^- + CO_2 \rightarrow e^- + CO_2^*(7.0eV)$, Excitation

$e^- + CO_2 \rightarrow e^- + CO_2^*(10.5eV)$, Excitation

$e^- + CO_2 \rightarrow e^- + e^- + CO_2^+$, Ionization

## A.4 Ethylene

$e^- + C_2H_4 \rightarrow e^- + C_2H_4$, Elastic

$e^- + C_2H_4 \rightarrow e^- + C_2H_4(V1)(0.11eV)$, Excitation

$e^- + C_2H_4 \rightarrow e^- + C_2H_4(V2)(0.361eV)$, Excitation

$e^- + C_2H_4 \rightarrow e^- + C_2H_4^*(3.80eV)$, Excitation

$e^- + C_2H_4 \rightarrow e^- + C_2H_4^*(5.00eV)$, Excitation

$e^- + C_2H_4 \rightarrow e^- + C_2H_4^*(7.00eV)$, Excitation

$e^- + C_2H_4 \rightarrow e^- + e^- + C_2H_4^+$, Ionization

## A.5 Ethane

$e^- + C_2H_6 \rightarrow e^- + C_2H_6$, Elastic

$e^- + C_2H_6 \rightarrow e^- + C_2H_6^-$, Attachment

$e^- + C_2H_6 \rightarrow e^- + C_2H_6(V24)(0.16eV)$, Excitation

$e^- + C_2H_6 \rightarrow e^- + C_2H_6(V13)(0.371eV)$, Excitation

$e^- + C_2H_6 \rightarrow e^- + C_2H_6^*(7.53eV)$, Excitation

$e^- + C_2H_6 \rightarrow e^- + C_2H_6^*(10.12eV)$, Excitation

$e^- + C_2H_6 \rightarrow e^- + e^- + C_2H_6^+$, Excitation

## A.6 Helium

$e^- + He \rightarrow e^- + He$, Elastic

$e^- + He \rightarrow e^- + He(23S)(19.82eV)$, Excitation

$e^- + He \rightarrow e^- + He(21S)(20.62eV)$, Excitation

$e^- + He \rightarrow e^- + He(23P)(20.96eV)$, Excitation

$e^- + He \rightarrow e^- + He(21P)(21.22eV)$, Excitation

$e^- + He \rightarrow e^- + He(33S)(22.726eV)$, Excitation

$e^- + He \rightarrow e^- + He(31S)(20.92eV)$, Excitation

$e^- + He \rightarrow e^- + He(33P)(23.01eV)$, Excitation

$e^- + He \rightarrow e^- + He(33D)(23.07eV)$, Excitation

$e^- + He \rightarrow e^- + He(31D)(23.07eV)$, Excitation

$e^- + He \rightarrow e^- + He(31P)(23.08eV)$, Excitation

$e^- + He \rightarrow e^- + He(43S)(23.593eV)$, Excitation

$e^- + He \rightarrow e^- + He(41S)(23.674eV)$, Excitation

$e^- + He \rightarrow e^- + He(43P)(23.708eV)$, Excitation

$e^- + He \rightarrow e^- + He(41D)(23.736eV)$, Excitation

$e^- + He \rightarrow e^- + He(43D)(23.736eV)$, Excitation

$e^- + He \rightarrow e^- + He(41F)(23.73eV)$, Excitation

$e^- + He \rightarrow e^- + He(43F)(23.737eV)$, Excitation

$e^- + He \rightarrow e^- + He(41P)(23.742eV)$, Excitation

$e^- + He \rightarrow e^- + He(53S)(23.972eV)$, Excitation

$e^- + He \rightarrow e^- + He(51S)(24.011eV)$, Excitation

$e^- + He \rightarrow e^- + He(53P)(24.028eV)$, Excitation

$e^- + He \rightarrow e^- + He(51D)(24.043eV)$, Excitation

$e^- + He \rightarrow e^- + He(53D)(24.043eV)$, Excitation

$e^- + He \rightarrow e^- + He(51S)(24.0431eV)$, Excitation

$e^- + He \rightarrow e^- + He(53F)(24.0432eV)$, Excitation

$e^- + He \rightarrow e^- + He(51P)(24.0458eV)$, Excitation

$e^- + He \rightarrow e^- + He(63S)(24.169eV)$, Excitation

$e^- + He \rightarrow e^- + He(61S)(24.191eV)$, Excitation

$e^- + He \rightarrow e^- + He(63P)(24.201eV)$, Excitation

$e^- + He \rightarrow e^- + He(63D)(24.2092eV)$, Excitation

$e^- + He \rightarrow e^- + He(61D)(24.2093eV)$, Excitation

$e^- + He \rightarrow e^- + He(61P)(24.211eV)$, Excitation

$e^- + He \rightarrow e^- + He(73S)(24.2846eV)$, Excitation

$e^- + He \rightarrow e^- + He(71S)(24.2983eV)$, Excitation

$e^- + He \rightarrow e^- + He(73P)(24.30429eV)$, Excitation

$e^- + He \rightarrow e^- + He(73D)(24.3095eV)$, Excitation

$e^- + He \rightarrow e^- + He(71D)(24.309eV)$, Excitation

$e^- + He \rightarrow e^- + He(71P)(24.311eV)$, Excitation

$e^- + He \rightarrow e^- + He(N3S)(24.3581eV)$, Excitation

$e^- + He \rightarrow e^- + He(N1S)(24.3672eV)$, Excitation

$e^- + He \rightarrow e^- + He(N3P)(24.3712eV)$, Excitation

$e^- + He \rightarrow e^- + He(N1D)(24.3747eV)$, Excitation

$e^- + He \rightarrow e^- + He(N3D)(24.3747eV)$, Excitation

$e^- + He \rightarrow e^- + He(81P)(24.3755eV)$, Excitation

$e^- + He \rightarrow e^- + He(91P)(24.4199eV)$, Excitation

$e^- + He \rightarrow e^- + He(101P)(24.4517eV)$, Excitation

$e^- + He \rightarrow e^- + He(111P)(24.4752eV)$, Excitation

$e^- + He \rightarrow e^- + He(24.4931eV)$, Excitation

$e^- + He \rightarrow e^- + He(N1P \quad SUM \quad HI)(24.5071eV)$, Excitation

$e^- + He \rightarrow e^- + e^- + He^+$, Ionization

# Bibliography


[1] Kenro Miyamoto et al. *Plasma physics for controlled fusion*, volume 92. Springer, 2016.

[2] Michael A Lieberman and Alan J Lichtenberg. *Principles of plasma discharges and materials processing*. John Wiley & Sons, 2005.

[3] Yuri P Raizer. Gas discharge physics. *Springer*, 1991.

[4] J.-M Torres and R S Dhariwal. Electric field breakdown at micrometre separations in air and vacuum. *Microsystem Technologies*, 6, 1999.

[5] DB Go and A Venkattraman. Microscale gas breakdown: ion-enhanced field emission and the modified paschens curve. *Journal of Physics D: Applied Physics*, 47(50):503001, 2014.

[6] Ayyaswamy Venkattraman. Theory and analysis of operating modes in microplasmas assisted by field emitting cathodesa). *Physics of Plasmas*, 2015.

[7] Irving Langmuir. Oscillations in ionized gases. *Proceedings of the National Academy of Sciences*, 14(8):627–637, 1928.

[8] Harold M Mott-Smith and Irving Langmuir. The theory of collectors in gaseous discharges. *Physical review*, 28(4):727, 1926.

[9] Weston M Stacey. *Fusion plasma physics*. John Wiley & Sons, 2008.

[10] John Nuckolls, Lowell Wood, Albert Thiessen, and George Zimmerman. Laser compression of matter to super-high densities: Thermonuclear (ctr) applications. *Nature*, 239(5368):139, 1972.

[11] Edison Liang. Comoving acceleration of overdense electron-positron plasma by colliding ultra-intense laser pulses. *Physics of plasmas*, 13(6):064506, 2006.

[12] Yong Jun Hong, Seung Min Lee, Gyoo Cheon Kim, and Jae Koo Lee. Modeling high-pressure microplasmas: Comparison of fluid modeling and particle-in-cell Monte Carlo collision modeling. *Plasma Processes and Polymers*, 2008.

[13] Hyun-Ha Kim. Nonthermal Plasma Processing for Air-Pollution Control: A Historical Review, Current Issues, and Future Prospects. *Plasma Processes and Polymers*, 2004.

[14] Muhammad Arif Malik, Abdul Ghaffar, Salman Akbar Malik, and O . Water purification by electrical discharges. *Plasma Sources Sci. Technol*, 10(01):82–91, 2001.

[15] John F Waymouth and Francis Bitter. Analysis of the plasma of fluorescent lamps. *Journal of Applied Physics*, 27(2):122–131, 1956.

[16] Takanori Ichiki, Ryo Taura, and Yasuhiro Horiike. Localized and ultrahigh-rate etching of silicon wafers using atmospheric-pressure microplasma jets Etching polyimide with a nonequilibrium atmospheric-pressure plasma jet Room-temperature atmospheric pressure plasma plume for biomedical applications Localized and ultrahigh-rate etching of silicon wafers using atmospheric-pressure microplasma jets. *Journal of Applied Physics Applied Physics Letters Applied Physics Letters Journal of Vacuum Science & Technology A: Vacuum, Surfaces, and Films Applied Physics Letters Journal of Applied Physics Journal of Applied Physics*, 95(3134):251504–221504, 2004.

[17] K. H. Becker, K. H. Schoenbach, and J. G. Eden. Microplasmas and applications, 2006.

[18] R. Foest, M. Schmidt, and K. Becker. Microplasmas, an emerging field of low-temperature plasma science and technology, 2006.

[19] Felipe Iza, Gon Jun Kim, Seung Min Lee, Jae Koo Lee, James L. Walsh, Yuantao T. Zhang, and Michael G. Kong. Microplasmas: Sources, particle kinetics, and biomedical applications, 2008.

[20] J. G. Eden, S. J. Park, C. M. Herring, and J. M. Bulson. Microplasma light tiles: Thin sheet lamps for general illumination. *Journal of Physics D: Applied Physics*, 2011.

[21] Akira Tonomura, Tsuyoshi Matsuda, Junji Endo, Hideo Todokoro, and Tsutomu Komoda. Development of a Field Emission Electron Microscope. *J. Electron Microsc*, 28(1):1–11, 1979.

[22] G. N. Fursey, V. I. Petrick, and D. V. Novikov. Low-threshold field electron emission from carbon nanoclusters formed upon cold destruction of graphite. *Technical Physics*, 2009.

[23] M. S. Peterson, W. Zhang, T. S. Fisher, and S. V. Garimella. Low-voltage ionization of air with carbon-based materials. *Plasma Sources Science and Technology*, 2005.

[24] David B Go, TS Fisher, SV Garimella, and V Bahadur. Planar microscale ionization devices in atmospheric air with diamond-based electrodes. *Plasma Sources Science and Technology*, 18(3):035004, 2009.

[25] Shashwati Sen, Prajakta Kanitkar, Ankit Sharma, K.P. Muthe, Ashutosh Rath, S.K. Deshpande, Manmeet Kaur, R.C. Aiyer, S.K. Gupta, and J.V. Yakhmi. Growth of SnO2/W18O49 nanowire hierarchical heterostructure and their application as chemical sensor. *Sensors and Actuators B: Chemical*, 2010.

[26] A. Venkattraman, A. Garg, D. Peroulis, and A. A. Alexeenko. Direct measurements and numerical simulations of gas charging in microelectromechanical system capacitive switches. *Applied Physics Letters*, 2012.

[27] Kunihide Tachibana. Current status of microplasma research. *IEEJ Transactions on Electrical and Electronic Engineering*, 2006.

[28] Karl H. Schoenbach and Weidong Zhu. High-pressure microdischarges: Sources of ultraviolet radiation, 2012.

[29] Christine K. Eun and Yogesh B. Gianchandani. Microdischarge-based sensors and actuators for portable microsystems: Selected examples. *IEEE Journal of Quantum Electronics*, 2012.

[30] J. G. Eden, S. J. Park, J. H. Cho, M. H. Kim, T. J. Houlahan, B. Li, E. S. Kim, T. L. Kim, S. K. Lee, K. S. Kim, J. K. Yoon, S. H. Sung, P. Sun, C. M. Herring, and C. J. Wagner. Plasma science and technology in the limit of the small: Microcavity plasmas and emerging applications. *IEEE Transactions on Plasma Science*, 2013.

[31] X. Lu, G. V. Naidis, M. Laroussi, and K. Ostrikov. Guided ionization waves: Theory and experiments, 2014.

[32] X. Lu, M. Laroussi, and V. Puech. On atmospheric-pressure non-equilibrium plasma jets and plasma bullets. *Plasma Sources Science and Technology*, 2012.

[33] Yuri P Raizer and John E Allen. *Gas discharge physics*, volume 2. Springer Berlin, 1997.

[34] A Venkattraman, A Garg, Dimitrios Peroulis, and Alina A Alexeenko. Direct measurements and numerical simulations of gas charging in microelectromechanical system capacitive switches. *Applied Physics Letters*, 100(8):083503, 2012.

[35] Friedrich Paschen. Ueber die zum Funkenübergang in Luft, Wasserstoff und Kohlensäure bei verschiedenen Drucken erforderliche Potentialdifferenz. *Annalen der Physik*, 1889.

[36] R. H. Fowler and L. Nordheim. Electron Emission in Intense Electric Fields. *Proceedings of the Royal Society A: Mathematical, Physical and Engineering Sciences*, 1928.

[37] R E Surgess and J M Houstqn. Corrected Values of Fowler-Nordheim Field Emission Functions v(y) and s(y).

[38] K.-F Chen and J G Eden. The plasma transistor: A microcavity plasma device coupled with a low voltage, controllable electron emitter. *Appl. Phys. Lett. Journal of Applied Physics*, 93(101), 2008.

[39] Pradeep Pai and Massood Tabib-Azar. SUB 3-micron gap microplasma fet with 50 v turn-on voltage. In *Proceedings of the IEEE International Conference on Micro Electro Mechanical Systems (MEMS)*, 2014.

[40] Anurag Garg, Venkattraman Ayyaswamy, Andrew Kovacs, Alina Alexeenko, and Dimitrios Peroulis. Direct measurement of field emission current in e-static MEMS structures. In *Proceedings of the IEEE International Conference on Micro Electro Mechanical Systems (MEMS)*, 2011.

[41] L. Michalas, A. Garg, A. Venkattraman, M. Koutsoureli, A. Alexeenko, D. Peroulis, and G. Papaioannou. A study of field emission process in electrostatically actuated MEMS switches. *Microelectronics Reliability*, 2012.

[42] P. Kisliuk. Electron emission at high fields due to positive ions. *Journal of Applied Physics*, 1959.

[43] L. H. Germer. Electrical breakdown between close electrodes in air. *Journal of Applied Physics*, 1959.

[44] M. Radmilovi??-Radjenovi??, J. K. Lee, F. Iza, and G. Y. Park. Particle-in-cell simulation of gas breakdown in microgaps. *Journal of Physics D: Applied Physics*, 2005.

[45] M. Radmilović-Radjenović and B. Radjenović. A particle-in-cell simulation of the breakdown mechanism in microdischarges with an improved secondary emission model. *Contributions to Plasma Physics*, 2007.

[46] Marija Radmilović-Radjenović and Branislav Radjenović. The influence of ion-enhanced field emission on the high-frequency breakdown in microgaps. *Plasma Sources Science and Technology*, 2007.

[47] Osamu Sakai, Takuya Shimomura, and Kunihide Tachibana. Negative refractive index designed in a periodic composite of lossy microplasmas and microresonators. *Physics of Plasmas*, 2010.

[48] O. Sakai, T. Sakaguchi, Y. Ito, and K. Tachibana. Interaction and control of millimetre-waves with microplasma arrays. In *Plasma Physics and Controlled Fusion*, 2005.

[49] S. J. Park, K. F. Chen, N. P. Ostrom, and J. G. Eden. 40 000 pixel arrays of ac-excited silicon microcavity plasma devices. *Applied Physics Letters*, 2005.

[50] Ayyaswamy Venkattraman. Cathode fall model and current-voltage characteristics of field emission driven direct current microplasmas. *Physics of Plasmas*, 2013.

[51] John P Verboncoeur, Maria Virginia Alves, Vahid Vahedi, and Charles Kennedy Birdsall. Simultaneous potential and circuit solution for 1d bounded plasma particle simulation codes. *Journal of Computational Physics*, 104(2):321–328, 1993.

[52] Ye A Bondar, V A Schweigert, and M S Ivanov. Modeling of the Hall-Effect Thruster Plume by Combined PIC-MCC / DSMC Method. *AIP Conference Proceedings*, 663(549), 2003.

[53] S. Hamaguchi. Modeling and simulation methods for plasma processing. *IBM Journal of Research and Development*, 1999.

[54] Gennady Markelov and Eric Gengembre. Modeling of plasma flow around SMART-1 spacecraft. In *IEEE Transactions on Plasma Science*, 2006.

[55] J P Boeuf. Plasma display panels: physics, recent developments and key issues. *J. Phys. D: Appl. Phys*, 36(03):53–79, 2003.

[56] Charles K Birdsall and A Bruce Langdon. *Plasma physics via computer simulation*. CRC press, 2004.

[57] HR Skullerud. Hr skullerud, j. phys. d: Appl. phys. 1, 1567 (1968). *J. Phys. D: Appl. Phys.*, 1:1567, 1968.

[58] Siegbert Kuhn, K-U Riemann, N Jelić, DD Tskhakaya Sr, D Tskhakaya Jr, and M Stanojević. Link between fluid and kinetic parameters near the plasma boundary. *Physics of plasmas*, 13(1):013503, 2006.

[59] Nikola Jelić, K-U Riemann, Tomaž Gyergyek, Siegbert Kuhn, Mladen Stanojević, and Jože Duhovnik. Fluid and kinetic parameters near the plasma-sheath boundary for finite debye lengths. *Physics of Plasmas*, 14(10):103506, 2007.

[60] GJM Hagelaar and LC Pitchford. Solving the boltzmann equation to obtain electron transport coefficients and rate coefficients for fluid models. *Plasma Sources Science and Technology*, 14(4):722, 2005.

[61] Elise N. Pusateri, Heidi E. Morris, Eric M. Nelson, and Wei Ji. Determination of equilibrium electron temperature and times using an electron swarm model with BOLSIG+ calculated collision frequencies and rate coefficients. *Journal of Geophysical Research*, 2015.

[62] Mohamed Rabie and Christian M Franck. Methes: A monte carlo collision code for the simulation of electron transport in low temperature plasmas. *Computer Physics Communications*, 203:268–277, 2016.

[63] Amanda M Loveless and Allen L Garner. Generalization of microdischarge scaling laws for all gases at atmospheric pressure. *IEEE Transactions on Plasma Science*, 45(4):574–583, 2017.

[64] J Dutton, MH Hughes, and BC Tan. Ionization coefficients in helium, neon and helium-neon mixtures. *Journal of Physics B: Atomic and Molecular Physics*, 2(8):890, 1969.

[65] AED Heylen. Ionization coefficients and sparking voltages from methane to butane. *International Journal of Electronics Theoretical and Experimental*, 39(6):653–660, 1975.

[66] MS Bhalla and JD Craggs. Measurement of ionization and attachment coefficients in sulphur hexafluoride in uniform fields. *Proceedings of the Physical Society*, 80(1):151, 1962.

[67] Clifton G Found. Ionization potentials of argon, nitrogen, carbon monoxide, helium, hydrogen and mercury and iodine vapors. *Physical Review*, 16(1):41, 1920.

[68] R-T Lee, H-H Chung, and Y-C Chiou. Arc erosion behaviour of silver electric contacts in a single arc discharge across a static gap. *IEE Proceedings-Science, Measurement and Technology*, 148(1):8–14, 2001.

[69] M Radmilović-Radjenović, B Radjenović, Š Matejčik, and M Klas. The breakdown phenomena in micrometer scale direct-current gas discharges. *Plasma Chemistry and Plasma Processing*, 34(1):55–64, 2014.

[70] Takahito Ono, Dong Youn Sim, and Masayoshi Esashi. Micro-discharge and electric breakdown in a micro-gap. *Journal of Micromechanics and Microengineering*, 10(3):445, 2000.

[71] M. Radmilović-Radjenović, B. Radjenović, S. Matejčik, and M. Klas. The breakdown phenomena in micrometer scale direct-current gas discharges. *Plasma Chemistry and Plasma Processing*, 2014.

[72] Jose Alejandro Buendia and Ayyaswamy Venkattraman. Field enhancement factor dependence on electric field and implications on microscale gas breakdown: Theory and experimental interpretation. *EPL (Europhysics Letters)*, 112(5):55002, 2015.